Analysis of the Dye/Titania Interface as Photo-Anode in Dye Sensitized Solar Cells

by

Herri Trilaksana

Thesis
Submitted to Flinders University
for the degree of

Doctor of Philosophy

Science and Engineering

23 August 2018

Table of Content

List of Figures

List of Tables

Abstract

The understanding of the unwanted process such as charge recombination, in Dye Sensitised Solar Cells (DSSCs) are still a challenging issue to gain the effort of improving this promising photovoltaic technique. The dye/titania and dye/electrolyte interfaces are playing a crucial factor of photovoltaic and this is the focus of this thesis. Four main issues have been chosen for investigations of this study which cover the corresponding influence of the electrolyte exposure, the organic and the metal-organic dyes-titania attachment in term of monolayer versus a multilayer, the aging effect, and the application of the co-adsorbent. The dye formation and the change of its electronic and molecular structure were studied.

Electron spectroscopy techniques including X-ray Photoelectron Emission Spectroscopy (XPS), Ultra-violet Photoelectron Spectroscopy (UPS) and Metastable Induced Electron Spectroscopy (MIES) have been employed to directly observe the changes with respect to the electronic structure representing the molecular restructuring and reorientation of the dye. Neutral Impact Collision Ion Scattering Spectroscopy (NICISS) is an ion spectroscopy technique used to study the molecular coverage and concentration depth profiling of the dye. These spectroscopic methods are capable in probing various depths where each technique is potentially able to determine the exact position of a component in the sample. FT-IR spectroscopy was used as a complementary method of electron and ion spectroscopy to determine the organic compound. FTIR is useful in determining the organic functional groups on the sample however it is not surface sensitive. FTIR is used to study sample with corresponding to the organic material such as co-adsorbent in this thesis.

The ruthenium-based dye N719 and Z907 are used to study the effect of the electrolyte exposure through the investigation of the iodine as a representative component of the electrolyte. The study investigated the changes of the electronic and molecular structure such as the indication of dipole layer formation, which can be attributed to the change of the work function, and the restructuring or reorientation of the outermost dye molecules.

The L0Br organic dye was used to investigate the formation of monolayer and multilayer dye molecule on the mesoporous titania semiconductor by determining the concentration depth profiles and its molecular coverage from the adsorption isotherm. The result showed that the L0Br formed more monolayer than the multilayer.

The effects of aging and electrolyte exposure were also observed using the PD2 and LEG1 organic dyes using two different electrolytes with containing and not containing the TBP. As a result of this study, it was observed that the LEG1 dye showed larger work-function changes than the PD2 and the electrolyte containing the TBP were affecting less to the formation of a dipole on the titania/dye interface which can be attributed to the change of the electronic structure or work-function of the dye.

The final chapter studied how the Chenodeoxycholic Acid (CDCA) as co-adsorbent influenced to the dye formation from the perspectives of the enhancement of the monolayer dye formation and preventing the dye aggregation. It was shown that the co-adsorbent suppressed the formation of multilayer dye and it was found to be dependent on the concentration of the co-adsorbent. These spectroscopic studies contribute to the better understanding of the electronic and molecular structure and also morphology of dye in titania/dye/electrolyte interface in DSSC.

Declaration

I certify this thesis does not incorporate without acknowledgement any material previously submitted for degree or diploma in any university; and that to the best of my knowledge and belief it does not contain any material previously published or written by another person except where due reference is made in the text.

Herri Trilaksana

Acknowledgements

<div align="right">

Herri Trilaksana

Flinders University

August 2018

</div>

Abbreviations

ARXPS	Angle Resolved X-ray Photoelectron Spectroscopy
CB	Conduction Band
CDCA	Chenodeoxycholic Acid
CE	Counter Electrode
DSSCs	Dye Sensitised Solar Cells
FTIR	Fourier-transform infrared spectroscopy
FTO	Fluorine Thin Oxide
FWHM	Full Width Half Maximum
HOMO	Highest Occupied Molecular Orbital
IPCE	Incident Photon to Current Efficiency
ITO	Indium Thin Oxide
LHE	Light Harvesting Efficiency
LUMO	Lowest Unoccupied Molecular Orbital
MIES	Meta Induced-Electron Spectroscopy
N719	Di-tetrabutylammonium cis-bis (isothiocyanate) bis (2,2'-bipyridyl-4,4' dicarboxylate) ruthenium (II))
NICISS	Neutral Impact Collision Ion Scattering Spectroscopy
RBS	Rutherford Back Scattering
TBP	4-tert-butylpyridine (TBP)
TOP	Tome of Flight
UPS	Ultra violet Photoelectron Spectroscopy
UHV	Ultra High Vacuum

VB	Valence Band
V_{OC}	Open-circuit Voltage
XPS	X-ray Photoelectron Spectroscopy
Z907	Cis-Bis(isothiocyanato) (2,2'-bipyridyl-4,4'-dicarboxylato)(4,4'-di-nonyl-2'-bipyridyl) ruthenium(II) were applied.L0Br

1 CHAPTER ONE: Introduction and Aims

1.1 Introduction

The world energy demand has been a crucial issue since the last few decades. Currently, solar energy is one of the promising future energy sources to replace the fossil fuel which has been the most common type of energy source in the world. The main difference between the solar cells technology and the technology based on the conventional fossil fuel energy source is because the solar cell is renewable and clean so it would not be harming to the environment because there is no CO_2 emission which is dangerous to the world environment. Compared to other types of photo voltaic technology, solar cell technologies based on the sensitized-dye on the mesoporous oxide films has attracted a massive concern of interest in the last few years. It is clearly because of its possibility to achieve moderate efficiency devices at low cost and employs abandoned materials. Thus, this technology could also be an interesting alternative effort to collect and convert the sunlight into the electricity in comparison with the conventional p-n junction solar cells. Since the last few decades, the use of mesoporous metal oxide structure has been very popular and attracted much attention of intense study and research. It was initiated after Gratzel et al achieved the first hybrid solar cells. The main reasons the Dye Sensitized Solar Cells (DSSCs) technology become very popular is because of the way to harvest the solar energy into electricity is promising. It is also due to their low cost production, high conversion efficiency, and unique structures.[1] By the DSSCs technology, it is becoming possible to completely migrate from the classical solid-state junction device, into the semiconductor with different charges transfer media in different phases such as liquid, gel or solid thereby forming a photo-electrochemical cells. However, some innovative efforts, intensive research, and investigation are still need needed to enhance the performance of the DSSCs in converting the solar radiation into the electricity.

1.2 Brief description of DSSC

The photovoltaic field, dominated mainly by inorganic solid-state junction cells, is now being challenged by the emergence of new devices based on nano-crystalline and conducting polymer films, which offer a very low-cost fabrication and attractive features such as transparency, flexibility, etc. that might facilitate the market entry. Among well known photo-voltaic technolgies, dye sensitized solar cells (DSSCs) are devices that have reached moderate efficiencies, thus being feasible competitors to conventional cells.

The configuration of the DSSCs is different compared to the conventional p-v junction semiconductor solar cells. The DSSCs consist of a nano-crystalline wide band gap semiconductor (usually TiO_2), which is deposited onto a transparent conductive substrate, and on whose surface a dye is adsorbed. This part is usually called photo-anode where the sunlight radiation will be collected and adsorbed by the dye active material. The cell is completed with a counter-electrode on the other side, and both electrodes are put into electrical contact by infiltrating a liquid electrolyte in between them. When the light is irradiated into the cell, the photon is absorbed by the dye and charges are separated at the interface between the dye and the metal oxide it is anchored to. The interaction between the dye and the metal oxide plays a crucial role in the operation DSSCs.

The optimization of the conversion efficiency is when the fraction of the light intensity that is converted into the electricity, is a key issue for the type of photovoltaic technologies. Many researchers have proposed different directions in handling the problems. Different modifications of the originally proposed cell, mainly based on the use of different semiconductors, dyes or ionic conductor, have been made in order to improve its performance. Employing nanostructures to improve solar energy conversion device[2] has also been very active and increasing of interest. Another interesting pathway to enhance the cell efficiency is to modify its optical design in order to improve the light harvesting efficiency (LHE) or adsorption within the cell.

Some crucial efforts have also been performed to improve the cell performance by modifying the structure of metal oxide. One of the important method that has been explored the most in modifying the optical design is the use of a diffuse scattering layer made of large TiO_2 colloids that are either deposited onto the nanocrystalline electrode or mixed with the nanocrystalline titania (nc-TiO_2) slurry. In both cases, they increase the optical light path within the absorbing layer and it leads the matter-radiation interaction time thus enhancing the probability of photon absorption by the dye molecules. However, it has to be taken into account that any structure introduced in the cell must permit the electrical contact between the electrolyte and the sensitized semiconductor slab, which forces it to have porosity capable of sustaining the flow of charges as the movement of the electrolyte and redox couple is necessary. Currently, different alternatives to enhance the performances of DSSCs are being proposed due to the development of novel porous periodic photonic nanostructures that can be easily integrated in these devices.

DSSCs combine the optical absorption and charge-separation processes by the association of a sensitizer as light-absorbing material with a wide band-gap semiconductor (usually titanium dioxide). In the early 1970s, it was found that titanium dioxide (TiO_2) from photo-electrochemical cells could split water with a small bias voltage when exposed to light [3]. However, the large band-gap of TiO_2 makes it transparent for visible light, resulted on the low conversion efficiency when using the sun as illumination source.

In addition, research on dye sensitization of semiconductor electrodes has been started since 1960s. The pioneering research involved a search of the extension of the system absorption range into the visible region, and the verification of the operating mechanism by injection of electrons from photo-excited dye molecules into the conduction band of the n-type semiconductor. Since only a monolayer of adsorbed dye molecules was photoactive, light absorption was low and limited when flat surfaces of the semiconductor electrode were employed. This inconvenience was solved by the introduction of polycrystalline TiO_2 (anatase) films with several hundreds of surface roughness factor [4, 5]. The use of mesoporous electrodes which provide a huge active surface area and the use of cells combining such as electrodes and a redox electrolyte based on iodide/triiodide couple could increase the amount of adsorbed dye even further by 7% conversion efficiencies [1]. The current highest energy conversion efficiency is over 11% [6], and further increase of the efficiency is possible by designing proper electrodes and sensitization dyes. Figure 1 shows both a scheme and an energy level diagram of a liquid electrolyte dye sensitized solar cell. The dye usually consists of one electrode made of a layer of a few micrometers of titanium dioxide nanocrystals (average crystal size around 20 nm), that have been sintered together to allow electronic conduction to take place. A monolayer of a sensitizer dye, typically a ruthenium polypyridyl complex, is attached to the surface of the nanocrystalline electrode. This mesoporous film is deposited onto a conductive, transparent substrate, typically indium tin oxide (ITO) or fluorinated SnO_2 (FTO), and soaked with a redox electrolyte, typically containing I^-/I_3^- ion pairs. This electrolyte is also in contact with a colloidal platinum catalyst coated counter-electrode. Sunlight is harvested by the dye producing photo-excited electrons that are injected into the conduction band of the nano-crystalline semiconductor network, and then into the conducting substrate. At the same time the redox electrolyte reduces the oxidized dye and transports the electron acceptors species (I_3^-) to the counter-electrode, where the I_3^- is

reduced back to I$^-$ and the electrical circuit is completed via electron migration through the external load.
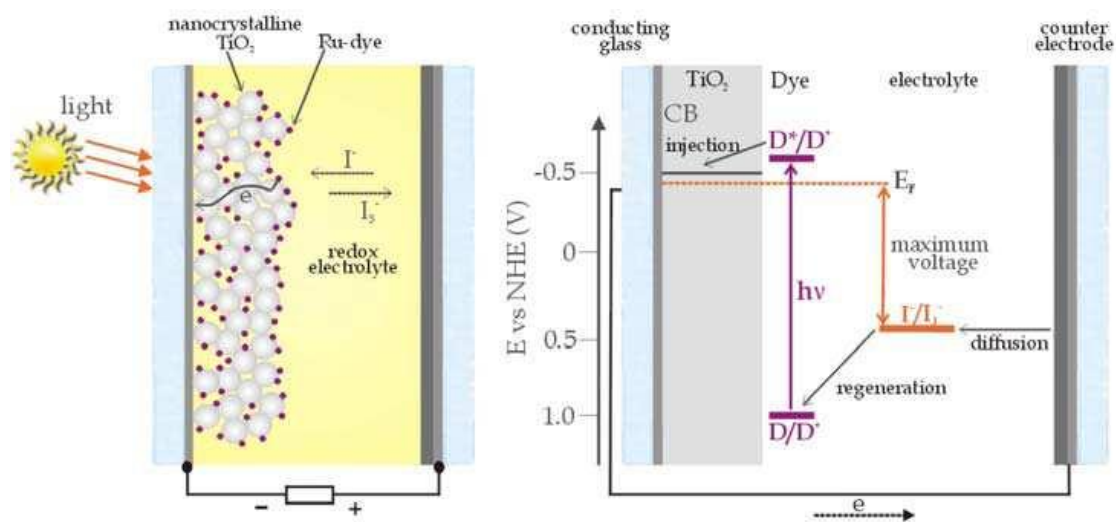
Figure 1-1 Cross section view of the design of a dye sensitized solar cell under illumination conditions (left), and energy levels of the different components of the cell that represent the energetics of operation of such devices (right).[6]Diagram is taken from a Book Chapter: Photon Management in Dye Sensitized Solar Cells by Silvia Colodrero page 415

In contrast to silicon devices, charge separation is primarily driven by the oxidation/reduction potentials of the different species at the TiO_2/dye/electrolyte interface, being produced electric field gradient in the TiO_2 electrode due to the high concentration of mobile ions employed in the liquid electrolyte.[8] Photo-induced charge separation takes place at the TiO_2/electrolyte interface. Thus, electron injection requires the dye excited state to be more reducing than the TiO_2 conduction band. In the same way, regeneration of the dye ground state by the redox couple requires the dye cation to be more oxidizing than the I^-/I_3^- redox couple.[9] The voltage output of the device is approximately given by the splitting between the TiO_2 Fermi level and the chemical potential of the redox electrolyte, being the former related with the density of injected electrons and the density of charge traps in the band gap of TiO_2. Under illumination conditions, the density of electrons injected into the semiconductor conduction band increases, raising the Fermi level towards the conduction-band edge and generating a photo-voltage in the external circuit. Charge transport processes within the cell are considered to be diffusive,[10-12] and are driven by concentration gradients generated in the device, thus making electrons to go towards the working electrode and triiodide ions towards the counter electrode. During the diffusion process, photo-generated electrons can recombine with acceptors species, such as dye

cations and triiodide ions. Another loss pathway includes decay of the dye excited state to ground [13]. Kinetic competitions between the different forward and loss pathways are therefore critical to determine the quantum efficiencies of charge separation and collection, and so the conversion efficiency. A diagram showing the kinetics of a DSSCs is presented in Figure 1-2. It should be noticed that not only energetics but also kinetics must be taken into account, and they constitute the key issues to achieve high energy conversion devices.
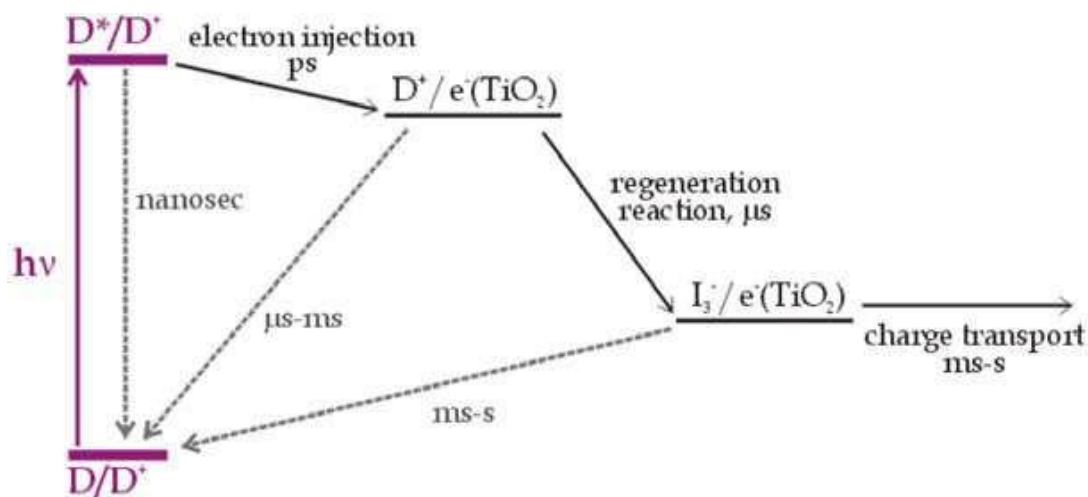
Figure 1-2 Kinetics and competitive processes involved in the conversion of light to electric power in DSSC.[12] Diagram is taken from a Book Chapter: Photon Management in Dye Sensitized Solar Cells by Silvia Colodrero page 416

1.3 Project aims

According to the prior studies in DSSCs and few information about where the iodine actually sit on the interfacial in DSSC, this research is going to contribute to investigate this issue particularly by using the surface sensitive technique. The primary aims of this research is to understand the dye adsorption process on the nanoparticle Titania layer in terms of the homogeneity and thickness of the dye layer and to investigate the distribution of the iodine components of the electrolyte near to the dye layer. These areas are major contributor to the overall efficiency and functionality of the cells. The focuses are distributed into four main research projects as the following.

The first study addresses the presence of iodine on the dye/titania interface in chapter 4 focuses on the in investigation of iodine across the dye/titania interface as the stability of unidirectional electron transport in DSSCs, is strongly influenced by the presence of I_3^- and I^- at the interface layer between the electrolyte and dye layer. This phenomenon is leading to the decrease of reintroducing dye, therefore decreasing the light conversion

efficiency of DSSCs. The titania/dye interface was studied using electron spectroscopy. The aim of this study is to investigate the presence of I_3^- and I^- into the dye layer and determine the iodine properties across the dye/titania interface. This research was using the N719 and Z907 ruthenium based dyes and NaI as source of the iodine component.

The second research addresses the modified L0 organic dye based on thiocyanate goup (L0Br) (chapter 5) and focuses on the investigation of its adsorption isothermal on the titania substrate using ion spectroscopy technique. From this research the concentration depth profiling of the dye molecule is obtained to reveal how the dye formation looks like when it sensitized on the titania.

The research working on the LEG1 and PD2 organic dyes (chapter 6) focuses on the effect of the aging and electrolyte exposing after the sensitized nanoporous anatase titania film applied in the real DSSC for hours. The technique used in this study is the electron spectroscopy techniques, because the ion spectroscopy technique was not able to be employed since the absence of heavier atom on the LEG1 and PD2 dye molecules.

The last research on this thesis is investigating the effect of Chenodeoxycholic acid as co-adsorbent to N719 dye sensitization on the titania substrate (chapter 7). It used the ion spectroscopy technique to observe the sensitized dye formation on the titania by determining the concentration depth profiling of the ruthenium on the titania obtained by deconvoluted the back scattered helium ion spectrum.

All dyes employed on the research in this thesis are synthesized on nanoporous anatase titania deposited on the Indium Thin Oxide (ITO) and Fluorine Thin Oxide (FTO) as the conductive layer.

References

1.   O'Regan, B. and M. Gratzel, A low-cost, high-efficiency solar cell based on dye-sensitized colloidal TiO2 films. Nature, 1991. **353**(6346): p. 737-740.

2.   Fujishima, A. and K. Honda, Electrochemical photolysis of water at a semiconductor electrode. Nature, 1972. **238**(5358): p. 37-8.

3.   Desilvestro, J., et al., Highly efficient sensitization of titanium dioxide. Journal of the American Chemical Society, 1985. **107**(10): p. 2988-2990.

4.   Vlachopoulos, N., et al., Very efficient visible light energy harvesting and conversion by spectral sensitization of high surface area polycrystalline titanium dioxide films. Journal of the American Chemical Society, 1988. **110**(4): p. 1216-1220.

5. Chiba, Y., et al., Conversion efficiency of 10.8% by a dye-sensitized solar cell using a TiO2 electrode with high haze. Applied Physics Letters, 2006. **88**(22): p. 223505.

6. Lozano, G., et al., Theoretical Analysis of the Performance of One-Dimensional Photonic Crystal-Based Dye-Sensitized Solar Cells. The Journal of Physical Chemistry C, 2010. **114**(8): p. 3681-3687.

7. Zaban, A., A. Meier, and B.A. Gregg, Electric Potential Distribution and Short-Range Screening in Nanoporous TiO2 Electrodes. The Journal of Physical Chemistry B, 1997. **101**(40): p. 7985-7990.

8. Nakade, S., et al., Dependence of TiO2 Nanoparticle Preparation Methods and Annealing Temperature on the Efficiency of Dye-Sensitized Solar Cells. The Journal of Physical Chemistry B, 2002. **106**(39): p. 10004-10010.

9. Soedergren, S., et al., Theoretical Models for the Action Spectrum and the Current-Voltage Characteristics of Microporous Semiconductor Films in Photoelectrochemical Cells. The Journal of Physical Chemistry, 1994. **98**(21): p. 5552-5556.

10. Cao, F., et al., Electron Transport in Porous Nanocrystalline TiO2 Photoelectrochemical Cells. The Journal of Physical Chemistry, 1996. **100**(42): p. 17021-17027.

11. Schwarzburg, K. and F. Willig, *Origin of Photovoltage and Photocurrent in the Nanoporous Dye-Sensitized Electrochemical Solar Cell.* The Journal of Physical Chemistry B, 1999. **103**(28): p. 5743-5746.

12. Huang, S.Y., et al., *Charge Recombination in Dye-Sensitized Nanocrystalline TiO2 Solar Cells.* The Journal of Physical Chemistry B, 1997. **101**(14): p. 2576-2582.

2 CHAPTER TWO: Dye Sensitized Solar Cells

In this chapter, the basic principle of Dye Sensitised Solar Cells (DSSCs) and its detail components are provided including the operational principle, working mechanism and kinetics, improvement of cell efficiency, and the main component on the DSSCs such as materials used in the cells.

2.1 Operation Principle of the Dye-Sensitized Nanocrystalline Solar Cells (DSSCs)

In a conventional p-n junction photovoltaic cell, the semiconductor assumes the functions of capturing sunlight to create an electron-hole pair and the transport of charge carriers simultaneously. On the other hand, in DSCs the dye is the element responsible for light absorption and charge generation, while charge transport occurs both in the semiconductor and in the electrolyte.[6]

In DSSCs, the semiconductor is a mesoporous oxide layer composed of nanometer-sized particles that have been sintered together to allow electronic conduction. This part is also named photo-anode or working anode. The material of choice has been TiO_2 (anatase) although alternative wide band gap oxides such as ZnO[7], and Nb_2O_5[8] have also been investigated. A monolayer of dye molecules (sensitizer) is loaded to the surface of the metal oxide, where excited electron is created when the dye is energised by solar radiation. Then the excited electron flows from the dye to the metal oxide surface upon light absorption, promoted into an excited state. As a result, electrons from the valence band (VB) are injected into the conduction band (CB) of the metal oxide semiconductor or charge separation, giving rise to formation of excited electrons and subsequent charge separation. The free electrons in the conduction band diffuse across the semiconductor toward the external circuit, performing electrical work. Once electrons reach the counter-electrode (CE), typically a thin layer of platinum, they react with the electrolyte that fills the space between the two electrodes, usually a solution of an ionic liquid solvent containing a triiodide/iodide redox system. The original state of the oxidized dye is subsequently restored by electron donation from the electrolyte, which is regenerated at the platinum counter electrode by reduction of triiodide.[6] DSSC The working mechanism of the dye-sensitized solar cell is summarized in Figure 2-1. Sunlight is absorbed by the dye, and the excited dye can inject an electron into the conduction band of TiO_2.
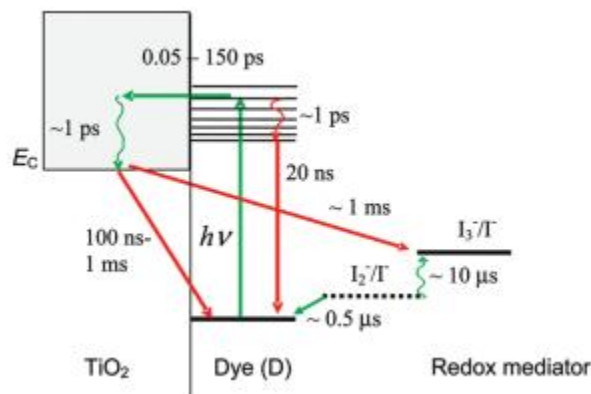
Figure 2-1 Kinetics of the cis-Ru(dcbpy)2(NCS)2-sensitized TiO2 solar cells with I^-/I_3^- redox mediator. Green arrows indicate typical time constants of the forward reactions and red arrows indicate recombination reactions. [1]

The time scale of this process is tens of femtoseconds to hundreds of picoseconds and depends on the electronic coupling and energetic overlap between donor and acceptor states.[9] The remaining oxidized dye is reduced by the iodide in the electrolyte. The half-time for regeneration of the most common sensitizer, cis-Ru(dcbpy)2(NCS)2, in the presence of about 0.5 M iodide is in the range of 100 ns to 10 µs, depending on the precise composition of the electrolyte.[10-14] The nature of the cation in the electrolyte plays a significant role. Pelet et al. observed faster dye regeneration when using electrolytes containing cations that adsorb at the TiO_2 surface. This was attributed to a higher local concentration of the iodide anion near the TiO_2/ electrolyte interface. Several studies report on the regeneration by iodide of other sensitizers, such as Ru and Os based complexes, metal-organic compounds such as phthalocyanines and porphyrins, and fully organic dyes.

2.2 Improvement of Eficiency of Dye-Sensitized Solar Cells

A number of researcher groups have been aiming to improve the DSSC performance in last two decades. They are modifying development in nano material level such as finding better configuration for each component and candidates for materials in DSSCs. Metal oxide semiconductor, sensitiser, electrolyte, and counter electrode are the important component DSSCs to capture the light and convert to electrical energy.

2.3 Main Component in DSSCs

There are couples of main components used in the DSSCs such as metal oxide as semiconductor, dyes as photo active material, electrolyte as hole transport medium, and

counter electrode where the electrolyte will collect the electrons after they are used in the external electric circuit.

2.3.1 Metal Oxide Semiconductor

Modification techniques to change the semiconductor profile in DSSC are still interesting research area recently. In a previous study it has been investigated that the performance of organized mesoporous TiO_2 films in dye sensitized solar cells is determined by structural parameters.[15] The TiO_2 films as photoanode materials for DSSCs consisted of up to 10 layers were crack-free, optically transparent, and had thicknesses exceeding 2 μm. The amount of adsorbed N3 or N719 dye was determined spectrophotometrically. The N3 sensitized electrode was dipped into 5.00 mL of 10×10^{-4} MNH4OH. The electrode sensitized with N719 was dipped into 3.00 mL of phosphate buffer (pH 7). The mixture was stirred, until complete desorption of the dye into the liquid took place. Thus resulting dye solution was analyzed by spectrophotometer. Those concentrations were determined by fresh standard solution, which were prepared by dissolving a known amount of crystalline dye in a respective solvent. The result showed that about one third of the ideal dye loading assumed for the (101) anatase face. In observation the thickness of mesoporous titania and the solar conversion allow conclusions to be drawn about the optimization of such mesoporous films for dye sensitized solar cells, which presents an interplay between the quality of anatase crystals and their surface area.[15]

Another metal oxide semiconductor in DSSCs is ZnO. Hundreds of experiments using ZnO layer as photoanode resulted a good performance in light conversion efficiency though they are still lower than TiO_2. There is a study investigated the use of dye N719 loaded to ZnO and they achieved 4.1% in light conversion efficiency.[16]

It is believed that there is a serious problem for dye loading of ZnO with Ru-complexes, such as N3 and N719. Because the dye-loading solution is relatively acidic due to protons derived from Ru-complexes and it will dissolve ZnO. As a result it is generating Zn^{2+}/dye aggregates. Such aggregates are harmful to the cells because they lower electron injection efficiencies and fill nano-scale pores of the ZnO photoanodes. The previous study has overcome this problem by adding base (KOH) to the dye-loading solution and shortening the loading time[17].

In order to understand the dye layer in DSSCs it is important to consider the mode of attachment to the Titania surface. Metal oxide surfaces like Titania are highly reactive and

it is very difficult to get an entirely exposed surface under vacuum, let alone in atmosphere. The photoactive dyes used in DSSCs and any contaminants are both adsorbed to the Titania nanoparticles. Adsorption is the term coined for molecules and atoms enter onto the substrate. Two types of adsorption are possible namely chemisorption and physisorption. Chemisorption is a stronger of the two, whereby adsorbates chemically bond to atom in the surface by covalent or ionic bonds- the sharing and exchange of electrons. Physisorption is a weaker bond, where the adsorbate is attracted to the surface via van der Waals forces and is often bound weakly enough that it is somewhat free to diffuse across the surface. The adsorption process can be complicated depending on surface morphology and the bonding possible however theoretical calculations are able to predict how adsorption will occur in simple systems. Often adsorption is a two-step process whereby an adsorbate atom or molecule contacts the surface with low enough kinetic energy that instead of being scattered away it can 'slide' across the surface in a physisorbed state until it reaches a favourable bonding site where chemisorption can take place.

Electron diffusion in metal oxide in DSSCs depends on the micro-profile of metal oxide and photoanode. Nakade[18] studied the difference in the diffusion coefficient of electrons between three different nano-porous TiO_2 films. The first two films was prepared via hydrolysis of Titanium tetra-isopropoxide in the presence of nitric acid, followed by autoclaving at 220^oC for 12 hours and hydrolysis of aqueous $TiCl_4$ solution followed by autoclaving at 220^oC for 13 hours respectively. The third film was commercially available TiO_2 (P25). Both experiments were studied with different annealing temperatures of the films. The films attached on an electrolyte containing $LiClO_4$ in methanol and irradiated by a pulsed laser (Quanta-Ray, Nd:YAG, 7ns, wavelength=355 nm). The result exhibited that nano-particles synthesized from hydrolysis of $TiCl_4$ showed a higher diffusion coefficient and the effect of Li^+ ion in an electrolyte on the diffusion coefficient revealed that larger concentration of Li^+ ion is required to exploit the faster electron diffusion.

2.3.2 Dye (sensitiser)

Many research groups have modified the dye used in DSCs and engaged in this research field more recently. For DSSCs, an ideal sensitizer should be able to absorb incident light of all wavelengths. The gap between the HOMO and LUMO levels in the dye molecule determine the wavelengths of light that are absorbed by these dyes and the LUMO level

matching to the conduction band of titania is a main factor in dye choice. Preferably, the energy level of the excited state corresponds to the conduction band of the semiconductor, and the ground state potential matches the redox level of the redox couple in the electrolyte, in order to avoid energetic losses during the processes of electron transfer and regeneration. (Figure 2-2) The dye is usually attaching to the surface of the nanostructured semiconductor (metal oxide) via its ligands, most often via carboxylate or phosphonate groups. A strong inter-linkage between the dye and the semiconductor requires that the dye should possess an anchoring group, which should react with surface hydroxyl groups of the semiconductor oxide to form chemical bonds. The standard anchoring group for sensitizers is carboxylic acid (-COOH) and its derivatives, such as ester, acid chloride, acetic anhydride, carboxylate salt, or amide, have also been used. By measuring the FT-IR to obtain vibrational data of dyes adsorbed on TiO_2 surfaces, we can determine the binding modes.[19] Many different photosensitizers including metal complexes, porphyrins, phthalocyanines and metal-free organic dyes have been designed and applied to DSCs in the past decades. The LUMO level matching to the conduction band of metal oxide can be adjusted through altering the ligand present, including isomerism of the traditional ligands.[20] Osmium complexes, organic dyes, ligand or functional group substitution and co-sensitization have all be implemented in attempts to increase the absorption spectrum and enable higher efficiency dyes.[20, 21]
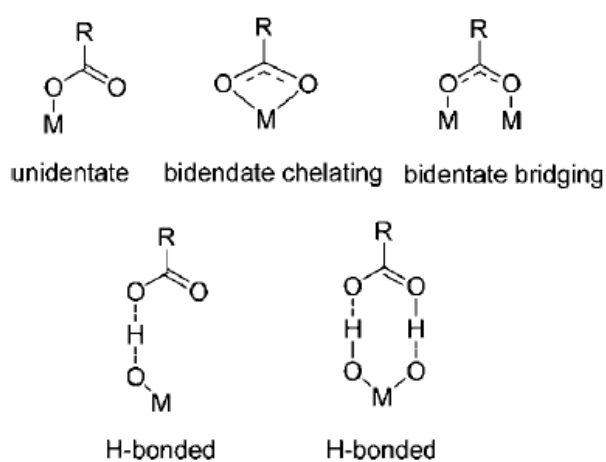
Figure 2-2 Binding modes for carboxylate unit on TiO_2 surface.[19]

Generally a measure of the chemical bond strength depends on the width of the energy band gap. TiO_2 is thus stable under illumination due to its wide band gap (3.2 eV), as a result it only absorbs the ultraviolet part of the solar spectrum while showing insensitivity to visible light. By sensitizing the semiconductor with a dye that absorbs visible light and

also transfers the charge carriers across the semiconductor-electrolyte junction, it increased the light-harvesting efficiency (Sommeling et al)[8]. Bignozzi et al[22] found that by coupling a sterically hindered dye with a mobile shuttle based on a transition metal complex allowed to reach a single device which 12% in efficiency.

Investigation of dye adsorbtion by Murakoshi and associates in 1995 measured the amount of dye desorbed via reflux with methanol to determine the coverage. An ideal flat surface coverage with monolayer ordering to be 1.3×10^{-10} mol.cm^{-1} was calculated.[23] This was not for the popular dyes N3 or N719, but rather for a similar dye : cisdi(thiocyanato)-N,N'-bis(2,2'-bipyridyl-4,4'-dicarboxylic acid)-ruthenium (II) dehydrate, (RuL2(NCS)2) 2H2O. They also did not clarify how they measured the surface area of their TiO2 films. A paper produced early by Marquet *et al* [24] described the adsorption isotherm of dye N719 using the adsorption depletion method with nanopartulate Titania. These results have recently been retaken using sintered mesoporous layers of nanoparticles and this study shown that the adsorption was overestimated and that in this case the adsorption was found to reach a constant coverage at a concentration of ca. 0.1 mmol/L.

2.3.3   Electrolyte

The electrolyte is one of key components for dye-sensitized solar cells and its properties have much effect on the conversion efficiency and stability of the solar cells. The research on the electrolyte has attracted much attention as the redox couple in electrolyte acting as electron donor is a key component on DSSCs. The electrolyte used in DSC is divided into three types: liquid electrolyte, quasi-solid, state electrolyte, and solid electrolyte. Liquid electrolyte could be divided into organic solvent electrolyte and ionic liquid electrolyte according to the solvent used.[21]

Regarding the electrolyte, the iodine/iodide redox couple has long dominated.[25] Although recent progress has been made on several other candidates, notably Co(III)/Co(II) and ferrocene/ferrocenium,[26-28] iodine/iodide still holds the certified records and best stability data. Li et al investigated the interaction of iodine with other components in the DSSC,[25] most notably the dye molecules.[29, 30] Iodine has been shown to bind to many organic donors, with a range of binding coefficients between single digits and 4 x 10^4.[31] Studies on the charge transfer complexes between iodine and electron donors containing sulphur atoms indicate that iodine binds to sulphur atom through its lone pair electron. Studies on the charge transfer complexes between iodine and electron donors containing sulphur

atoms indicate that iodine binds to sulphur atom through its lone pair electron.[32] Iodine binding to the thiocyanate anion has been measured in water and acetonitrile.[33, 34] The previous study has indicated that the interaction between iodine and dyes adsorbed on TiO$_2$ surface in dye-sensitised solar cells influences cell performance. The binding of iodine to dyes, such as phthalocyanines,[30] porphyrins[35] and ruthenium dyes,[29] has been suggested to increase recombination of conduction band electrons to the electrolyte. We now believe that this recombination proceeds by the reduction of iodine (as opposed to the reduction of I_3^-).[36] The studied has been studied by Richards et. all by investigating two aspects. Firstly, they need to determine the prominent pathway for electron transfer process from TiO2 to Iodine/iodide electrolytes. Secondly, they measured the electron lifetime while independently varying free iodine or triiodide (I^{3-}) concentration. They found that the lifetime is correlated with free-iodine concentration and independent of I3- concentration. The increase in recombination from dye–iodine binding could result from an increase the local iodine concentration near the TiO$_2$ surface. They have shown that adsorption of *p*-aminobenzoic acid on the TiO$_2$ surface decreases the recombination lifetime and the cell V_{oc}, likely due to iodine binding to the amine group.[37] Recently, the intermolecular interaction between organic dye molecules with thiophene ligands and iodine or triiodide, and its effect on recombination has been described.[38] Despite the rising interest in dye–iodine interactions, direct evidence for dye–iodine binding has not yet been published.

Gerrit Boschloo and Anders Hagfeldt[1] described that the redox couple also potentially affecting to the electrochemical potential of the TiO$_2$ electrode through the recombination kinetics between electrons in TiO$_2$ and oxidized redox species. It therefore appears that the iodide/triiodide couple will probably be unsurpassed as a redox mediator for dye sensitized solar cells. Figure 2-3(a) and 2-3(b) below show the relative electrochemical potential in redox couple system and the diagram of photo-voltage depends on redox couple respectively.
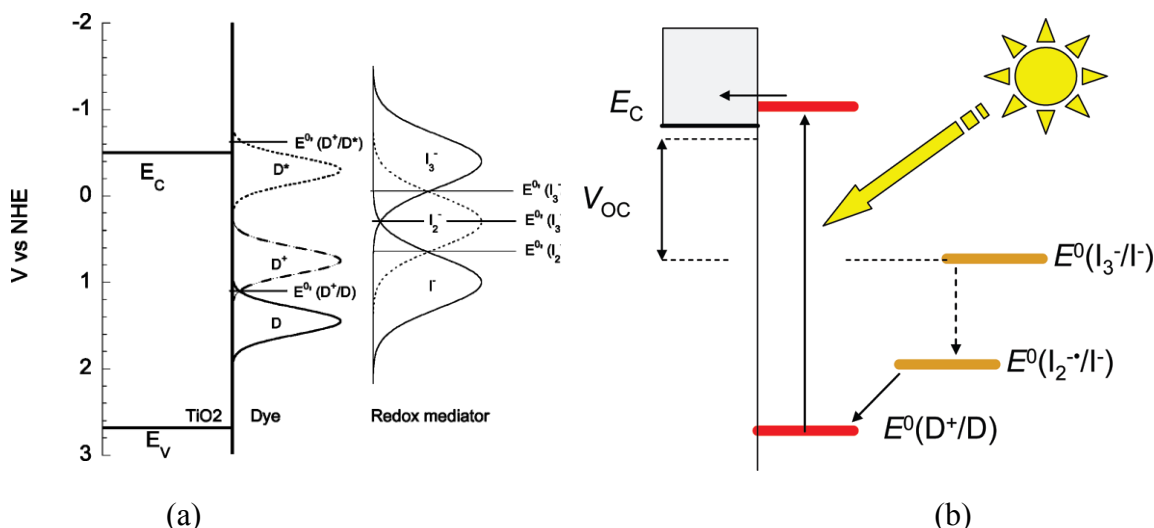
Figure 2-3 Redox reactions of the iodide-iodine system and their relative electrochemical potentials.[1]

The kinetics of recombination between electrons in the TiO_2 and triiodide in the electrolyte are extremely slow and favorable compared with most alternatives investigated to date. When the DSSCs is illuminated under open circuit conditions, the net rate of electron injection from dyes into the TiO_2 is balanced by the net rate of electron transfer from the electrode to the electrolyte. Because the V_{OC} depends on the electron concentration in the TiO_2, changes in V_{OC} can be related to the recombination process. In addition the regeneration of the oxidized dye is rapid, but this comes at the high cost of a potential loss of about 0.75 V. This potential lost is due to the unstable I_2^- radical, which is formed during dye regeneration, is converted to I_3^-. There is still limited room for improvement for DSSCs with I^-/I_3^- as the redox mediator.[1]

In terms of being the electron transport mediators, triiodide/iodide has been so far the most efficient and commonly used redox system. The reason is that I^- allows for a fast regeneration of the oxidized dye with small recombination losses. The electronic recapture involving I_3^- is kinetically so slow on both TiO_2 and SnO_2 surfaces, under short circuit conditions, most of electrons survive the transit through the mesoporous titania film and the SnO_2 surface and appear in the external circuit.[22] Recently, a number of different redox couples as candidates to replace traditional I^-/I_3^- system have been introduced into DSSCs. However, most of the metal-complexes-based redox couples still have drawbacks such as fast back electron recombination and slow diffusion constant. Such one-electron, outer-sphere redox couple often yield shorter electron lifetimes when used in the DSSCs. To contribute to the photocurrent the photo-injected electrons must diffuse through

hundreds of nanoparticles in close proximity to the oxidized redox species (electron acceptors) in solution and, in the absence of an electrostatic barrier, interfacial recombination may result as a major energy loss mechanism. Therefore, the overall efficiency of DSSCs is limited.[27]

Interfacial energetics and kinetics are far more important in DSSCs than in conventional solar cells. Gregg[39] stated that since the nanoporous metal oxide devices has a huge interfacial area, and electrolyte is able to penetrate throughout the bulk, it involves a number of unusual physical characteristics from dark currents cannot be compared to photocurrents quantitatively for longer time to the open circuit photovoltage is controlled by the photoinduced interfacial chemical potential gradient instead of the built-in equilibrium potential difference. The properties of surface states induced by UV illumination can lead the photoconversion process in contrast to their detrimental role in silicon crystalline cell. They revealed the result that recombination rates can be substantially decreased by modifying the semiconductor/electrolyte interface, rather than by optimizing bulk properties. Gregg et al also argued that surface states induced by UV illumination are able to increase the photo-conversion process in contrast to their destructive role in conventional cells based on silicon. Finally, he stated that by modifying the semiconductor/electrolyte interface the recombination rates can be substantially decreased, rather than by optimizing bulk properties.

There are number of results exhibit the performance of tri-iodide in some polymers. Durr et al have shown the behavior of tri-iodide ion in nanoporous TiO_2-polymer gel networks. They described that tri-iodide exhibits good diffusion properties in a polymer gel electrolyte consisting of Polyethylene Oxide (PEO) dissolved in a mixture of 1:1 Propylene Carbonate (PC) and ethylene carbonate (EC). They used the porous TiO_2 layer contains of particles with an average diameter of 20 nm and was sintered directly onto a platinum electrode at $450°C$. They also varied the thickness of the TiO2 layer between 2 and 12 μm by using different mesh sizes for the screen-printing process, whereas the layer thickness of the electrolyte bulk material was maintained constant by the use of a 6- μm-thick spacer foil. They used 15 mM of iodine and 0.15 M of iodide as a standard concentration in the resulting electrolyte. The porosity of the TiO_2 films they used were determined by means of nitrogen adsorption techniques.[40] They observed the characteristic of current density vs voltage taken at a sweep velocity of 50 mV/s using

initial iodine concentration in 15 mM. Then they investigated the concentration changes of iodide ion in this reaction:

$$I_2 + I^- \rightarrow I_3^- \tag{2.1}$$

Once the initial iodine (I_2) concentration is much lower, thus the reaction is almost completed and so the initial iodine concentration is equal to the tri-iodide (I_3^-) concentration.

Rowley and Meyer studied the reduction of I_2/I_3^- by Titanium dioxide.[41] They designed a photo-electrochemical cell that allowed iodide oxidation photoproduct to be generated proximate to TiO_2, similar to utilized in a DSSC. The photo-electrochemical cell was designed in the absence of molecular sensitizers. Nanosecond transient absorption studies of the mesoporous TiO_2 thin film under forward bias in 0.5 M TBAI/acetonitrile revealed that there was no evidence for a reaction between $TiO_2(e^-)$ and $I_2^{\bullet-}$, even with $I_2^{\bullet-}$ concentrations twice as large as those for I_3^-. They also found that the found that the I_3^- concentration decreased rapidly in the presence of $TiO_2(e^-)$, indicating that I_3^-, or $I_2^{\bullet-}$ which is in equilibrium with I_3^-, is the relevant electron acceptor.
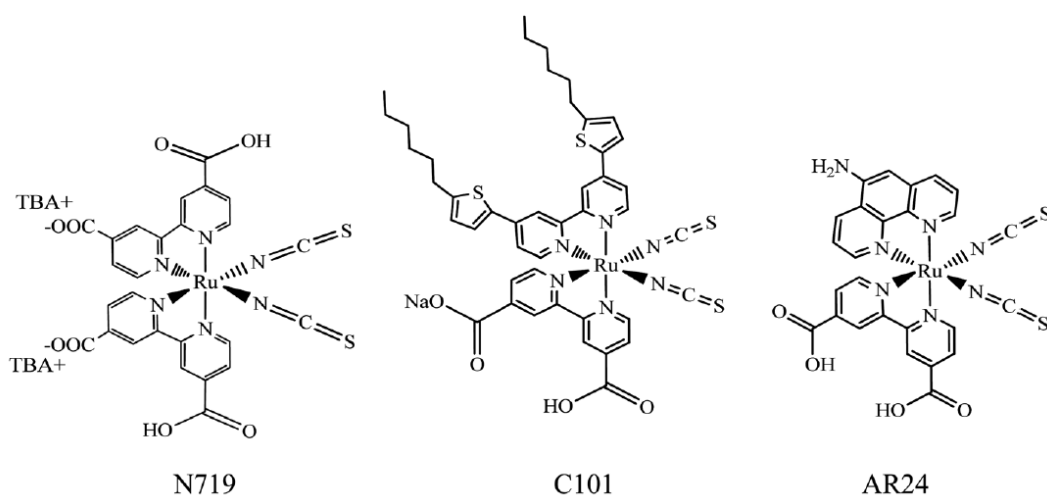
Figure 2-4 Chemical structures of N719, C101 and AR24

Previous study investigated the binding coefficients of iodine to three dyes used in Dye Sensitized Solar Cells (DSSCs).[25] The binding coefficients were quantified via the effect of iodine binding on the UV-vis spectrum of dye. Using iodine titration curves of dye sensitized TiO_2 films, they found that the binding coefficients of iodine to the three different dyes are in the range of 2000-4000 M^{-1}. They have measured the interaction between iodine and three ruthenium dyes, N719, C101 and AR24.19. Their molecular

structures are shown in Figure 2-4. Iodine could bind to these three dyes via various electron donor groups, such as thiocyanate, thiophene (in C101dye) and amine (in AR24 dye).

To quantify the binding strength they use changes in the dye absorption spectra with iodine binding. They use FTIR to identify the likely site of the binding. The binding constant for the dye–iodine complex was extracted from the FTIR spectra and by plotting the change in OD vs the iodine concentration and fitting with a Langmuir isotherm equation (2).[42]

$$\frac{\Gamma}{s_\Gamma} = \frac{K_f C}{1+K_f C} = \frac{C}{\left(C+\frac{1}{K_f}\right)} \tag{2.2}$$

In their work, they found the evidence of iodine binding to three dyes used in Dye Sensitised Solar Cells (DSSCs) via the sulphur and/or nitrogen atoms of dyes resulting in blue/red shifts in dye absorption spectra. These spectrum shifts can be related to the change of dyes orbitals' energy levels and the *Voc* loss in cells. The interaction between iodine and the NCS groups takes place through the sulphur atom, and in the case of AR24, it also takes place through the amino substituent. Figure 2-5 depicts the scheme of the interaction between N719 (left) and AR24 (right) and iodine. This additional interaction in the AR24 dye causes a seven-fold increase in the recombination rate, resulting in a decreased V_{QC} and efficiency of the cell.
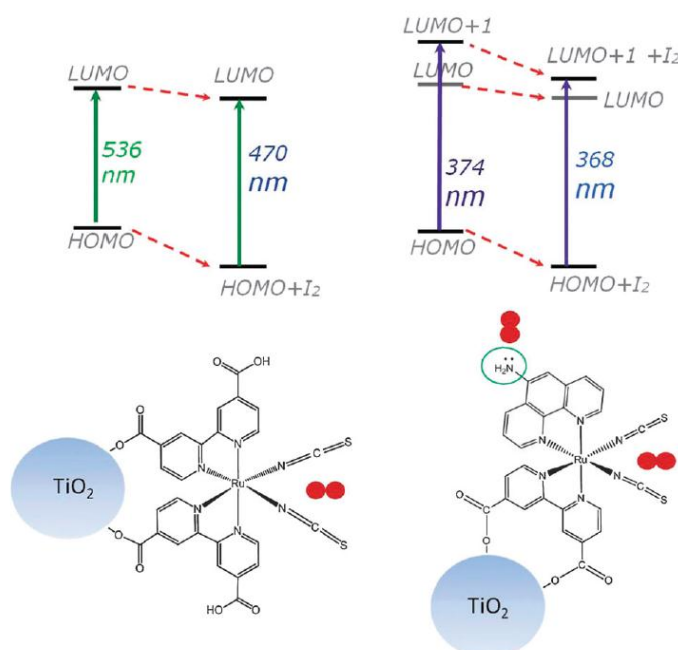
Figure 2-5 Scheme of the interaction between N719 (left) and AR24 (right) and iodine. [25]

Critical factors related to the electrolyte which are dominant in performance of DSSCs are the influence of electrolyte on the charge recombination and electron injection efficiency. Zhang et al[43] investigated the electron lifetime by Electrochemical Impedance Spectroscopy (EIS). This method assumes that electrochemistry cells responses are similar to the electronic circuit response such as resistor and capacitance circuit. Zhang et al argue that in electrochemical impedance spectroscopy (EIS), the potential applied to a system is perturbed by a small sine wave modulation and the resulting sinusoidal current response (amplitude and phase shift) is measured as a function of modulation frequency. The impedance is defined as the frequency domain ratio of the voltage to the current and is a complex number. For a resistor (R), the impedance is a real value, independent of modulation frequency, while capacitors (C) and inductors (L) yield imaginary impedance, whose value varies with frequency. The impedance spectrum of an actual system, that is, the impedance measured in a wide range of frequencies, can be described in terms of an equivalent circuit consisting of series and parallel connected elements R, C, L, and W, which is the Warburg element that describes diffusion processes. Electrochemical impedance spectra for the DSCs depicted that the addition of Methylbenzimidazole (MBI) in the electrolyte which is consist of LiI could enhance the electron lifetime and lower the rate constant (k_{et}) for I_3^- reduction with electrons in the TiO_2 metal oxide conduction band.

Rowley and Meyer made a photoelectrochemical cell to characterize interfacial electron transfer at potentiostatically controlled mesoporous nanocrystallyne (anatase) TiO_2 thin film electrodes.[44] They wanted to observe the reactivity of TiO_2 with di-and tri-iodide in acetonitrile solution. In their works, they stated that there was no direct evidence for a reaction between TiO_2 and di-iodide ($I_2^{\bullet-}$), even when the concentration of trapped electrons was increased with a forward bias. They also found that di-iodide is disproportionate to yield tri-iodide, I_3^- and iodide with a disproportionation rate constant in fluid acetonitrile solution, k=3×10^9 M^{-1}s^{-1}. However, they observed the spectroscopic evidence for a reaction between electron in TiO_2 and tri-iodide (I_3^-). Other group presented the adsorption of organic dyes on TiO_2 surfaces in dye-sensitised solar cells.[45] In their investigation, they proposed an integrated strategy which combines FT-IR measurements with DFT calculations to individuate the energetically favourable TiO_2 adsorption mode of acetic acid, as a meaningful model for realistic organic dyes. They presented that a bridged bidentate structure was found to closely match the FT-IR frequency pattern, and also being calculated as the most stable adsorption mode by calculations in solution. This adsorption

mode was found to be the most stable binding also for realistic organic dyes bearing cyanoacrylic anchoring groups. Then this group also investigated the adsorption mode and I_2 binding of prototype organic dyes. In the effect of the dye adsorption mode and the recombination with the electrolyte, despite the accepted knowledge that the adsorbed dyes act as an isolating layer, keeping the reduced electrolyte far from the direct contact with the oxide surface,[46-48] some authors [29, 49-52] suggested that particular atoms or chemical groups can also provide binding sites for I_2, increasing its concentration close to the TiO_2 surface and thus accelerating the recombination process. Evidence of stable Ru-complex–I_2 adducts has been reported by Tuikka et al.,[52] which isolated N_2-I_2 crystals. O'Regan et al.[29] found that the replacement of two oxygen ligand atoms with two sulfur atoms in a Ru(II)-dye caused a 2-fold increase in the recombination rate. This was ascribed to the stronger tendency of ethylthioether compared to ethylether to bind I_2. An extensive investigation on the effects of dye molecular structure and electrolyte composition on the recombination dynamics has been reported by Miyashita et al.,[49]

2.3.4   Counter Electrode

At the Counter Electrode the reduction of triiodide to iodide occurs. However, to ensure fast reaction kinetics and to provide the high activation energy of the two-electron transfer, a catalyst is needed. Platinum is traditionally used as the most efficient catalyst not only because it provides high exchange current densities, but also because it is transparent. A method for fabrication of highly transparent platinum counter electrodes (CEs) has been developed based on spray coating of Pt nanoparticles (NPs) on hot substrates. The Pt NP layer is over 88% transparent, leading to overall transparency of 80% when incorporated with indium tin oxide/glass substrates for functional counter electrodes. The counter electrode prepared by sputter deposition method is completely opaque while the Pt NP counter electrode appears highly transparent in the visible light spectrum.

Among other materials, carbon,[53] carbon black,[54] graphite,[55] activated carbon[56] or single-wall carbon nanotubes,[57] and conductive polymers[58] have been used as CEs in DSCs.

Electrochemical properties of counter electrode material are also very important. The properties of porous carbon black layer as an electron injector into iodide redox couple have been observed by Kim et al. According to the electrochemical impedance spectroscopy analysis and a new circuit model the electrochemical parameters are able to

be identified. The experimental result shows that the catalytic activity is improved while the Carbon Black (CB) particle size is decreased. The same phenomena arose when the CB electrode thickness increased therefore led to the low transfer resistance at the interface between electrolyte and counter electrode.[59]

Those are some details of theory and principle related to the achievement in DSSC including crucial parts such as photo anode, electrolyte, dye, and counter electrode. In this thesis, the main focus of the work is on the study of photo anode in particular the formation and morphology of the dye on TiO_2. Also the interaction between dye and the electrolyte or dye and titania has been investigated.

References

1. Boschloo, G. and A. Hagfeldt, *Characteristics of the Iodide/Triiodide Redox Mediator in Dye-Sensitized Solar Cells.* Accounts of Chemical Research, 2009. **42**(11): p. 1819-1826.

2. O'Regan, B. and M. Gratzel, A low-cost, high-efficiency solar cell based on dye-sensitized colloidal TiO2 films. Nature, 1991. **353**(6346): p. 737-740.

3. Fujishima, A. and K. Honda, *Electrochemical photolysis of water at a semiconductor electrode.* Nature, 1972. **238**(5358): p. 37-8.

4. Lozano, G., et al., Theoretical Analysis of the Performance of One-Dimensional Photonic Crystal-Based Dye-Sensitized Solar Cells. The Journal of Physical Chemistry C, 2010. **114**(8): p. 3681-3687.

5. Huang, S.Y., et al., *Charge Recombination in Dye-Sensitized Nanocrystalline TiO2 Solar Cells.* The Journal of Physical Chemistry B, 1997. **101**(14): p. 2576-2582.

6. Andrade, L., et al., Impedance characterization of dye-sensitized solar cells in a tandem arrangement for hydrogen production by water splitting. International Journal of Hydrogen Energy, 2010. **35**(17): p. 8876-8883.

7. Sayama, K., H. Sugihara, and H. Arakawa, *Photoelectrochemical Properties of a Porous Nb2O5 Electrode Sensitized by a Ruthenium Dye.* Chemistry of Materials, 1998. **10**(12): p. 3825-3832.

8. Sommeling, P.M., et al., *Long-term stability testing of dye-sensitized solar cells.* Journal of Photochemistry and Photobiology A: Chemistry, 2004. **164**(1–3): p. 137-144.

9. Haque, S.A., et al., Charge Separation versus Recombination in Dye-Sensitized Nanocrystalline Solar Cells: the Minimization of Kinetic Redundancy. Journal of the American Chemical Society, 2005. **127**(10): p. 3456-3462.

10. Haque, S.A., et al., Charge Recombination Kinetics in Dye-Sensitized Nanocrystalline Titanium Dioxide Films under Externally Applied Bias. The Journal of Physical Chemistry B, 1998. **102**(10): p. 1745-1749.

11. Pelet, S., J.-E. Moser, and M. Grätzel, Cooperative Effect of Adsorbed Cations and Iodide on the Interception of Back Electron Transfer in the Dye Sensitization of Nanocrystalline TiO2. The Journal of Physical Chemistry B, 2000. **104**(8): p. 1791-1795.

12. Clifford, J.N., et al., Dye Dependent Regeneration Dynamics in Dye Sensitized Nanocrystalline Solar Cells: Evidence for the Formation of a Ruthenium Bipyridyl Cation/Iodide Intermediate. The Journal of Physical Chemistry C, 2007. **111**(17): p. 6561-6567.

13. Montanari, I., J. Nelson, and J.R. Durrant, *Iodide Electron Transfer Kinetics in Dye-Sensitized Nanocrystalline TiO2 Films.* The Journal of Physical Chemistry B, 2002. **106**(47): p. 12203-12210.

14. Mori, S.N., et al., Investigation of the Effect of Alkyl Chain Length on Charge Transfer at TiO2/Dye/Electrolyte Interface. The Journal of Physical Chemistry C, 2007. **111**(8): p. 3522-3527.

15. Zukalová, M., et al., Structural parameters controlling the performance of organized mesoporous TiO2 films in dye sensitized solar cells. Inorganica Chimica Acta, 2008. **361**(3): p. 656-662.

16. Kakiuchi, K., E. Hosono, and S. Fujihara, *Enhanced photoelectrochemical performance of ZnO electrodes sensitized with N-719.* Journal of Photochemistry and Photobiology A: Chemistry, 2006. **179**(1–2): p. 81-86.

17. Keis, K., et al., Studies of the Adsorption Process of Ru Complexes in Nanoporous ZnO Electrodes. Langmuir, 2000. **16**(10): p. 4688-4694.

18. Nakade, S., et al., Electron transport in electrodes consisting of metal oxide nano-particles filled with electrolyte solution. Physica E: Low-dimensional Systems and Nanostructures, 2002. **14**(1–2): p. 210-214.

19. Hagfeldt, A., et al., *Dye-Sensitized Solar Cells.* Chemical Reviews, 2010. **110**(11): p. 6595-6663.

20. Robertson, N., *Optimizing Dyes for Dye-Sensitized Solar Cells.* Angewandte Chemie International Edition, 2006. **45**(15): p. 2338-2345.

21. Kong, F.-T., S.-Y. Dai, and K.-J. Wang, *Review of Recent Progress in Dye-Sensitized Solar Cells.* Advances in OptoElectronics, 2007. **2007**: p. 1-13.

22. Bignozzi, C.A., et al., *The role of transition metal complexes in dye sensitized solar devices.* Coordination Chemistry Reviews, 2013. **257**(9–10): p. 1472-1492.

23. Murakoshi, K., et al., Importance of binding states between photosensitizing molecules and the TiO2 surface for efficiency in a dye-sensitized solar cell. Journal of Electroanalytical Chemistry, 1995. **396**(1–2): p. 27-34.

24. Marquet, P., et al., Molecular Scale Characterization of the Titania−Dye−Solvent Interface in Dye-Sensitized Solar Cells. Langmuir, 2010. **26**(12): p. 9612-9616.

25. Li, X., et al., Measured binding coefficients for iodine and ruthenium dyes; implications for recombination in dye sensitised solar cells. Physical Chemistry Chemical Physics, 2012. **14**(44): p. 15421-15428.

26. Zhou, D., et al., Efficient organic dye-sensitized thin-film solar cells based on the tris(1,10-phenanthroline)cobalt(II/III) redox shuttle. Energy & Environmental Science, 2011. **4**(6): p. 2030-2034.

27. Yella, A., et al., Porphyrin-Sensitized Solar Cells with Cobalt (II/III)–Based Redox Electrolyte Exceed 12 Percent Efficiency. Science, 2011. **334**(6056): p. 629-634.

28. Daeneke, T., et al., High-efficiency dye-sensitized solar cells with ferrocene-based electrolytes. Nat Chem, 2011. **3**(3): p. 211-215.

29. O'Regan, B.C., et al., Structure/Function Relationships in Dyes for Solar Energy Conversion: A Two-Atom Change in Dye Structure and the Mechanism for Its Effect on Cell Voltage. Journal of the American Chemical Society, 2009. **131**(10): p. 3541-3548.

30. O'Regan, B.C., et al., Catalysis of Recombination and Its Limitation on Open Circuit Voltage for Dye Sensitized Photovoltaic Cells Using Phthalocyanine Dyes. Journal of the American Chemical Society, 2008. **130**(10): p. 2906-2907.

31. Rao, C.N.R., S.N. Bhat, and P.C. Dwedi, *Spectroscopy of Electron Donor-Acceptor Systems.* Applied Spectroscopy Reviews, 1972. **5**(1): p. 1-170.

32. auml, C. ther, and M. Bolte, Investigations on the Interaction Between sp2-Sulfur Atoms and Iodine Molecules Using the Cambridge Structural Database. Phosphorus, Sulfur, and Silicon and the Related Elements. **178**(3): p. 453-464.

33. Lewis, C. and D.A. Skoog, *Specrophotometric Study of a Thiocyanate Complex of Iodine.* Journal of the American Chemical Society, 1962. **84**(7): p. 1101-1106.

34. Ashour, S., Spectrophotometric microdetermination of thiocyanate and azide anions in acetonitrile using iodine. Journal of Analytical Chemistry, 1999. **54**(6): p. 538-542.

35. Splan, K.E., A.M. Massari, and J.T. Hupp, *A Porous Multilayer Dye-Based Photoelectrochemical Cell That Unexpectedly Runs in Reverse.* The Journal of Physical Chemistry B, 2004. **108**(13): p. 4111-4115.

36. Richards, C.E., et al., The Mechanism of Iodine Reduction by TiO2 Electrons and the Kinetics of Recombination in Dye Sensitized Solar Cells. The Journal of Physical Chemistry Letters, 2012. **3**(15): p. 1980–1984.

37. O'Regan, B.C. and J.R. Durrant, Kinetic and Energetic Paradigms for Dye-Sensitized Solar Cells: Moving from the Ideal to the Real. Accounts of Chemical Research, 2009. **42**(11): p. 1799-1808.

38. Zhang, M., et al., Redox couple related influences of [small pi]-conjugation extension in organic dye-sensitized mesoscopic solar cells. Chemical Science, 2011. **2**(7): p. 1401-1406.

39. Gregg, B.A., *Interfacial processes in the dye-sensitized solar cell.* Coordination Chemistry Reviews, 2004. **248**(13–14): p. 1215-1224.

40. Durr, M., et al., Diffusion-limited transport of I[sub 3][sup -] through nanoporous TiO[sub 2]-polymer gel networks. The Journal of Chemical Physics, 2004. **121**(22): p. 11374-11378.

41. Rowley, J. and G.J. Meyer, *Reduction of I2/I3− by Titanium Dioxide.* The Journal of Physical Chemistry C, 2009. **113**(43): p. 18444-18447.

42. Atkins, P. and J. Paula, *Physical Chemistry.* 2002. **7th edn**.

43. Zhang, C., et al., *Electrolyte effects on photoelectron injection and recombination dynamics in dye-sensitized solar cells.* Journal of Photochemistry and Photobiology A: Chemistry, 2010. **213**(2–3): p. 87-92.

44. Rowley, J.G. and G.J. Meyer, *Di- and Tri-iodide Reactivity at Illuminated Titanium Dioxide Interfaces.* The Journal of Physical Chemistry C, 2011. **115**(13): p. 6156-6161.

45. Anselmi, C., et al., Adsorption of organic dyes on TiO2 surfaces in dye-sensitized solar cells: interplay of theory and experiment. Physical Chemistry Chemical Physics, 2012. **14**(46): p. 15963-15974.

46. Koumura, N., et al., *Alkyl-Functionalized Organic Dyes for Efficient Molecular Photovoltaics.* Journal of the American Chemical Society, 2006. **128**(44): p. 14256-14257.

47. Ito, S., et al., High-conversion-efficiency organic dye-sensitized solar cells with a novel indoline dye. Chemical Communications, 2008(41): p. 5194-5196.

48. Burke, A., et al., The Function of a TiO2 Compact Layer in Dye-Sensitized Solar Cells Incorporating "Planar" Organic Dyes. Nano Letters, 2008. **8**(4): p. 977-981.

49. Miyashita, M., et al., Interfacial Electron-Transfer Kinetics in Metal-Free Organic Dye-Sensitized Solar Cells: Combined Effects of Molecular Structure of Dyes and Electrolytes. Journal of the American Chemical Society, 2008. **130**(52): p. 17874-17881.

50. Planells, M., et al., Energy levels, charge injection, charge recombination and dye regeneration dynamics for donor-acceptor [small pi]-conjugated organic dyes in mesoscopic TiO2 sensitized solar cells. Energy & Environmental Science, 2011. **4**(5): p. 1820-1829.

51. Bai, Y., et al., Engineering Organic Sensitizers for Iodine-Free Dye-Sensitized Solar Cells: Red-Shifted Current Response Concomitant with Attenuated Charge Recombination. Journal of the American Chemical Society, 2011. **133**(30): p. 11442-11445.

52. Tuikka, M., et al., Halogen bonding-a key step in charge recombination of the dye-sensitized solar cell. Chemical Communications, 2011. **47**(15): p. 4499-4501.

53. Kitamura, T., et al., Improved Solid-State Dye Solar Cells with Polypyrrole using a Carbon-Based Counter Electrode. Chemistry Letters, 2001. **30**(10): p. 1054-1055.

54. Murakami, T.N. and M. Grätzel, *Counter electrodes for DSC: Application of functional materials as catalysts.* Inorganica Chimica Acta, 2008. **361**(3): p. 572-580.

55. Kay, A. and M. Grätzel, Low cost photovoltaic modules based on dye sensitized nanocrystalline titanium dioxide and carbon powder. Solar Energy Materials and Solar Cells, 1996. **44**(1): p. 99-117.

56. Imoto, K., et al., *High-performance carbon counter electrode for dye-sensitized solar cells.* Solar Energy Materials and Solar Cells, 2003. **79**(4): p. 459-469.

57. Suzuki, K., et al., Application of Carbon Nanotubes to Counter Electrodes of Dye-sensitized Solar Cells. Chemistry Letters, 2003. **32**(1): p. 28-29.

58. Tennakone, K., et al., An efficient dye-sensitized photoelectrochemical solar cell made from oxides of tin and zinc. Chemical Communications, 1999. **0**(1): p. 15-16.

59. Kim, J.-M. and S.-W. Rhee, Electrochemical properties of porous carbon black layer as an electron injector into iodide redox couple. Electrochimica Acta, 2012. **83**(0): p. 264-270.

3 CHAPTER THREE: Methods and Techniques

In this chapter, the detail of the experimental techniques and also the materials used in this thesis is provided.

3.1 Experimental Methods

Generally the techniques used in this research employed on the electron and ion spectroscopy. They were applied to investigate the dye surface and the dye/titania interface. X-ray Photo-electron Emission Spectroscopy (XPS), also known as Electron Spectroscopy for Chemical Analysis (ESCA), is a widely used technique to investigate the chemical composition of surfaces. Ultra-violet Photoelectron Spectroscopy (UPS) and Metastable Induced Electron Spectroscopy (MIES) were carried out to measure electronic structure of material and determine the molecular orientation on the top most atomic layer and also the density of state (DOS) as MIES is the most surface sensitive capable to do surface analysis. The more detail about electron spectroscopy techniques is described below.

3.2 Surface Analysis using Electron and Ion Spectroscopy

In this section, it will be described the surface analysis techniques based on electron and ion spectroscopy used in this thesis. They are XPS, UPS, and MIES for electron spectroscopy and NICISS for ion spectroscopy. In general, the differences among them are classified from their sensitivity in term of how much energy they have available to transfer for the emission of electrons from the sample or material. The higher energy they have the easier for the electrons to be emitted from the sample or material. For ion spectroscopy, it uses projectile from a rare gas to interact with the sample.

3.2.1 Photoelectron Spectroscopy (PES)

PES is a surface analysis technique that has been in use since the middle of last century and takes advantage of the photoelectric effect. The photoelectric effect, observed in 1887 by Heinrich Hertz and explained in 1905 by Albert Einstein, describes the ejection of an electron (also termed photoelectron) from an atom upon absorption of a photon of appropriate energy. Photoelectron spectroscopy techniques used in this thesis are XPS and UPS which was carried out in low pressure chamber. This low pressure related to the condition of the emitted electrons not losing their kinetic energy when they travel from the sample to the detector. It is called inelastic mean free path indicating how far

an electron on average travels through a solid before losing energy. It is usually such that we see 3 lambda of the sample.[1] However, it is important to notify that the contribution of electron emission decreases with depth and the estimation of the information depth as 3 lamda is a rough approximation used as a guideline for the depth range of XPS.

The kinetic energy of the photoelectron after it has been emitted from an electron orbital indicates the energy of the state it resided in and can be calculated using the photoelectric equation below (Equation 3.1). The surface sensitivity of UPS and indeed any photoelectron spectroscopy stems from the mean free path of electrons in solids and liquids. This is the distance that an electron that has been liberated from its orbital or energy level can travel before it is attenuated by collisions with a few nm which depends upon the energy of the electron and the material. The plot of the inelastic mean free path (IMFP) for the electron is shown in Figure 3-1 below.
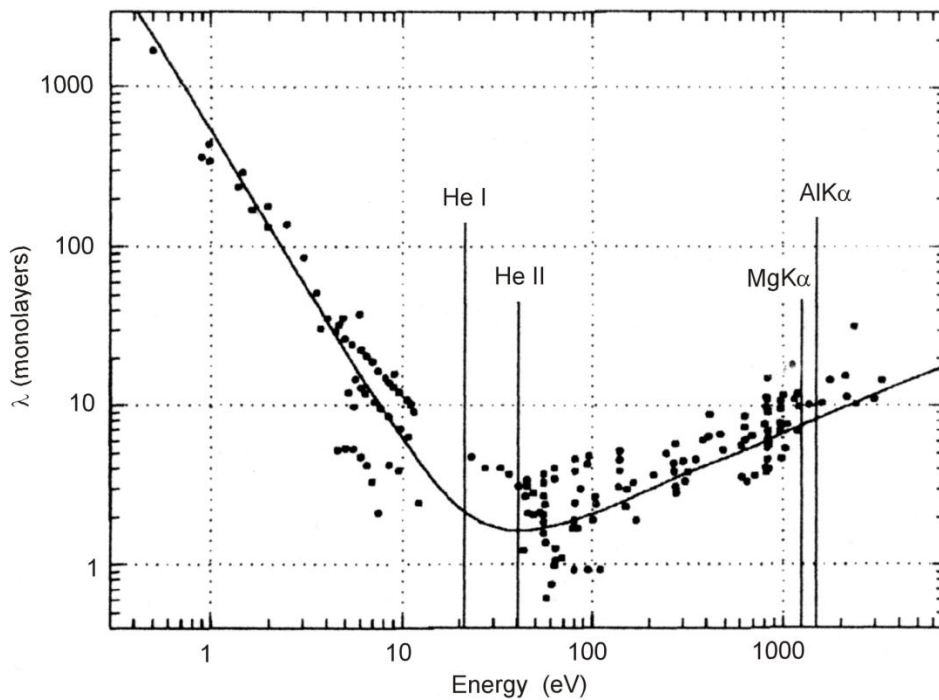
Figure 3-1. Plot of the inelastic mean free path of the electron

$$E_k = E_p - (E_B + \phi) \tag{3.1}$$

E_k =kinetic energy of photoelectron

E_p = energy of incident photon

E_B =binding energy of photoelectron

ϕ =work function of spectrometer

3.2.1.1 X-ray Photoelectron Spectroscopy (XPS)

XPS is one of the electron emission spectroscopic techniques, which employs X-ray to emit electrons from the sample surface. XPS uses X-ray photons to ionise electrons from the surface via the photoelectric effect. The X-ray is shown to the surface and its x-ray photon energy will be absorbed then the electron will be emitted from the surface and collected on the energy analyser. Since X-rays have a high frequency and therefore high energy, X-rays are able to ionise the more tightly bound electrons found in the core of the atoms in the surface. Each of electron energy corresponds to a unique element, thus the component of the sample could be assigned thoroughly. This XPS technique is used to investigate the electrons in the core energy level and it is able to ascertain the chemical composition, electronic state, and binding energies of the sample.

The Kinetic Energy is detected and using Equation 3.1 and the binding energy of the electrons is determined. Core electrons, even when present in lattices, are still confined to individual atoms and as such their binding energy is only affected in a small part by their environment. For this reason XPS is capable of identifying surface elements easily and relating slight shifts in energy and peak areas to environment and relative concentrations respectively and these are the primary uses of this technique.

In this work a Phoibos HSA100 as a hemi-spherical electron energy analyser and a retractable SPECS XR-50 dual X-ray anode which produces Mg or Al X-rays was used. For this project the Mg anode was used at a voltage of 12 kV and power output of 100W. Mg X-ray has photon energy of 1253.6 eV and the binding energy scale is determined using Equation 3.1. Each spectrum was calibrated to the C 1s spectral line at 284.8 eV.

Angle Resolve X-ray Photoelectron Spectroscopy (ARXPS) is a modified XPS technique just by varying the X-ray incident angle. By doing this, the depth of X-ray could be varied so the origin of emitted electron could be changing as a function of the X-ray incident angle. In this study, the ARXPS was also employed to investigate the dye surface properties semi quantitatively.

3.2.1.2 Ultraviolet Photoelectron Spectroscopy (UPS)

UPS was developed in 1962 when David Turner first published ionisation potentials of noble and organic gases using a He discharge lamp. Ultraviolet photons will eject electrons from the Valence electron energies in atoms and solids, which are present in molecular orbitals and bonding states. Since the Photon Energy and spectrometer work

function for UPS instruments are known, by detecting the electrons emitted for valence band of the sample with certain Kinetic Energies and using Equation 3.1, the work function of the valence bands at surfaces is determined In this way UPS is surface sensitive to the first 10nm of a substrate making it ideal for investigating components of interfaces and surfaces.

UPS is similar to the XPS but the excitation source used in the UPS is a helium discharge source. Depending on the operating conditions of the source the photon energy can be optimized for He I = 21.22eV or He II = 44.8eV which is significantly lower energy than what the XPS used. In consequence, this lower photon energy is that only the low binding energy valence electrons may be excited using the He source. The valence stages are responsible for crystal/molecular bonding and charge transfer. A further consequence of the low photon energy is that the UPS is becoming more surface sensitive than XPS and thus very sensitive to surface contamination as well. UPS is very useful as a technique to determine the work function or electronic structure of the material being analysed.

3.2.2 Metastable Induced Electron Spectroscopy (MIES)

MIES is not one of the photoelectron spectroscopy technique because it uses ionised helium gas atom to interact with the top most atom on the sample. MIES is more surface-sensitive technique using He I lines. It is able to investigate just a few angstroms below the surface. MIES is a method to determine quantitatively the composition and electronic structure of the outermost layer of a sample. Its surface sensitivity is caused because of the object carrying the energy used to excite the target electrons cannot penetrate through the material in its excited state. The metastable atom releases its energy to the surface at a distance of a few Å below the surface. Thus in a MIES experiment, the surface sensitivity does not originate from the mean free path of the emitted electrons but from the fact that only electrons in the outermost layer can be excited. Therefore, MIES probes the composition of that region which is important for interactions and reactions at surfaces or interfaces. MIES spectra are evaluated quantitatively and directly reveal the density of states (DOS) of the valence electrons. The MIES spectrum and its molecular orientation are shown in Figure 3-2.
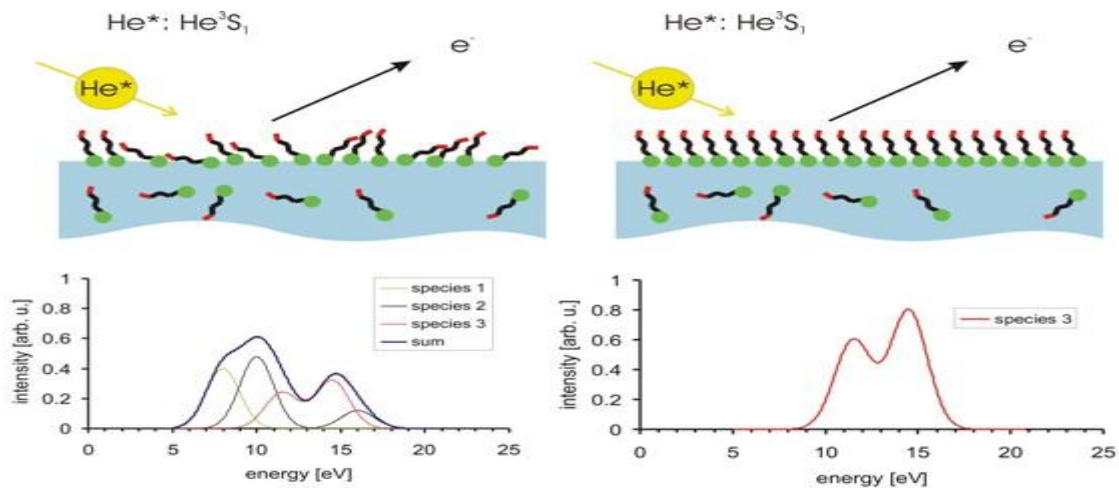
Figure 3-2. The MIES technique and the spectrum associated with the surface

A MIES provides much of the same information that UPS does, in that it indicates the density of states of the valence bands, however this technique is completely surface sensitive. This is due to the metastable Helium atoms used to ionise the surface electrons. MIES and UPS as the information gained from this technique largely contribute to the electronic structure and the configuration of the top most atoms on the surface.

Metastable Induced Electron Spectroscopy (MIES) is a technique whereby an atom (usually Helium) in a metastable state is directed to a surface. In the case of Helium, the atoms are excited to the 2S which has a lifetime of ~4000s and energy of 19.82eV.

The 2s ➞1s transition is dipole forbidden ($\Delta l = \pm 1$ for dipole allowed transitions, yet the 2s ➞1s has $\Delta l=0$) and so the excited atom (He*) can decay more easily via other pathways provided by the surface it impacts with, which result in information about the valence electron levels present in the surface.

Electron emission of the metastable He* upon approaching within angstroms of the surface occurs in a number of ways and the specific process is governed by the surface constituents. For metals with work functions above ~3.5 eV the process is resonant ionization of the excited electron into the surface valence band followed by Auger neutralization. The spectrum in these cases represents a convolution of the density of electron energy states in the first surface layer. For surfaces with low work functions there is no resonance with the He 2s state and the surface so the He* undergoes Auger de-excitation with the spectra representing the valence band density of states. The Auger neutralization process involves the surface donating an electron to the 1s hole in the He^{+} ion from the valence band. However this electron donation leaves the atom in the surface

with too much energy, so another valence band electron is ionized. This final emitted electron is collected and analyzed. Auger de-excitation involves a surface electron tunneling into the 1s hole in the He* after which the metastable electron in the 2s state is ionized with the remaining energy from the surface. MIES is an ultrahigh vacuum technique (UHV, 10^{-10} mbar) which can look at both dry and liquid samples. It is one of the only techniques capable of liquid surface analysis under vacuum, and most MIES systems are capable of UPS and XPS in conjunction with MIES. Schematic for a MIES apparatus is shown in Figure 3-3.

An advantage of the MIES technique is that it is completely surface sensitive due to the large cross section for the de-excitation of the He* atom. The metastable atom does not penetrate into the bulk and therefore only the surface properties are revealed. This is especially important when investigating the surface structure of interfaces.
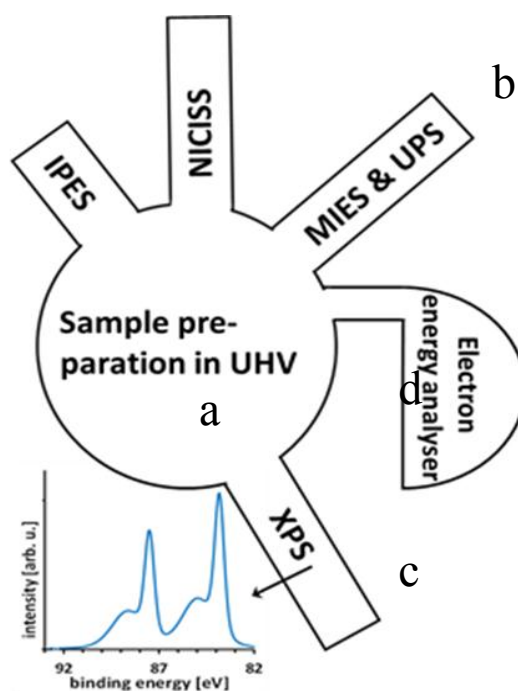
Figure 3-3. The XPS/UPS/MIES apparatus: Ultra High Vacuum chamber (a) MIES and UPS source (b) X-ray source (c) concentric hemispherical energy analyzer (d).

3.2.3 Neutral Impact Collision Ion Scattering Spectroscopy (NICISS) and Concentration Depth Profiles

In principle, NICISS experiment is very similar with rutherford back scattering (RBS) experiment. The difference is just in the energy. NICISS is a surface sensitive technique

capable for determining the concentration depth profiles of the elements and has been employed extensively for soft matter surfaces up to a depth of about 20 nm and with a depth resolution of a few angstroms in the near-surface area.[2] This ion spectroscopic technique utilises an ionised rare gas atoms (usually Helium) as projectiles as just several keV and detects backscattered neutral helium atoms.[3] Its kinetic energy is between 3 keV (2860 eV used here) collides with the surface and is backscattered from the sample as a neutral atom at a scattering angle close to 180°. In the present case the scattering angle is 164°). With its kinetic energy, the projectiles can be backscattered from a depth of up to 30 nm or it will probe just around 300 Å below the surface.[3, 4] The energy loss during the scattering process leads to the velocity of the backscattered helium projectile. The method is applied at high vacuum (~10^{-5}Torr) or lower pressure.

The projectile is used to bombard the sample and the back scattered projectiles neutralised by the target atoms is captured by a time of flight (TOF) detector. By knowing the time of flight of each helium trajectory from the target to the detector, the energy of each projectile can be employed to trace back the position of the target atom.

There are two components of this energy loss, the largest being the backscattering process where conservation of momentum is responsible for the resulting velocity of the projectile (the neutralisation process involved in backscattering plays a smaller role). This collision is largely elastic and as such the velocity of the backscattered He atom is strongly dependent upon the mass of the target atom. The second component of the energy loss for projectiles is found in the small angle scattering undergone within the sample. This small angle scattering occurs both prior to and post backscattering and relates the depth of the target atom in the surface to the final energy of the backscattered He.

The projectiles lose energy during the backscattering process, and the energy transfer depends on the mass of the target atom. There are two energy losses upon the projectiles in NICISS. The largest being the backscattering process where conservation of momentum is responsible for the resulting velocity of the projectile (the neutralisation process involved in backscattering plays a smaller role). These energy losses obtained when the projectiles lose energy during the backscattering process when they interact with the target atoms. The energy transfer from the projectile to the target relates to the mass of the target atom. In principle, the first type of energy loss can be used to identify the element from which depth a projectile is backscattered. Additionally, the projectiles continuously lose energy on their trajectory through the bulk due to small angle scattering from and electronic

excitations of the molecules constituting the target. This energy loss, known as stopping power, is used to determine the depth of the atom from which the projectile is backscattered. By combining the two loses, the concentration depth profile of the sample will be known. The scheme of NICISS principle is shown in Figure 3-4.

A typical NICISS spectrum consists of energy loss spectra for each element constituting the sample. The shape of the spectrum measured of a single element is determined by its concentration depth profile in the sample. The depth resolution of NICIS spectra are mainly influenced by small angle scattering of the projectile. The small angle scattering depends on the trajectory of the projectiles within the sample. The magnitude of the small angle scattering increases with increasing length of the trajectory. Small angle scattering of the projectile is least in the top several Å of the surface, leading to a depth resolution of only a few Å.
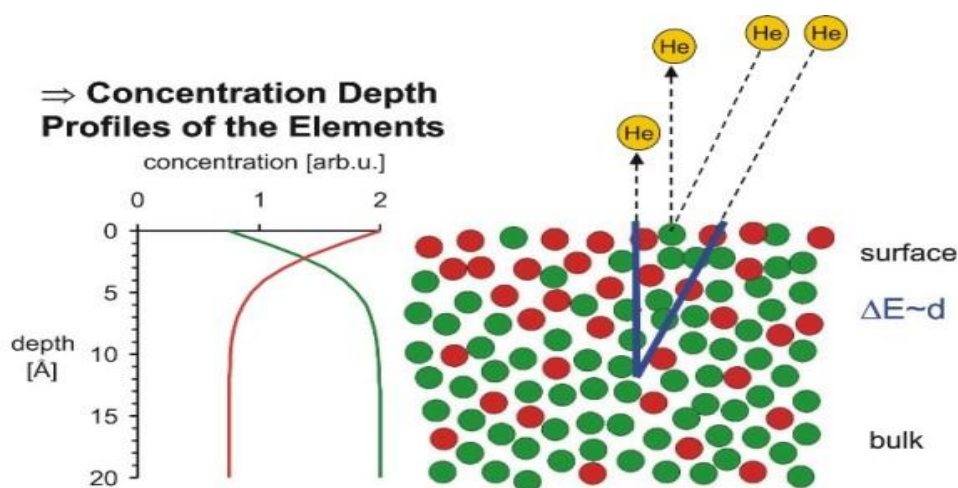
Figure 3-4. The schematic of NICISS principle

The spectra are also influenced by the distribution of inelastic energy losses during the backscattering process and the straggling of the energy loss caused by low angle scattering and electronic excitations [5]. The inelastic energy loss during the backscattering process can be determined from the NICIS spectra of the respective elements in the gas phase. The energy loss straggling of low energy projectiles has been determined experimentally.[6]

The inelastic energy loss during backscattering and the energy loss straggling of projectiles in the bulk is known experimentally, and thus it is possible to deconvolute the measured profiles to obtain more details of the concentration depth profiles. The deconvolution is performed with a program based on the genetic algorithm[3]. In the

genetic algorithm the result of the deconvolution is independent of the starting conditions of the program and that the statistical error of all suitable solution can be used to determine the error bars of the deconvoluted profile. In order to determine the energy of a projectile backscattered from an element in the outermost layer of the sample, NICIS spectra of the elements in a low density gas jet are employed[3].

The following Time of Flight (TOF) of the He atom to the detector is recorded and this relates primarily to the element He backscattered from and secondarily to the depth into the surface the target atom resided, showing the prevalence of different elements at depths within the sample (concentration depth profiles). The equations shown below give the conversion between the time of flight spectra and the energy of the projectile (Equation 3.2) and the energy loss associated with the scattering process to the mass of the target atom (Equation 3.3).

The last equation (Equation 3.4) converts the energy lost to the depth profiles.

$$I_i(E) = I_i(t) \frac{\Delta t}{\Delta E} \frac{1}{d\sigma/d\Omega(E)} \frac{1}{\det(E)} \tag{3.2}$$

However in this term $\left(\frac{\partial E}{\partial t}\right)_0 \left(\frac{\partial \delta}{\partial \omega}\right)_0$

These values are standard values which can be anything. Then we always use a normalisation factor for the absolute concentration.

$$E_{final} = E_0 \frac{\left(\cos\theta + \left(A^2 - (\sin\theta)^2\right)^{1/2}\right)^2}{(1+A)^2} - Q_{initial} \tag{3.3}$$

$$I(d) = I(E) \frac{dE}{dz} f \tag{3.4}$$

Where E = Energy of projectile

$I_i(E)$ = the energy loss spectrum

$I_i(t)$ = contribution of the element I in the TOF spectrum

t = time of flight

$\frac{d\sigma}{d\Omega}$ = the differential impact cross section of target elements for projectiles

θ = detector angle $\sim 164^0$

$$A = \frac{m_{\text{target element}}}{m_{\text{projectile}}}$$

Q_{in} = Inelastic energy loss during backscattering

$I(d)$ = depth profile

z = depth

f =factor relating the concentration to the yield of backscattered projectiles

Equations for determining the energy of scattering processes are found by first looking at the conservation of momentum which leads to the main term in Equation 3.3. Inelastic energy loss of the back scattering process adds a term Q initial to the final energy in Equation 3.3. The energy loss attributed to small angle scattering is known as the nuclear stopping power and can be treated as continuous and related to the depth. There is also energy lost in excitation of electrons, known as electronic stopping power, however at low projectile energy the nuclear stopping power is dominant over the electronic stopping power.

The NICISS technique is similar to Rutherford Backscattering (RBS), although RBS is 3 orders of magnitude more energetic and has a lower depth resolution[7]. RBS is a depth profiling technique with a standard resolution of ~ 100 Å. NICISS however has a minimum feature resolution of ~ 2 Å near the surface.

A NICISS apparatus consists of a vacuum chamber, ion source, time of flight (TOF) detector and an electrostatic deflection unit. A schematic of the apparatus is shown below in Figure 3-5. Helium is commonly used as the scattering ion as it is light enough to detect the lighter elements such as Carbon, Nitrogen and Oxygen. The use of Helium also reduces the sputtering of Hydrogen over the use of heavier projectiles.
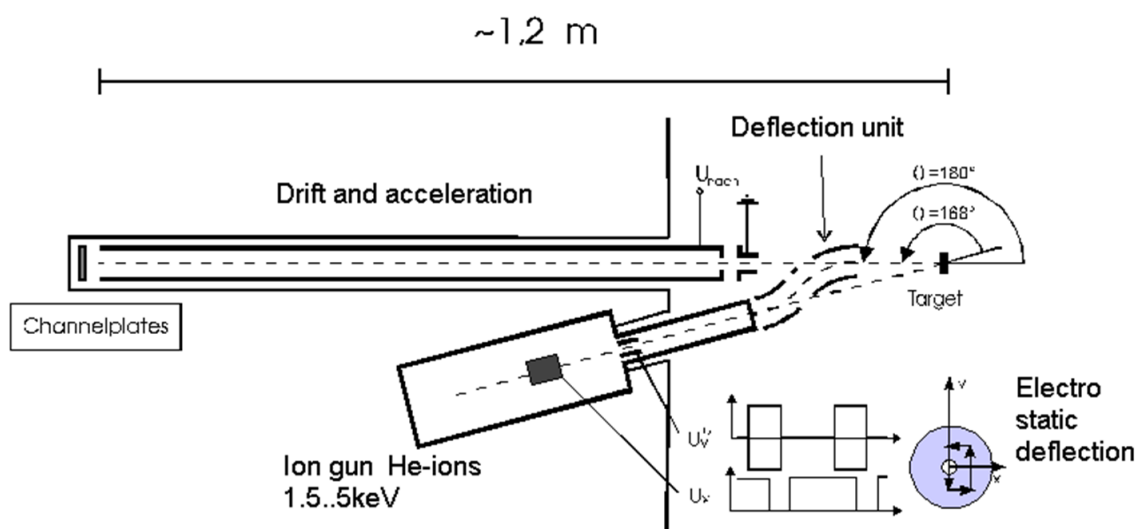
Figure 3-5. NICISS apparatus diagram

The Helium ion is likely to be neutralised on its approach to the sample, when it comes within a few angstroms of the surface. This can occur via three paths. The first path is

resonant neutralisation, whereby an electron from the substrate tunnels into the 2s orbital of the He$^+$, forming an excited Helium atom. The second path is Auger neutralisation, by which a substrate electron tunnels into the 1s state in He$^+$, leaving the surface with an excess of energy which causes the emission of an Auger electron from the surface. Thirdly, Auger de-excitation can also neutralise the helium atom, which is similar to resonant neutralisation except that it results in the release of an Auger electron from the surface. Detecting the neutral atoms rather than the backscattered ions increases the count rate of the experiment, as greater than 99% of ions are neutralized when incident on the surface [5].

3.3 Fourier Transform Infra-Red Spectroscopy (FT-IR)

FT-IR is an optical technique particularly for identifying organic chemicals in a various applications although it also can be able to characterise some inorganic constituents. It is an effective way to identify the presence of certain functional groups in complex molecules. Also, the FT-IR can be used to analyse the unique collection of absorption bands to confirm the identity of a pure compound or to detect the presence of specific impurities. When some of the infrared radiation is absorbed by the sample and some of it is passed through (transmitted), some functional group will be vibrating due to their natural frequency then they produce spectrum represents the molecular absorption and transmission, create a molecular fingerprint of the corresponding sample. Since the output is like a fingerprint, then no two unique molecular structures are able to produce the same typical infrared spectrum. Considering this reason then it makes infrared spectroscopy as a useful and powerful technique for identifying organic chemicals in several types of chemical analysis. The main difference between the IR and FT-IR spectroscopy is the use of interferometer on the FT-IR. The spectrum collected by FT-IR is commonly called as an interferogram which is unique for each organic compound. From the interferogram, it can be seen that every data point which makes up the signal has information about every infrared frequency coming from the source[8].

This technique facilitates various advanced analysis in chemical binding properties due to its sensitivity, speed, and improved data processing. This technique is also able to covers a wide range of chemical applications, especially for polymers materials and organic compounds. In this thesis, FT-IR and electron/ion scattering spectroscopy are complementary. FT-IR is very good for identifying compounds but is not surface sensitive. However, ion scattering and electron spectroscopy are surface sensitive but are lesser

useful for identifying exact chemical compounds. FT-IR was used to observe the presence of the co-adsorbent namely Chenodeoxycholic Acid (CDCA) in the sensitized titania (chapter 7).

3.4   Materials and Sample Preparation

The meso-porous layer of TiO_2 in this research was prepared using the DSL 18NR-T paste produced by Dyesol, the most common supplier company for DSSC materials. The TiO_2 paste was used as it was namely in batch 278 which is containing 19.4% of TiO_2 loading. The size of the nano-porous titania is averaging around 20 nm. There are three different molecular structures for nano-porous titania, they are anatase, brokite, and rutile. The titania nano-particles batch 378 used in this research are predominantly in the anatase structure [9]. The deposited titania film surface will be prepared by the doctor blade method. The titania nano-porous slurry is deposited on a clean conductive indium tin oxide (ITO) coated glass substrate [10]. The thickness of the titania layer is estimated around the thickness of the tape frame used in both left and right side when the doctor blade is dragged across the conductive ITO surface. Subsequently, the ITO/titania, substrate will be sintered in an oven for 30 minutes and the temperature is kept at a constant around 450 ± 20 ^{o}C to form the nano-porous structure of titania thus it can be applied as the semiconductor substrate. The temperature is increased and decreased slowly to avoid cracking of the titania layer as the cracking titania surface leads to the uncovered ITO surface thus it will affect to the dye molecules attachment on the titania layer. The slurry titania contains some organic fillers, as well as an organic plasticizer. The solvent for the titania paste is normally terpineol. Within the sintering process, all of the filler materials are burnt off and it helps to control the formation of the porosity of the nano-porous titania layer.

Once the nano-porous titania films were prepared, before being used as a substrate to be sensitized by the dye molecule, the ITO/titania substrates were heated to 80 ^{o}C for 15 minutes. It was supposed to remove contaminants that probably present on the titania surface before the dye loading process was taken place when the titania film exposed into the dye solution. For the dye loading process, N719 dye solution was provided by dissolving some amount of the dye powder into ethanol as a solvent. Starting from the high concentration then followed by some dilution was more recommended to consider the use of the dye material wisely. It was important to remember that the literature reveals ethanol[4,11-14] are typical solvents for dye loading process of titania for both ionic and non-

ionic dyes. A certain concentration of dye has been determined. The titania film is dyed for 24 hours in approximately 4 ml solution. The sensitized titania film samples was kept in sealed containers to protect the photo-anode from light exposure as the dyed titania film is sensitive to the light exposure. The typical sample size was prepared approximately less than 1 cm^2 because it needs to be considered as the sample holder of the electron spectroscopy apparatus can mount 1 cm^2 sample in size. It is about 0.8 cm in width by 1 cm in length.

A various dyes were used in this research. The first dyes are Ruthenium complex which are N719 and Z907, and the second ones are organic dyes which are L0Br, PD2 and LEG1. The molecule structure of each dyes are shown in Figure 3.3.
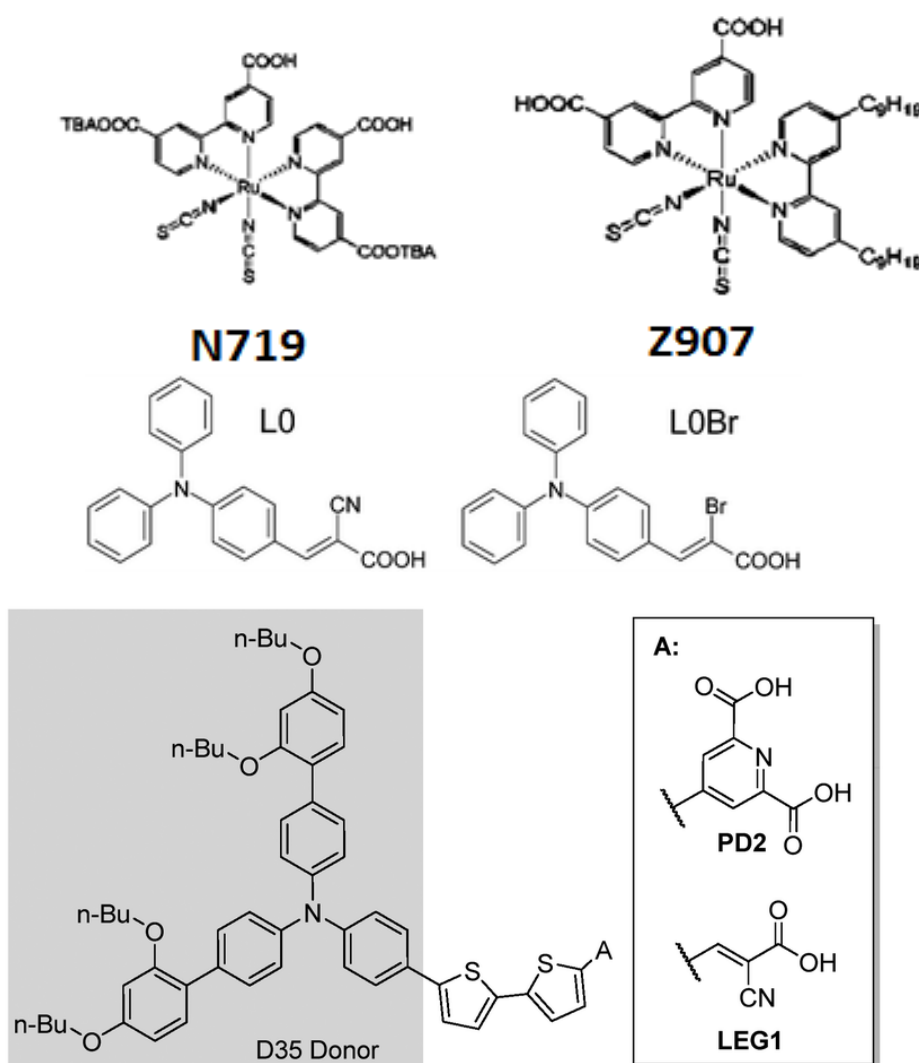
Figure 3-6. Molecular structure for Ruthenium complexes (N719 and Z907) and organic dye (L0Br, PD2 and LEG1).

3.5 The Limitation of Techniques Used in this Research

The NICISS is a specific spectroscopic technique used to investigate concentration depth profile of the component on the substrate. It is very powerful technique as the projectile ion will interact with the atomic target representing the interested molecule on the substrate. Its interaction depends on the mass of target atom thus the presence of the heavier atom on the sample is required in the NICISS. In term of its depth range, NICISS has 30 nm maximum and the outermost layer is hard to be exact regarding the composition. Not existing or less presence of the heavier atom on the sample will take longer time to investigate the concentration depth profile of the component. The XPS is one of the photo electron spectroscopy techniques which employ the photon electron interaction in the core level. In one hand, it is very thorough method to reveal the composition of material we interested on the substrate. However, as the X ray energy in XPS will excite the electron in the core level, in consequence it will not be very surface sensitive on the other hand and it is hard to measure non-monotonic profiles. The UPS is another technique we used on the research to determine the electronic structure of material on the substrate which capable to measure the work function. However it could not be able to determine the exact energy band gaps between the LUMO and HOMO level of material as it is being the limitation of UPS without the IPES techniques beside its depth range which is less than XPS. MIES is the most surface sensitive technique and it does not include on the Photo Electron Spectroscopy as it employs thermal interaction between excited gas atom and the topmost layer atom on the sample surface. Regarding on the depth probing of the MIES technique, it would be a powerful surface analysis technique or sensitive for outermost layer only but no depth information. It would not be much useful without the existing information about the functional group on the material composition on the study. Thus it requires sometime the theoretical calculation about the molecular orbital contribution to interpret which orbital is contributing to the MIE spectrum. FT-IR is optical spectroscopy uses the molecule vibration after the are interacting with light. It is an established technique in chemistry to determine the functional group presenting on the sample. However, its limit of detection is sometimes relatively higher in comparison of the surface analysis techniques. Thus it highly depends on the amount of the presented material on the sample surface.

3.6 Conclusion

There are various spectroscopy techniques used in this study to reveal the interface properties and some physical phenomena across the interface on DSSCs mainly XPS, UPS, MIES and NICISS in electron and ion spectroscopy techniques but also FT-IR as an optical spectroscopy to determine the organic functional group on the dye which attached on the titania.

Reference

1. Burger, K. and A. Buvari, Inorg. Chem. Acta, 1974. **11**(25).

2. Andersson, G. and C. Ridings, *Ion scattering studies of molecular structure at liquid surfaces with applications in industrial and biological systems.* Chemical reviews, 2014. **114**(17): p. 8361-8387.

3. Andersson, G. and H. Morgner, *Impact collision ion scattering spectroscopy (ICISS) and neutral impact collision ion scattering spectroscopy (NICISS) at surfaces of organic liquids.* Surface Science, 1998. **405**(1): p. 138-151.

4. Katoh, R., K. Yaguchi, and A. Furube, *Effect of dye concentration on electron injection efficiency in nanocrystalline TiO2 films sensitized with N719 dye.* Chemical Physics Letters, 2011. **511**(4–6): p. 336-339.

5. Andersson, G. and H. Morgner, *Determining the stopping power of low energy helium in alkanethiolates with Neutral Impact Collision Ion Scattering Spectroscopy (NICISS).* Nuclear Instruments and Methods in Physics Research Section B: Beam Interactions with Materials and Atoms, 1999. **155**(4): p. 357-368.

6. Andersson, G., *Energy-loss straggling of helium projectiles at low kinetic energies.* Physical Review A, 2007. **75**(3): p. 032901.

7. Paxton, A.T. and L. Thiên-Nga, *Electronic structure of reduced titanium dioxide.* Physical Review B, 1998. **57**(3): p. 1579-1584.

8. Connes, J. and P. Connes, *Near-Infrared Planetary Spectra by Fourier Spectroscopy. I. Instruments and Results.* Journal of the Optical Society of America, 1966. **56**(7): p. 896-910.

9. Zaban, A., et al., *The Effect of the Preparation Condition of TiO2 Colloids on Their Surface Structures.* The Journal of Physical Chemistry B, 2000. **104**(17): p. 4130-4133.

10. Topoglidis, E., et al., *Protein adsorption on nanoporous TiO 2 films: a novel approach to studying photoinduced protein/electrode transfer reactions.* Faraday Discussions, 2000. **116**(0): p. 35-46.

11. Hwang, K.-J., et al., *Analysis of adsorption properties of N719 dye molecules on nanoporous TiO2 surface for dye-sensitized solar cell.* Applied Surface Science, 2010. **256**(17): p. 5428-5433.

12.   Yu, Y., K. Wu, and D. Wang, *Dye-sensitized solar cells with modified TiO[sub 2] surface chemical states: The role of Ti[sup 3 +].* Applied Physics Letters, 2011. **99**(19): p. 192104-3.

13.   Zhang, J. and A. Zaban, *Efficiency enhancement in dye-sensitized solar cells by in situ passivation of the sensitized nanoporous electrode with Li2CO3.* Electrochimica Acta, 2008. **53**(18): p. 5670-5674.

14.   Ishihara, T., et al., *Effect of ligand carboxylation on adsorption and photosensitization in Ru(II)-complex dye-sensitized nanocrystalline TiO2 solar cell.* Japanese Journal of Applied Physics, Part 1: Regular Papers and Short Notes and Review Papers, 2005. **44**(4 B): p. 2780-2782.

4 CHAPTER FOUR: Effect of Iodine in Dye/Titania Interface of Dye Sensitized Solar Cells Using Photoelectron Spectroscopy Techniques: XPS, UPS and MIES

Abstract

The location of iodine as part of the electrolyte in the dye layer of dye sensitized solar cells was investigated using a range of spectroscopy techniques. The interaction of iodine with the dye molecule has not been understood well since the position of iodine around the dye molecule has not been revealed clearly. Iodine has been known as a constituent in the electrolyte as hole transfer medium in DSSC, thus by knowing its properties in particular of its interaction with the dye molecule has been an important thing as part of attempt to improve the cells performance. In this study, two different dyes N719 and Z907 have been used to look at how the iodine behaves around the two different chemical boundaries. The UP and MIE spectra which have measured have been analyzed to identify the position of iodine relatively either to the dye/substrate interface or the top of dye surface.

4.1 Introduction.

Dye-sensitized solar cells (DSSCs) are considered as a lower cost alternative to silicon-based photovoltaic (PVs).[1, 2] The demand on the purity of the materials in DSSCs is not as strong in comparison with silicon based photovoltaic giving the first an advantage in regard to production costs compared to the latter. However, record efficiencies for dye-sensitized cells (~11%)[3] are lower than those for silicon cells (~26%).[4] The DSSC technology still has some difficulties in regard to efficiency and durability. An important factor in lifetime and efficiency could be the presence of iodide in the dye layer which can lead to the recombination reaction of electrons in the titania or dye and the holes in the electrolyte. This is one of the reasons why the electrolyte is one of key components in dye-sensitized solar cells (DSSCs) and has a strong influence on the conversion efficiency and stability of the solar cells.

Three types are usually used in DSSC application. They are different in the phase for some reasons. Those three types are: liquid electrolyte, quasi-solid state electrolyte, and solid

electrolyte. According to the solvent they are used, the liquid electrolyte that commonly used could be divided into organic solvent electrolyte and ionic liquid electrolyte.[5]

The iodide/tri iodide redox ($3I^-/I_3^-$) couple was for a long time the most frequently used electrolyte in DSSCs.[6] Research have paid much concern on the usage of other materials for the electrolyte based on cobalt and ferrocene such as Co(III)/Co(II) and ferrocene/ferrocenium,[7-9] however, the iodine species is still the best redox couple in DSSC application that able to show the certified records and best stability data.[10, 11] The interaction of the iodine molecule to other material in DSSC interface has already investigated by Li et al,[7] in first instance with the dye molecules.[12, 13] The strength of the binding of iodine to many organic donors group is related to the binding coefficients between single digits and 4×10^4.[14] Studies also found that the iodine bound to the sulfur atom on the NCS groups of N719 through their lone pair electrons.[15] Another research using water and acetonitrile revealed that the binding of iodine to the dye molecules were facilitated thiocyanate group.[16,17] It also influences the performance of the cells. The binding of iodine to dye molecules, such as phthalocyanines,[13] porphyrins[18] and ruthenium dyes,[12] has shown the evidence that it increased the recombination rate of conduction band electrons to the electrolyte. It is now widely assumed that the recombination proceeds by the reduction of iodine rather than the reduction of I_3^-.[19] However, another research also revealed that there is a positive effect that the recombination rate can be suppressed. The adsorption of p-aminobenzoic acid on the TiO_2 surface can decrease the recombination lifetime therefore it increases the open-circuit voltage of the cell (V_{OC}). The reason behind this is potentially pointing that the binding of iodine to the amine group.[12] The technique used in the research to reveal the iodine properties performed by Li et al was the FT-IR spectroscopy. In the research, the main focus was on the interaction between the iodine and dye molecules.[6] Another study has also revealed that the function of thiophene group plays a crucial rule to perform the change transfer from donor to the semiconductor substrate.[20]

Gerrit Boschloo and Anders Hagfeldt described that the I^-/I_3^- redox couple also potentially affect to the electrochemical potential of the TiO_2 electrode through the recombination kinetics between electrons in TiO_2 and oxidized redox species. Although the electron life time of electron diffused into the titania is reasonably long, but the regeneration of oxidized iodide is much faster, then the recombination process between the electron on the

dye and the I^-/I_3^- could be suppressed. Overall, the iodide/triiodide couple has some positive effects. Not only having a good solubility, it does not absorb too much light too, and it has a suitable redox potential. It also provides rapid dye regeneration. But the best properties of this $I-/I3-$redox species related to our study here is that it has the very slow recombination kinetics between electrons in TiO2 and the oxidized part of the redox couple, triiodide.[21] Thus the comparison between how fast the dye regeneration and the electron transfer from the dye into titania is the crucial parameter of a favorable electrolyte, and iodine has this property.

In this study, we are investigating the interaction of the $3I^-/I_3^-$ interaction with the dye layer attached to the titania surface. We are aiming to determine the position of iodine across the dye-titania interface using direct measurement by electron spectroscopy techniques such as X-ray photoelectron spectroscopy (XPS), UV photoelectron spectroscopy (UPS) and Metastable Induced Electron Spectroscopy (MIES). We are also aiming to determine the influence of the presence of iodine or iodide on the orientation of the dye molecules on the titania surface. In summary, the aim of the present work is to understand how the presence of iodine across the dye/titania interface influences the electronic energy levels and the orientation and conformation of the dye molecules.

4.2 Material and Techniques

4.2.1 Material

In this study the most commonly used organometallic dyes, N719 dye (Di-tetrabutylammoniumcis-bis (isothiocyanate) bis (2,2'-bipyridyl-4,4' dicarboxylate) ruthenium (II)) and Z907 dyecis-Bis(isothiocyanato) (2,2'-bipyridyl-4,4'-dicarboxylato) (4,4'-di-nonyl-2'-bipyridyl) ruthenium(II) were applied. The structure of N719 is significantly different to that of Z907 in regard to their ligands. The N719 dye is ionic and polar and this will form a hydrophilic surface while the Z907 is lesser polar than N719 and will form more a hydrophobic surface due to its long alkyl ligand on it. However, both dyes have four pyridyl groups and also two thiocyanate ligands. The N719 and Z907 dye molecular structures are shown in Figure 4.1.
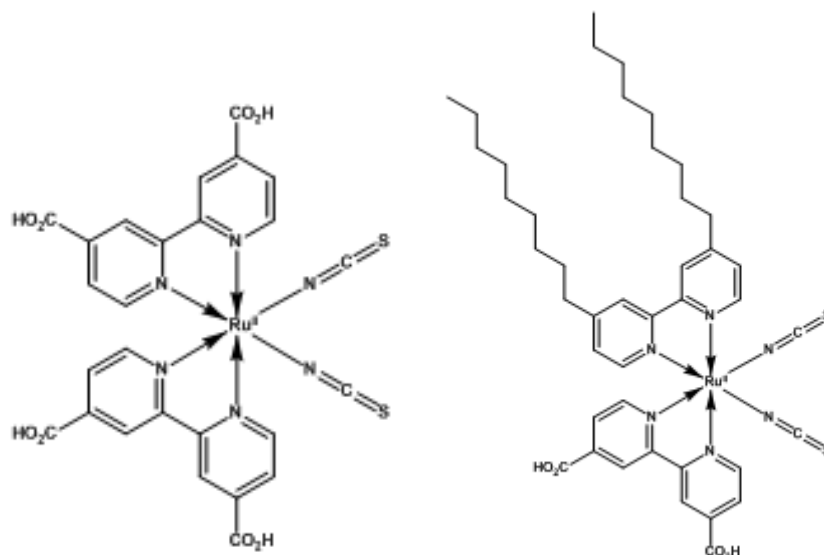
Figure 4-1. N719 and Z907 dye molecular structure. Redrawn from previous studies.[22]

As the N719 and the Z907 dyes are the most popular ruthenium based dye, the most attractive properties of the N719 and Z907 have been shown in some real cell application and broaden DSSC research. The N719 and Z907 have been purchased from Dyesol (Australia).

4.2.2 Sample Preparation

Mesoporous layers of TiO_2 as a substrate were prepared using the DSL 18NR-T paste from Dyesol. The paste was used as received. This paste contains 19.4% TiO_2 loading with particle size averaging around 20nm. A 10 mm x 8 mm nanoporous titania films were prepared by applying the doctor blade method. Subsequently the TiO_2 film was sintered at 450 °C for 30 minutes to burn the organic filler in the titania paste.[23] During the sintering process the filler will be removed leaving behind only the nano-porous titania film on the substrate. Indium Thin Oxide (ITO) was used as the substrate because it has a conductive layer on the side where the titania needs to be deposited on. Indium doped Tin Oxide (ITO) coated glass slides were used as the substrate from Kintec (China) with 1.1 mm in thickness and its sheet resistivity is 15 ohm/sq.

Subsequently the nano-porous titania film were immersed into either an N719 or Z907 dye solutions for 24 hours which results in a dye covered titania surface. The concentrations used for the N719 dye in ethanol and the Z907 dye in acetonitrile were 0.005 mM[23] and 0.03 mM[24], respectively. The concentrations were chosen based on previous work determining the adsorption isotherms on titania. At these concentrations the titania surface

is covered almost completely with the respective dye[23]. Each titania film was immersed into a fresh dye solution for 24 hours and then rinsed with the respective solvent. All vials with the dye solutions were stored in darkness at room temperature before being used. Subsequently the dyed nano-porous titania was investigated with XPS, UPS and MIES. These spectra are used as reference spectra for the pristine sample, i.e. samples not having been exposed to the electrolyte. Subsequently the samples were immersed into the NaI electrolyte solutions for 24 hours. When the samples were taken out from the electrolyte solutions, one of them was rinsed with 15 drops of solvent and the other one was further used without rinsing. These two rinsing procedures have been chosen because the influence of rinsing on the surface structure of the dye layers exposed to the electrolyte solution is not known.

4.2.3 Electron Spectroscopy

The use of XPS, UPS and MIES has already been detailed on chapter 3 but brief overviews are given here. The dyed titania layer was investigated with a range of electron spectroscopy techniques XPS, UPS, and MIES. All of the instrument are installed at the same apparatus using the same ultrahigh vacuum (UHV). The emitted electrons from the sample after the irradiation by the X-ray source are collected with a hemispherical Phoibos 100 energy analyzer from SPECS then the spectra are recorded.

The fitting procedure needs to be carried out to evaluate the XP spectra. High resolution XP spectra were fitted using combined Gaussian-Lorentzian peaks. When we fit the spectra, the suitable background needs to be taken into account. In this study, we used a Shirley background method as it is commonly used in the analysis of the XP spectra.[26] MIE and UP spectra were fitted with Gaussian curves the secondary electron background was considered with the exponential curve.[27] In electron spectroscopy, secondary electrons are generated when electrons are on elastically scattered. As a result, these secondary electrons then can excite additional secondary electrons in a cascading process that produces a background signal in the measured spectrum, the shape of which can be approximated accurately using an exponential function.

4.2.4 Analysis of the valence electron spectra

The UP and MIE spectra were fitted with Gaussian curves and only the minimum number of Gaussian curves was used to fit a spectrum. The fitted peaks represent the electron orbital contributions or DOS centered at a specific binding energy. The full width half

maximum (FWHM) of the Gaussian curves is used as a fitting parameter. One Gaussian curve can cover a range of electron orbital. The purpose of the fitting procedure is to determine to which degree a specific electron orbital is present in the electron spectra.

The computer calculation is aiming to determine the binding energy of each contribution of the orbital functional groups from the dye molecule. By doing ab-initio method it can be determined which orbital contributes to the electron emission with a specific energy. This calculation is used as a reference for identifying the binding energy of the fitted peaks to assign the electron orbitals for the respective functional groups of the sample.

In the computer calculation, there are some assumptions used to approach the experiment. The N719 and Z907 dye molecules and their interaction with TiO_2 model slabs were studied using density functional theory calculations (DFT). All calculations were carried out using the program package Gaussian 09. The molecular dye structures were geometrically optimized, and the TiO_2 slab models kept geometrically frozen in the calculations. Single-point energy and geometry optimization calculations were performed using the cam-B3LYP hybrid functional. Solvent effects were not included in the calculations.

A small TiO_2 slab was constructed from the anatase type structure of formal composition $Ti_{15}O_{28}$, formally with one Ti(IV) in excess and thus a total charge of +4. The small (100) surface was exposed to the N719 and Z907 dyes and the TiO_2 slab was kept tethered during the geometry optimizations. Upon coordination of the N719 and Z907 dyes, two protons from the same bypyridyl ligand were removed mimicking the expected experimental adsorption effects and rendering the dyes a formal -2 charge. Exchange of the SCN^- ligands for I^- and/or I_3^- ligands does not change the overall charge of the system.

As the full width half maximum (FWHM) of a spectrum is important, it should be taken into account while the spectra need to be fitted before it is ready to be evaluated. In general, the main factors that influence the FWHM of an electron spectroscopy spectrum are the natural line width of a peak, the resolution of the spectrometer, and the energy distribution of the excitation energy. The spectra for condensed phase element are usually broader than peaks of the same substance in the gas phase. It is potentially caused by the interaction between the atoms or molecules in the condensed phase. However, the FWHM of a given state is usually broader that the energy difference to the neighbor states. For this reason a single peak could represents usually more than one electronic state.

4.3 Result and Discussion

From the UP spectra we will determine the change in work function of the dyed titania surface when exposed to the electrolyte solution. The MIE spectra will be used to determine whether the dipole at the dye/titania interface changes subsequent to the exposure of the dye layer to the electrolyte solution and also whether the composition of the outermost layer of the dye layer has been influenced such as through reorientation of the dye molecules or restructuring of the top most molecular structure of the dye layer. XPS will be used to quantify the composition of the dye layer on titania exposed to the electrolyte solution. We will first describe the N719 results and then the Z907 results.

4.3.1 N719.

XP spectra of N719 have been taken from the pristine samples and treated by non-rinsing and rinsing with solvent subsequent to the exposure to the electrolyte solution. The regions for Carbon, Oxygen, Sulphur, Nitrogen, Ruthenium, Titanium, Iodine and Sodium were recorded in XP spectra in case the respective element was found in the survey spectrum. Table 4.1 shows the elemental composition of the samples. The peak positions are used to determine the chemical nature of the elements found. N is found at (399.9 ± 0.1) eV and is attributed to the organometallic functional groups involving N [28, 29] as the N719 is an organometallic dye based. Carbon is found mainly at 285. There are also other C peaks. It is not unambiguous to identify to which functional group these further C peaks are related to. They could be related to the dye, but they also could be related some residual solvent or adventitious hydrocarbons. But analysing the nature of these C peaks is not important because the study is focussing mainly on the change in composition and on Iodine. From the change in intensity of the other C peaks is will be difficult to derive any information. O is found at 529.8 ± 0.1 eV and is mainly attributed to O in TiO_2.[30] Ru is found at the same position 280.8 ± 0.1 eV for the pristine and the treated samples and is attributed to Ru in N719. It is worth noting that this binding energy of Ru correspondence to double oxidised Ru[31, 32] with the Ru being the central atom in the N719 dye. Ti is found at 458.6 ± 0.1 and is attributed to Ti in TiO_2.[33, 34] Iodine is found at 618.7 ± 0.0eV and attributed to iodide.[35] Iodine or I_3^- should occur at a somewhat higher binding energy. Na is found at 1071.6 ± 0.1eV and is attributed to the presence of NaI as iodine source due to the electrolyte exposure. S is found at 162.0 ± 0.1eV for the pristine, then 162.1 ± 0.1eV and 161.6 ± 0.1eV for iodine exposure. All of them are attributed coming from the cyanate group in N719. Generally, the chemical states of the samples due to the treatment of the

iodine exposure were not significantly changed. The intensity increased for the Iodine, and Sodium due to the electrolyte exposure. However, elements other than I and Na do not change significantly due to the exposure to electrolyte solutions.

Table 4-1. Chemical composition of N719 sample from XPS . Peak positions can be averaged because there is little variation across the samples.

Element	% Intensity			Calibrated Peak Position			Average Position
	Pristine	Non-Rinsing	Rinsing	Pristine	Non-Rinsing	Rinsing	
N	(3.6 ± 1.1)	(3.7 ± 1.1)	(2.8 ± 1.1)	(399.9 ± 0.1)	(399.9 ± 0.1)	(399.8 ± 0.1)	(399.9 ± 0.1)
Na	(2.3 ± 0.8)	(16.0 ± 0.8)	(12.2 ± 0.8)		(1071.6 ± 0.1)	(1071.6 ± 0.1)	(1071.6 ± 0.0)
O	(54.1 ± 11.8)	(37.3 ± 11.8)	(46.1 ± 11.8)	(529.8 ± 0.1)	(529.8 ± 0.1)	(529.9 ± 0.1)	(529.8 ± 0.1
C	(27.5 ± 15.2)	(29.1 ± 15.2)	(25.1 ± 15.2)	(285.0 ± 0.0)	(285.0 ± 0.0)	(285.0 ± 0.0)	(285 ± 0.1
Ru	(0.3 ± 0.2)	(0.4 ± 0.2)	(0.3 ± 0.2)	(280.8 ± 0.2)	(280.8 ± 0.2)	(280.8 ± 0.2)	(280.8 ± 0.0
Ti	(12.5 ± 3.8)	(7.6 ± 3.8)	(9.2 ± 3.8)	(458.6 ± 0.1)	(458.7 ± 0.1)	(458.7 ± 0.1)	(458.6 ± 0.1
I		(5.4 ± 0.0)	(3.4 ± 0.0)		(618.7 ± 0.0)	(618.7 ± 0.0)	(618.7 ± 0.0
S	(0.6 ± 0.1)	(0.5 ± 0.1)	(0.5 ± 0.1)	(162.0 ± 0.2)	(162.1 ± 0.2)	(162.6 ± 0.2)	(162.2 ± 0.3

Figure 4-2 shows the UP spectra for N719. From the UP spectra it can be seen that the secondary electron cut-offs are shifting by 0.21 eV and 0.17 eV for the non-rinsing and rinsing sample, respectively (Shown in table 4.2). No shift of the position of the HOMO level is found (indicated with a red arrow in Figure 4.2). The change in secondary electron cut-off is a measure for the change of the work function as provided in table 4-2. For the non-rinsed and rinsed sample, the work function has changed for (0.21 ± 0.02) and (0.17 ± 0.02)eV respectively (shown in table 4-2). From Figure 4.2 it also can be seen that there is additional contribution at around 3.8 eV after the electrolyte exposure. The intensity around 3.8 eV goes up higher for non-rinsing treatment (blue curve) showing that there is additional contribution in this region. It will be shown below that this additional contribution can most likely be attributed to the presence of the iodine.

The MIE spectra as shown in Figure 4-3 also show the occurrence of a peak at 3.8 eV which is consistent with the changes in the UP spectrum in Figure 4-2 at around 3.8 eV as shown by the purple arrow. This additional contribution attributed to the presence of iodine after the iodine exposure. It means that the composition of the outermost layer is changing and it is due to the presence of the iodine. It can also be seen that the MIE and UP spectra do not shift indicating that there is not a change in the dipole formed at the dye/titania interface. It thus can be concluded that iodine does not penetrate through the dye/titania interface. Which functional group is reoriented and will be evaluated using the molecular orbital assignment by comparing between the calculation and the fitted MIE spectrum.
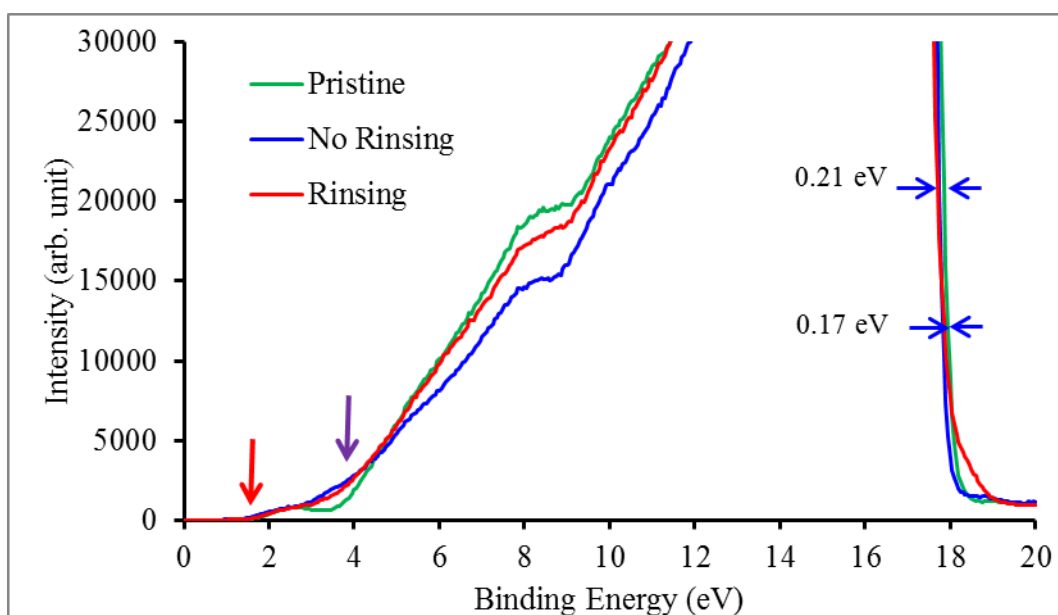
Figure 4-2. The UP Spectra and the additional peak around 3.8 eV due to the iodine exposure of the N719 dye. The red arrow is showing the position of the HOMO level of the material

Table 4-2. The work function of the N719 sample and its change after iodine exposure

Sample	Work Function (eV)	Change of work Function relative to pristine sample (eV)
N719	3.45 ± 0.04	
No Rinsing	3.60 ± 0.02	0.21
Rinsing	3.62 ± 0.02	0.17
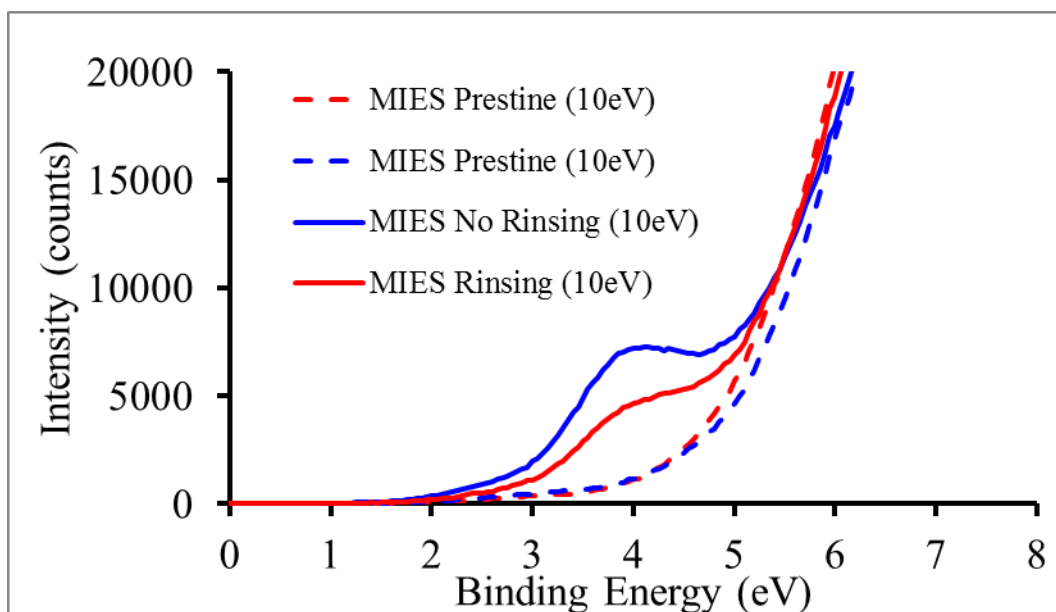
Figure 4-3. MIE Spectra for N719 showing there was additional peak in lower binding energy region as a the iodine present at the surface.

Figure 4-4a and 4-4b show how the peaks used to fit the measured MIE spectrum are correlated to the functional groups identified through the molecular orbital calculation of the dye molecule. The functional groups occur at the specific binding energies and the change in intensity in MIE spectra is identified as a change in how this functional group is accessible by He* thus forms the outer layer configuration. Our system in this study is the N719 dye and it seems that there is a possibility that one iodine atom bounded to the thiocyanate functional group representing the presence of iodine to the dye layer. By matching between fitted peak and the calculated position from the molecular orbital calculation, then the molecular orbital can be assigned as such each functional group. For the N719 we assign the possible peak where the certain functional group are located at (4.1 ± 0.05) eV, (6.8 ± 0.05) eV, (8.8 ± 0.05) eV, and (11.0 ± 0.05) eV. The vertical bars in Figure 4-4 are representing the calculation of molecular orbital obtained from the model or theoretical calculation. Each Gaussian curve used to fit the MIE spectrum is then identified with functional groups of the dye molecule based on the computer calculation. Figure 4-4a is shows the MIE spectrum of the pristine sample and Figure 4-4b that of the sample exposed to the electrolyte solution with subsequent rinsing. Then the intensity variations of each peak are drawn in Figure 4-5 as index 1 to 3 indicates pristine, non-rinsing, and rinsing treatment and each curve is representing the changes of representative peak, thus we can easily see the changes over the treatment.
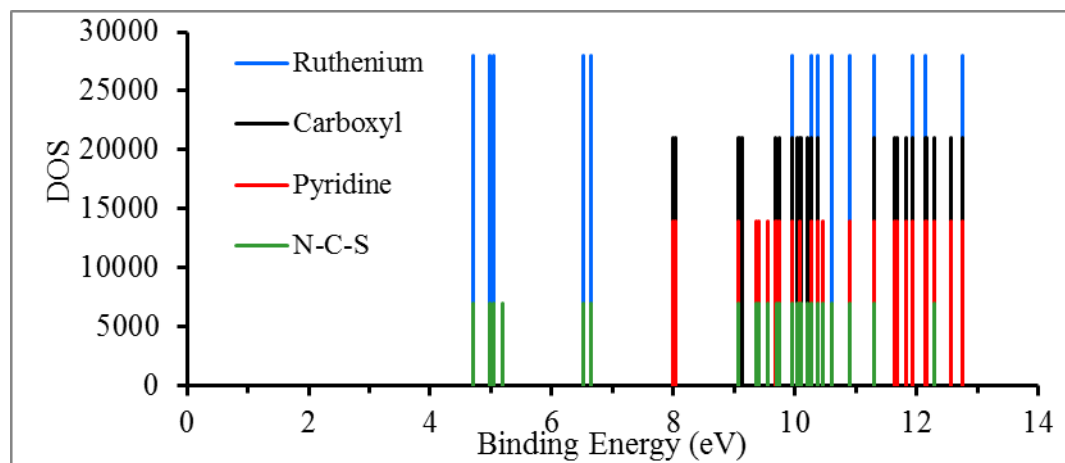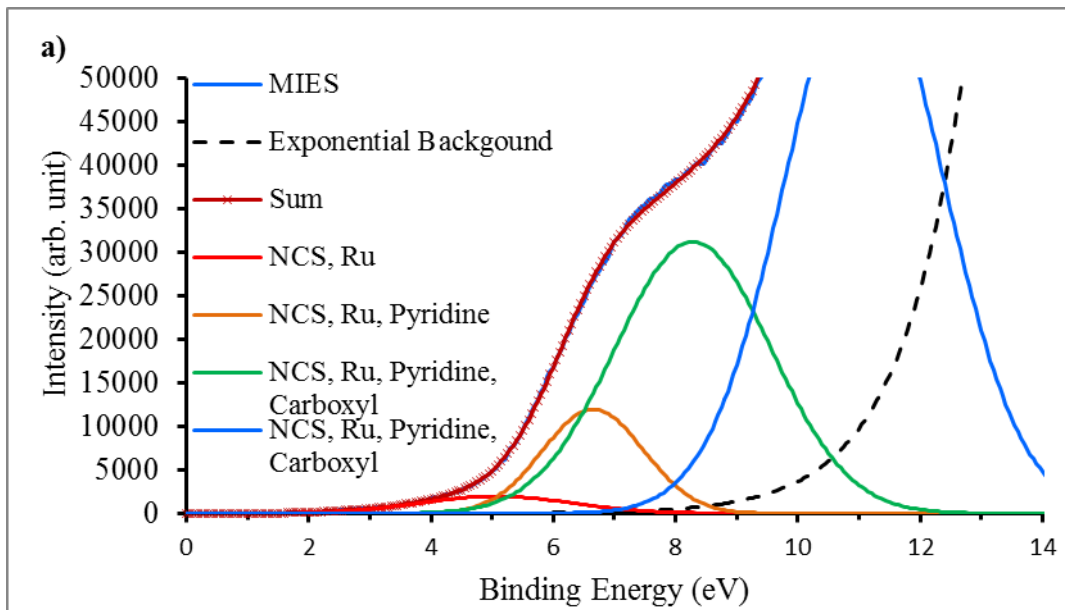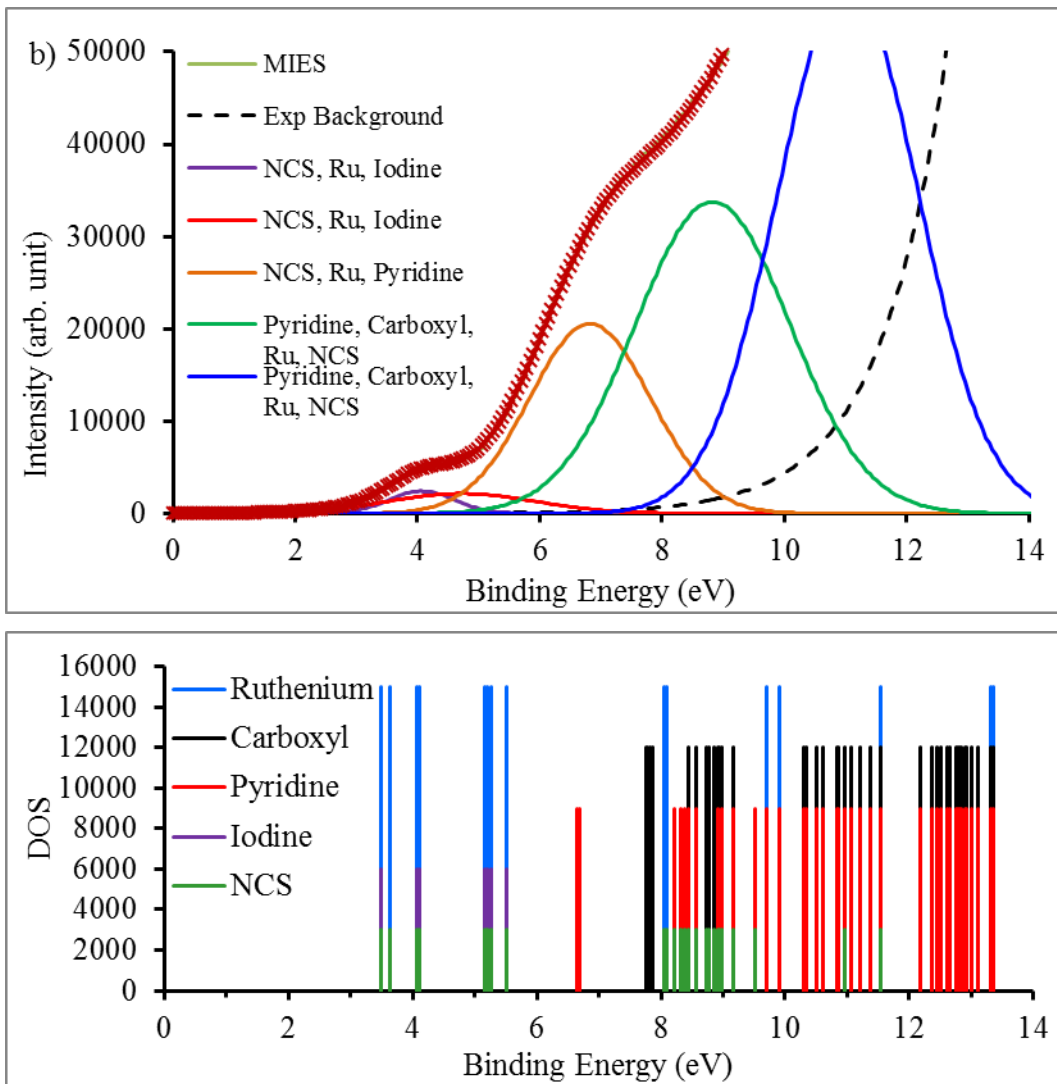
Figure 4-4. Molecular orbital contribution and MIE Spectrum for (a) pristine N719 dye sample and (b) after immersed into the electrolyte solution with rinsing.
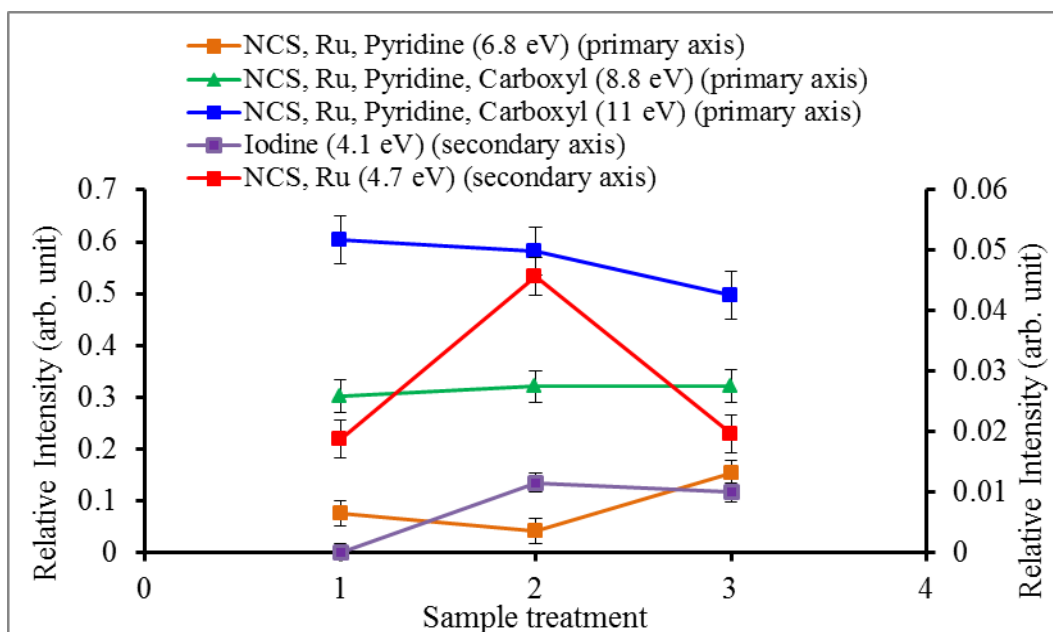
Figure 4-5. The peak changes of N719 dye associated with the change of the relative intensity due to the Iodine exposure with rinsed and non-rinsed treatment.

The peak intensities are not corrected for the transmission function of the analyser and the relative sensitivity of MIES for the functional groups. Thus only changes in intensities of individual peaks will be discussed and not the intensity ratios of the four peaks. The orbital assignment of respective peaks associates to each functional group on the dye molecule is provided in table 4-3.

Table 4-3. Peak position of respective functional group of N719 dye

Peak position (eV)	Functional groups	Intensity		
		Non-Exposed	Non-Rinsed	Rinsed
4.7	NCS, Ru	0.018 ± 0.003	0.05 ± 0.003	0.02 ± 0.003
6.8	NCS, Ru, Pyridine	0.07 ± 0.02	0.04 ± 0.02	0.15 ± 0.02
8.8	NCS, Ru, Pyridine, Carboxyl	0.30 ± 0.03	0.32 ± 0.03	0.32 ± 0.03
11	NCS, Ru, Pyridine, Carboxyl	0.60 ± 0.05	0.58 ± 0.05	0.50 ± 0.05
4.1	Iodine	0	0.011 ± 0.001	0.009 ± 0.001

Figure 4-5 describes the intensities variation of fitted Gaussian curve contribution of MIE spectra between the pristine sample and after the iodine exposure. There are four peaks which each of them are occupied by several functional groups as shown in Figure 4.5. The only strong variation occurring on those peaks are at 4.1 eV and 4.7 eV which is most likely caused by not being able to separate the 4.1 and 4.7 eV peaks.

4.3.2 Z907

XP spectra of Z907 have been taken in similar way as the N719 dye. The regions were recorded as well in case the respective element was found in the survey spectrum similar with the N719. Table 4-4 shows the elemental composition of the samples. The majority peaks for carbon are at 285 eV. Other carbon contribution can be from dye molecule,or some residual solvent or adventitious hydrocarbon. However, neither the presence of solvent or adventitious hydrocarbons influences the interpretation of XPS. N is found at (400.1 ± 0.5) eV. The position are associated with organo-metallic[28, 29] as the Z907 is one of the organometallic dye. Oxygen peak are found at (530.2 ± 0.4) eV. This positions is attributed to the metal oxide[30]. Ru is found at (281.1 ± 0.3) eV attributed to double oxide[31][32] as the central atom in the N719 dye. Titanium is found at (459.0 ± 0.4) eV for the non-exposed This position is attributed to double oxide[33, 34] related to the TiO$_2$ of the substrate. Iodine is found at (619.2 ± 0.5) eV and it is attributed to the form of iodide[35] as iodine exposure treatment. Na is found at (1071.8 ± 0.4) eV and is attributed to the presence of NaI as iodine source due to the electrolyte exposure. However, the sodium was also found in the non-exposed sample which can be attributed to the impurity as the intensity in this sample is a small amount of sodium impurity. S is found at (162.3 ± 0.5) eV and it is attributed coming from the cyanate group. If we look at the chemical states of the samples due to the treatment, it was not significantly changed. The main feature of the change of the intensity is that the intensity of non-exposed sample is higher than the exposed one. Then the intensity of sodium and iodine is lower after rinsing treatment.

Table 4-4 Chemical composition of Z907 sample from XPS

Element	% Intensity			Calibrated Peak Position			Average Position (eV)
	Non-exposed	Non-Rinsed	Rinsed	Non-exposed	Non-Rinsed	Rinsed	
N	4.8 ± 0.6	4.8 ± 0.6	4.1 ± 0.6	399.6 ± 0.1	400.5 ± 0.1	400.2 ± 0.1	400.1 ± 0.5
Na	1.1 ± 0.6	2.4 ± 0.6	3.1 ± 0.6	1071.4 ± 0.0	1072.2 ± 0.0	1071.9 ± 0.0	1071.8± 0.4
O	39.9 ± 0.4	38.4 ± 0.4	38.3 ± 0.4	529.8 ± 0.1	530.5 ± 0.1	530.2 ± 0.1	530.2 ± 0.4
C	44.6 ± 0.5	43.1 ± 0.5	43.8 ± 0.5	285.0 ± 0.0	285.0 ± 0.0	285.0 ± 0.0	285.0 ± 0.0
Ru	0.4 ± 0.0	0.4 ± 0.0	0.4 ± 0.0	280.8 ± 0.1	281.4 ± 0.1	281.1 ± 0.1	281.1 ± 0.3
Ti	9.4 ± 0.2	8.8 ± 0.2	8.9 ± 0.2	458.7 ± 0.1	459.4 ± 0.1	459.0 ± 0.1	459.0 ± 0.4
I		1.7 ± 0.0	1.0 ± 0.0		619.5 ± 0.0	618.8 ± 0.0	619.2 ± 0.5
S	0.7 ± 0.1	0.4 ± 0.1	0.4 ± 0.1	161.7 ± 0.2	162.6 ± 0.2	162.5 ± 0.2	162.3 ± 0.5

Table 4-5 The work function of the Z907 dye and its change after iodine exposure

Sample	Work Function (eV)	Change of work Function relative to pristine sample (eV)
Z907	3.15 ± 0.04	
No Rinsing	3.78 ± 0.05	0.62
Rinsing	3.35 ± 0.05	0.20
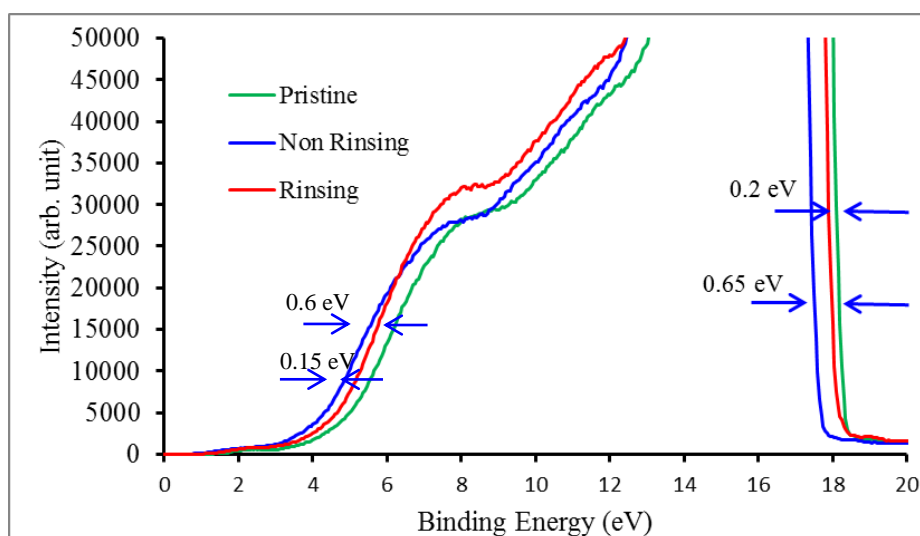
Figure 4-6. The UP Spectra of Z907 dye.

Figure 4-6 shows the UP spectra of Z907 adsorbed onto titania and exposed to the electrolyte solution. The figure shows that there is a shift of the UP spectra but also a change in the secondary electron cut-off. The secondary electron cut-off shifted in the

spectra around 0.65 and 0.2 eV for non-rinsing and rinsing treatment respectively, and the HOMO position shifted around 0.6 and 0.15 eV. It indicated that the more iodine affects larger shift of HOMO position and also work function change as shown in table 4.5. However, there is very little change in the shape of the UP spectra. The shift of the whole UP spectrum is very similar to the change in work function which is an indication that the origin of the shift of the spectrum and the change in work function is the same.

The MIE spectrum as shown in Figure 4.7 is also showing a shift. A shift of UP and MIE spectra is the evidence for a change in dipole on the sample. The UP spectra are only due to the dye layer and not the titania. XPS has shown that the Iodine has penetrated into the sample. Together with the UPS result showing that iodine must be presenting in a deeper layer it can be considered to be likely that the iodine is present at the dye/titania interface inducing a change in dipole. The fact that there is no additional contribution in the UP and MIE spectra, indicates that there is no change in composition or change in orientation of the molecules up to the probing depth of UPS and MIES. For this reason it can be concluded that the dipole is formed at the interface below the probing depth of UPS because what we need to see here is the shift of the whole spectra. then and it can be assumed that the dipole is at the dye/titania interface.[36]
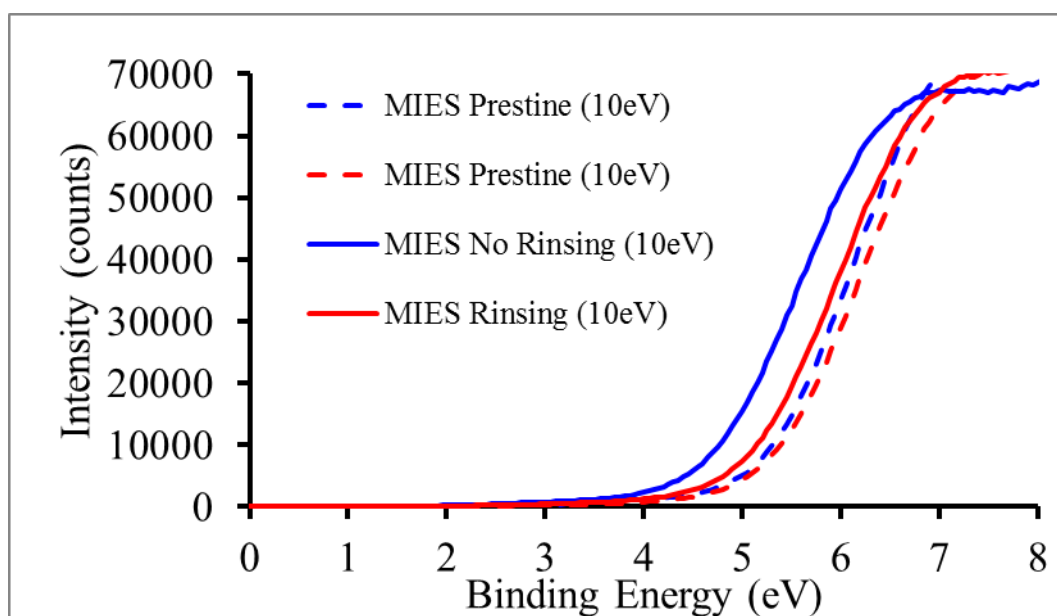
Figure 4-7. MIE Spectra for Z907 showing there was a significant shift between the dye and the substrate indicating the formation of dipole layer across the dye/titania interface occurred.

The quantification of the contributions to the MIE spectra can be used to substantiate the evidence of the above drawn conclusion regarding iodine penetrating through to the

dye/titania interface. Similar as for the quantification of the N719 MIE spectra, Figure 4.8a and Figure 4.8b are showing the process of correlating the calculated molecular orbital to the peaks fitted to the MIE spectra. We find four peaks at $3.4 \pm 0.1eV$, $7.2 \pm 0.1eV$, $9.2 \pm 0.1eV$, and $11.2 \pm 0.1eV$, which are occupied by several possible functional groups. This means that there is no additional peak in the MIE spectra on Figure 4.7, and it seems that the Z907 does not show any significant reorientation or restructuring on the top most atomic layer distribution.
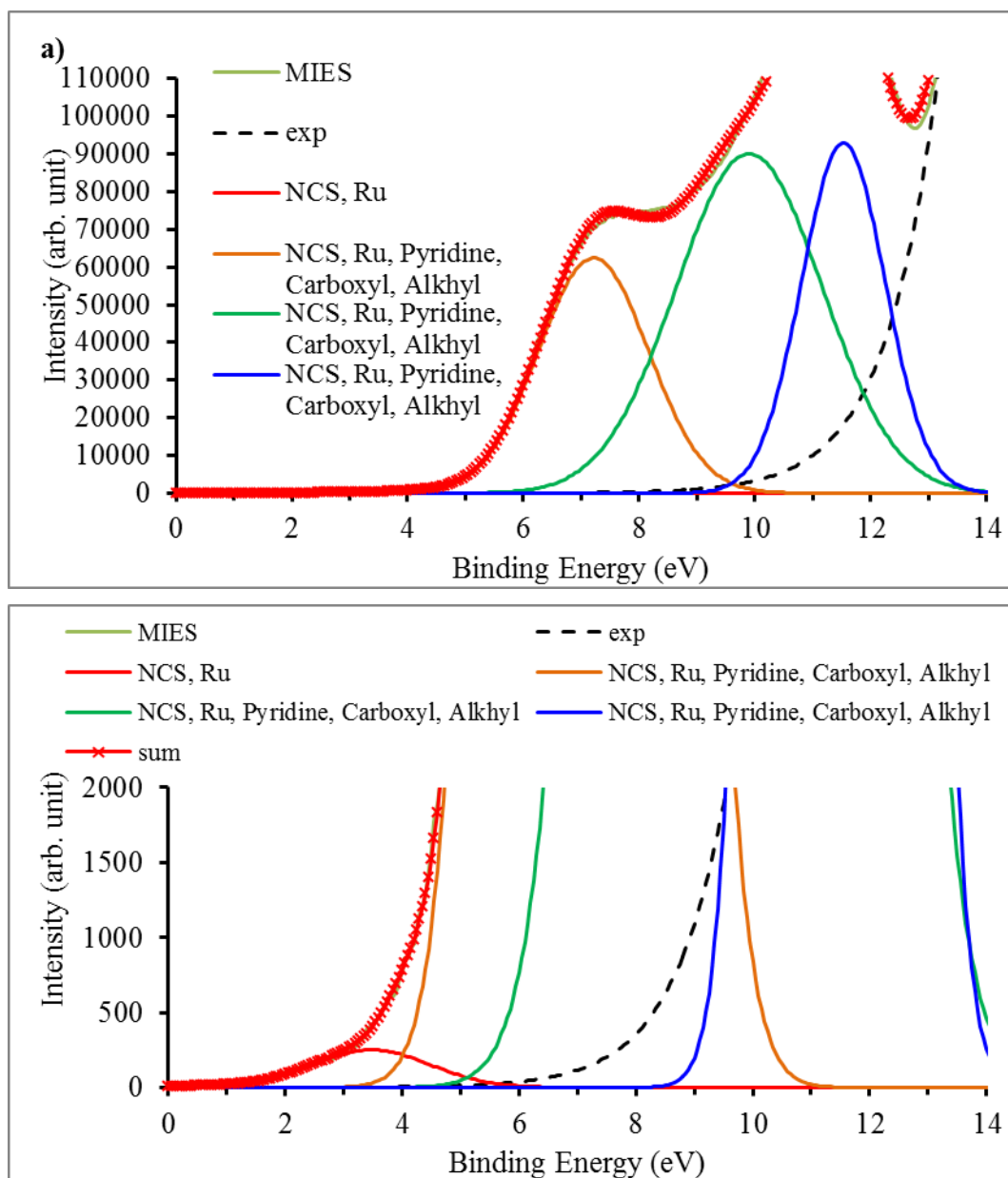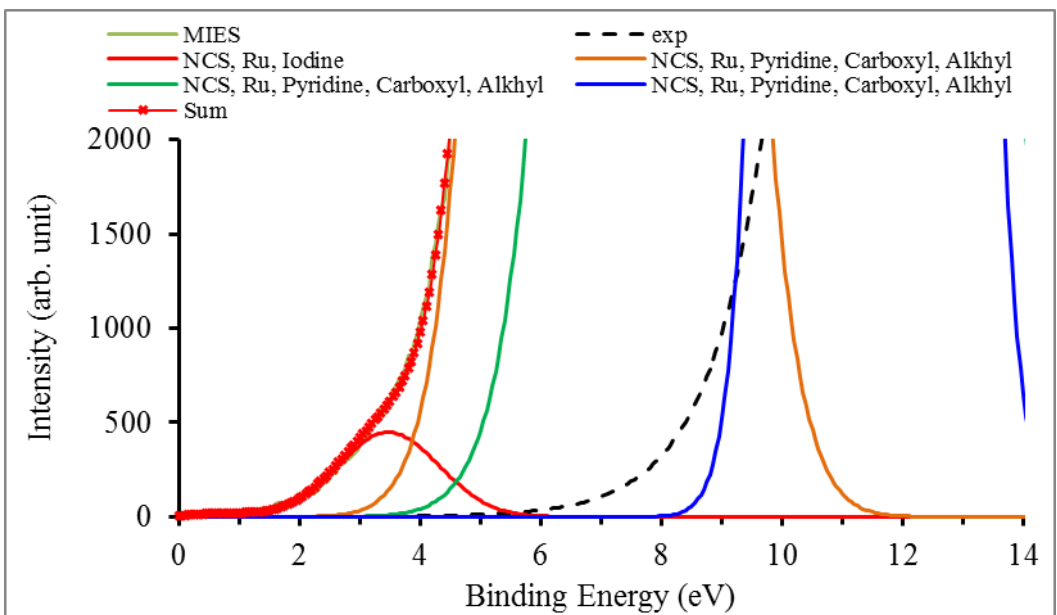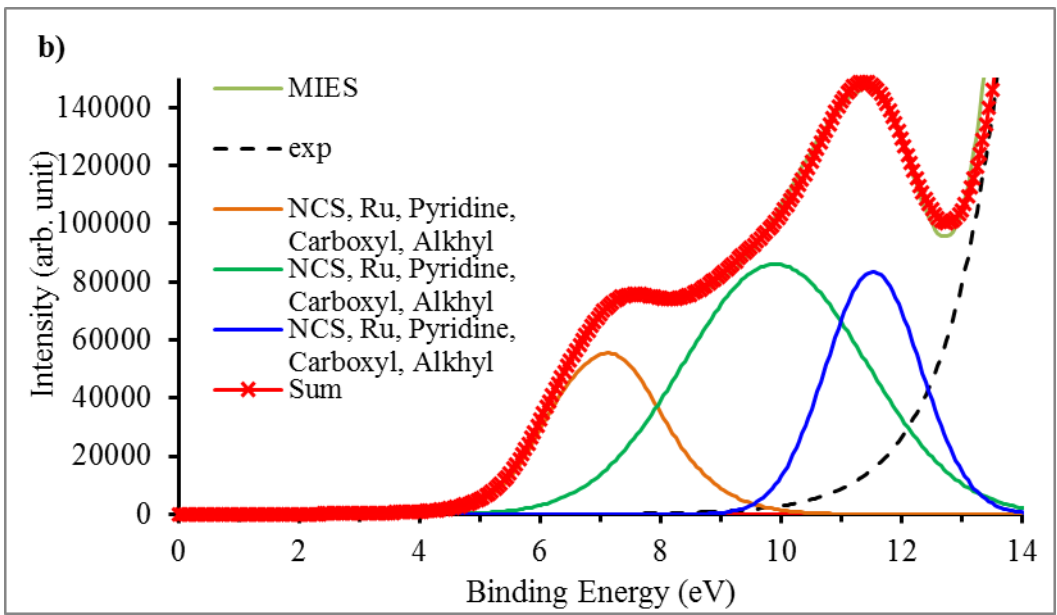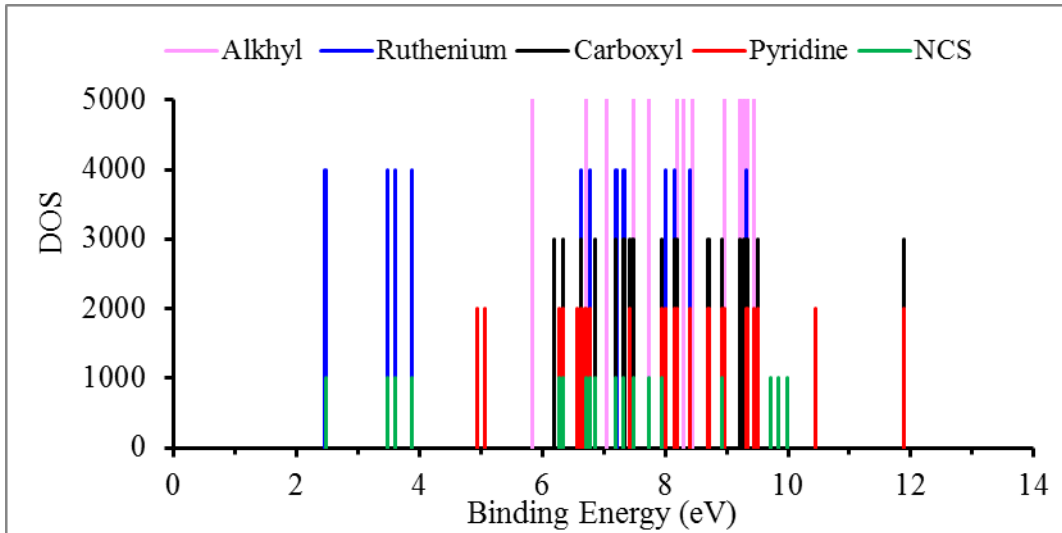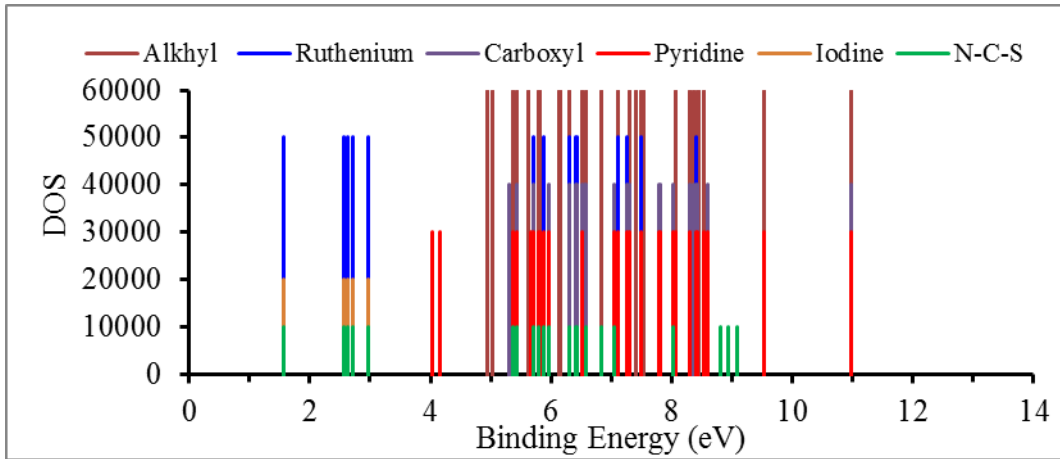
Figure 4-8. Figure molecular orbital contribution and MIE Spectrum for (a) pristine Z907 dye and (b) after immersed into the electrolyte solution with rinsing.
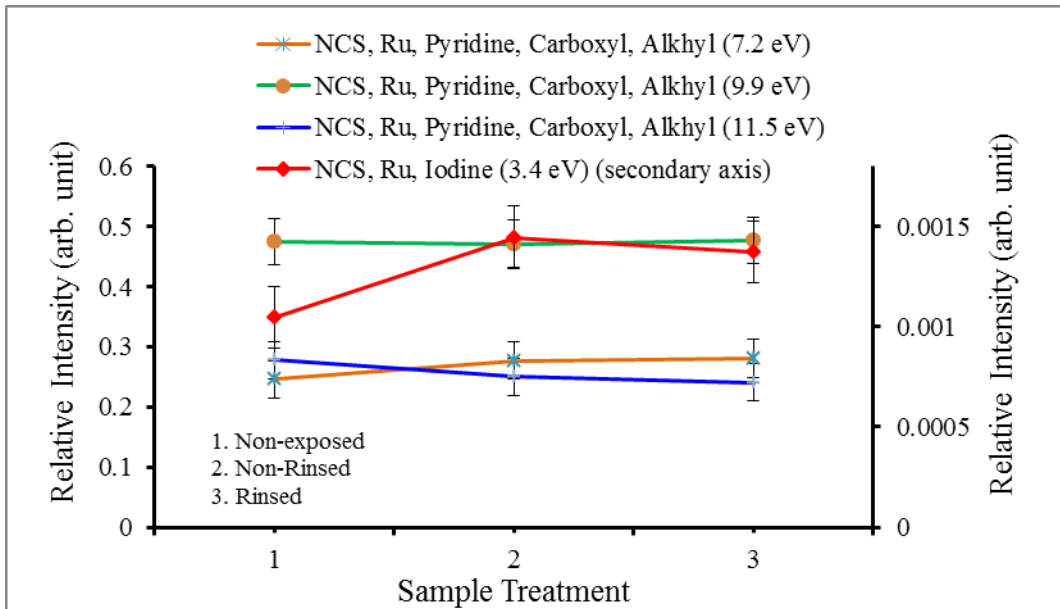
Figure 4-9 The peak changes of Z907 dye associated with the change of the relative intensity due to the Iodine exposure with rinsing and no rinsing treatment.

Table 4-6 Peak position, functional groups and relative intensity of Z907 dye MIE spectra

Peak number	Functional Group	Non-exposed		Non-Rinsed		Rinsed	
		Intensity	Position (eV)	Intensity	Position (eV)	Intensity	Position (eV)
1	NCS, Ru, Iodine	0.00105	3.4 ± 0.1	0.00144	2.8 ± 0.1	0.00137	3.3 ± 0.1
2	NCS, Ru, Pyridine, Carboxyl, Alkhyl	0.246	7.2 ± 0.1	0.277	6.6 ± 0.1	0.281	7.1 ± 0.1
3	NCS, Ru, Pyridine, Carboxyl, Alkhyl	0.474	9.9 ± 0.1	0.471	9.3 ± 0.1	0.477	9.8 ± 0.1
4	NCS, Ru, Pyridine, Carboxyl, Alkhyl	0.2781	11.5 ± 0.1	0.25	10.9 ± 0.1	0.241	11.4 ± 0.1

Each curve on Figure 4-9 is indicating the intensity changes over the treatment of the samples. The intensity changes are evaluated to determine the influence of the presence of iodine as one of the electrolyte component on the surface. It more likely seems that the

iodine molecule also goes deeper as the iodine contribution was detected on the XPS but was not detected on the UPS and MIES which indicates that the iodine is also able to reach until the dye/titania interface and produced the formation of dipole layer, therefore the work function was significantly changed. It also can be seen from Figure 4.9 that the peak occupied by NCS, Ru, and Iodine (red plot) shows intensity change due to the small contribution of iodine but less than what occur on the N719. While the other peak contributions do not show significant changes in intensity means that the change of reorientation and restructuring of the dye molecule does not occur.

4.4 Conclusion

We have investigated the effect of iodine on the dye adsorbed onto titania using electron spectroscopy. For the interacting iodine/dye system we have been able to determine the change of the dye formation due to the presence of the iodine after exposed to the electrolyte solution. For the N719 dye, the iodine goes not deeper until the dye titania interface and its presence can be observed up to the probing depth of UPS and MIES. The N719 dyes showed that due to the presence of the iodine after iodine exposure, it showed the additional peak around low binding energy in the MIE spectra. The Z907 dye on the other hand showed significant changes of the work function due to the iodine exposure. The Z907 dye does not clearly show an additional peak after iodine exposure which can be clearly associated with the presence of iodide. From considering XPS, UPS and MIES of Z907 spectra we conclude that the iodine is in a deeper layer and we assume at the dye/titania interface. The Z907 more likely formed stronger dipole layer across the dye/titania interface rather than the N719 dye. However, for the N719 dye, the more iodine on the surface, more dye molecule reorientation occurred and presence of iodide, but it does not affect significantly to the change of its work function.

References

1. O'Regan, B. and M. Gratzel, A low-cost, high-efficiency solar cell based on dye-sensitized colloidal TiO2 films. Nature, 1991. **353**(6346): p. 737-740.

2. Kroon, J.M., et al., *Nanocrystalline dye-sensitized solar cells having maximum performance.* Progress in Photovoltaics: Research and Applications, 2007. **15**(1): p. 1-18.

3. Mathew, S., et al., Dye-sensitized solar cells with 13% efficiency achieved through the molecular engineering of porphyrin sensitizers. Nat Chem, 2014. **6**(3): p. 242-247.

4.   Green, M.A., et al., *Solar cell efficiency tables (version 49).* Progress in Photovoltaics: Research and Applications, 2017. **25**(1): p. 3-13.

5.   Kong, F.-T., S.-Y. Dai, and K.-J. Wang, *Review of Recent Progress in Dye-Sensitized Solar Cells.* Advances in OptoElectronics, 2007. **2007**: p. 1-13.

6.   Li, X., et al., Measured binding coefficients for iodine and ruthenium dyes; implications for recombination in dye sensitised solar cells. Physical Chemistry Chemical Physics, 2012. **14**(44): p. 15421-15428.

7.   Zhou, D., et al., Efficient organic dye-sensitized thin-film solar cells based on the tris(1,10-phenanthroline)cobalt(II/III) redox shuttle. Energy & Environmental Science, 2011. **4**(6): p. 2030-2034.

8.   Yella, A., et al., Porphyrin-Sensitized Solar Cells with Cobalt (II/III)–Based Redox Electrolyte Exceed 12 Percent Efficiency. Science, 2011. **334**(6056): p. 629-634.

9.   Daeneke, T., et al., High-efficiency dye-sensitized solar cells with ferrocene-based electrolytes. Nat Chem, 2011. **3**(3): p. 211-215.

10. Sauvage, F., et al., *Butyronitrile-Based Electrolyte for Dye-Sensitized Solar Cells.* Journal of the American Chemical Society, 2011. **133**(33): p. 13103-13109.

11. Stergiopoulos, T., et al., *High boiling point solvent-based dye solar cells pass a harsh thermal ageing test.* Solar Energy Materials and Solar Cells, 2016. **144**(Supplement C): p. 457-466.

12. O'Regan, B.C., et al., Structure/Function Relationships in Dyes for Solar Energy Conversion: A Two-Atom Change in Dye Structure and the Mechanism for Its Effect on Cell Voltage. Journal of the American Chemical Society, 2009. **131**(10): p. 3541-3548.

13. O'Regan, B.C., et al., Catalysis of Recombination and Its Limitation on Open Circuit Voltage for Dye Sensitized Photovoltaic Cells Using Phthalocyanine Dyes. Journal of the American Chemical Society, 2008. **130**(10): p. 2906-2907.

14. Rao, C.N.R., S.N. Bhat, and P.C. Dwedi, *SPECTROSCOPY OF ELECTRON DONOR-ACCEPTOR SYSTEMS.* Applied Spectroscopy Reviews, 1972. **5**(1): p. 1-170.

15. auml, C. ther, and M. Bolte, Investigations on the Interaction Between sp2-Sulfur Atoms and Iodine Molecules Using the Cambridge Structural Database. Phosphorus, Sulfur, and Silicon and the Related Elements. **178**(3): p. 453-464.

16. Lewis, C. and D.A. Skoog, *Specrophotometric Study of a Thiocyanate Complex of Iodine.* Journal of the American Chemical Society, 1962. **84**(7): p. 1101-1106.

17. Ashour, S., Spectrophotometric microdetermination of thiocyanate and azide anions in acetonitrile using iodine. Journal of Analytical Chemistry, 1999. **54**(6): p. 538-542.

18. Splan, K.E., A.M. Massari, and J.T. Hupp, *A Porous Multilayer Dye-Based Photoelectrochemical Cell That Unexpectedly Runs in Reverse.* The Journal of Physical Chemistry B, 2004. **108**(13): p. 4111-4115.

19. Richards, C.E., et al., The Mechanism of Iodine Reduction by TiO2 Electrons and the Kinetics of Recombination in Dye-Sensitized Solar Cells. The Journal of Physical Chemistry Letters, 2012. **3**(15): p. 1980-1984.

20. Zhang, M., et al., Redox couple related influences of [small pi]-conjugation extension in organic dye-sensitized mesoscopic solar cells. Chemical Science, 2011. **2**(7): p. 1401-1406.

21. Boschloo, G. and A. Hagfeldt, *Characteristics of the Iodide/Triiodide Redox Mediator in Dye-Sensitized Solar Cells.* Accounts of Chemical Research, 2009. **42**(11): p. 1819-1826.

22. Zedler, L., et al., Ruthenium dye functionalized gold nanoparticles and their spectral responses. RSC Advances, 2012. **2**(10): p. 4463-4471.

23. Ellis-Gibbings, L., et al., Formation of N719 Dye Multilayers on Dye Sensitized Solar Cell Photoelectrode Surfaces Investigated by Direct Determination of Element Concentration Depth Profiles. Langmuir, 2012. **28**(25): p. 9431-9439.

24. Johansson, V., et al., On the correlation between dye coverage and photoelectrochemical performance in dye-sensitized solar cells. Physical Chemistry Chemical Physics, 2014. **16**(2): p. 711-718.

25. Seah, M.P. and W.A. Dench, Quantitative electron spectroscopy of surfaces: A standard data base for electron inelastic mean free paths in solids. Surface and Interface Analysis, 1979. **1**(1): p. 2-11.

26. Shirley, D.A., High-Resolution X-Ray Photoemission Spectrum of the Valence Bands of Gold. Physical Review B, 1972. **5**(12): p. 4709-4714.

27. Li, X., Z. Zhang, and V.E. Henrich, *Inelastic electron background function for ultraviolet photoelectron spectra.* Journal of Electron Spectroscopy and Related Phenomena, 1993. **63**(3): p. 253-265.

28. C.D. Wagner, A.V. Naumkin, A. Kraut-Vass, J.W. Allison, C.J. Powell, J.R.Jr. Rumble, NIST Standard Reference Database 20, Version 3.4 (web version) (http:/srdata.nist.gov/xps/) 2003.

29. G. Beamson, D. Briggs, High Resolution XPS of Organic Polymers - The Scienta ESCA300 Database Wiley Interscience, 1992.

30. G. Beamson, D. Briggs, High Resolution XPS of Organic Polymers - The Scienta ESCA300 Database, Wiley Interscience, 1992, Appendices 3.1 and 3.2.

31. Morgan, D.J., *Resolving ruthenium: XPS studies of common ruthenium materials.* Surface and Interface Analysis, 2015. **47**(11): p. 1072-1079.

32. Varughese, B., S. Chellamma, and M. Lieberman, *XPS Study of Self-Assembly of Ruthenium Dimers [((acac)2Ru)2bptz]0,+ on Hydrophobic and Hydrophilic SAMs.* Langmuir, 2002. **18**(21): p. 7964-7970.

33. Diebold, U. and T.E. Madey, *TiO2 by XPS.* Surface Science Spectra, 1996. **4**(3): p. 227-231.

34. Ji, G.-J. and Z.-M. Shi, *AFM and XPS Study of Glass Surface Coated with Titania Nanofilms by Sol-Gel Method.* Chinese Physics Letters, 2010. **27**(9): p. 096801.

35. Zangmeister, R.A., *Application of X-ray Photoelectron Spectroscopic Analysis to Protein Adsorption on Materials Relevant to Biomanufacturing.* Journal of Pharmaceutical Sciences. **101**(4): p. 1639-1644.

36. Ishii, H., et al., Energy Level Alignment and Interfacial Electronic Structures at Organic/Metal and Organic/Organic Interfaces. Advanced Materials, 1999. **11**(8): p. 605-625.

Chapter Five

Investigation of L0Br Dye Morphology on Nanoporous Titania Using Ion Spectroscopy (NICISS)

This chapter is a reformatted of the paper published in *ACS Applied Materials & Interfaces*, Year 2017, Vol. 9, Pages. 19773−19779

Author Contribution:

Herri Trilaksana: Designed and performed experiments, data analysis and interpretation, prepared the first draft of the manuscript.

Prof Gunther Andersson: Intellectual contribution in conceptualising experiment, data interpretation and revision of manuscript.

This paper publication is a collaborating research with Prof. Lars Kloo's Research Group in KTH, Sweden. Significant intellectual contribution to understanding and interpretation of result were made during my PhD, which justifies inclusion in this dissertation

5 CHAPTER FIVE: Investigation of L0Br Dye Morphology on Nanoporous Titania Using Ion Spectroscopy (NICISS)

Abstract

Organic material in dye sensitized solar cells (DSSCs) application has been intensively studied to reveal its properties, which is able to improve the performance of solar cells. Since the monolayer formation of dye plays a crucial role in electron injection from the dye into the conduction band of titania semiconductor, the attachment mode of the dye molecule needs to be investigated confirming whether the dye forms a mono layer or multilayer on the tiania. In this study, one of the organic dye namely L0Br has been sensitized on the nanoporous titania substrate deposited on the conductive ITO. By using NICISS (Neutral Impact Collision Ion Scattering Spectroscopy) as one of ion spectroscopy techniques, the morphology of sensitized dye molecules on the nano-porous titania substrate and its concentration depth profile can be determined. The analysis of the deconvoluted spectrum of the concentration depth profile of the L0Br dye shows that the dye molecules more likely form monolayer dye formation rather than multilayer.

5.1 Introduction

Organic dyes with cyanoacrylic group has been investigated because they have cis and trans transformation states in their cyano group which affects to lower the efficiency of charge transfer from donor to acceptor in molecule dye. In this study the L0 organic dye has been modified with bromine atom, thus the cis and trans transformation could be eliminated. Therefore, the presence of the bromine atom on the dye molecule (L0Br) enables ion spectroscopic technique to investigate. NICISS is an ion spectroscopy technique is able to measure the concentration depth profile of the L0Br sensitized onto mesoporus titania.

5.2 Experimental Section

5.2.1 Materials and Sample Preparation

This experiment used nanoporous titania as a substrate. The semiconductor in DSSCs is a mesoporous oxide layer composed of nanometer-sized particles that have been sintered together to allow electronic conduction. This mesoporous layers of TiO_2 were prepared using the DSL 18NR-T paste from Dyesol. The TiO_2 slurry was used as received containing 19.4% TiO2 loading with particle size averaging at 20 nm. The molecular structure of the titania paste here after the sintering process is in anatase structure[1] and prepared on a clean indium tin oxide (ITO) coated glass substrate by doctor blade method. The thickness of the layer was controlled roughly by the thickness of the tape frame used.

This experiment used a series of titania films which were sintered in an oven for 30 minutes at (450 ± 20) ^0C. The temperature was increased and decreased slowly to avoid cracking of the titania layer. The titania slurry paste contains some organic fillers, an organic plasticiser, and terpineol as solvent. These organic components are burnt off during the sintering process and control the porosity of the layer.[2]

The dye molecules (sensitizer) were adsorbed onto the surface of the metal oxide, by immersing each sample directly into a dye solution for 24 hours with the respective dye concentration subsequently after the sintering process. The range of dye solution concentration is from 0.1 mM down to 0.0025 mM and each dye solution was freshly prepared. The sample was rinsed by methanol after it was taken out of the solution. The rinsing is needed to release the L0Br molecule excess from the mesoporous titanium surface.

5.2.2 NICISS

NICISS is an ion spectroscopy technique for determining the concentration depth profiles of the elements. It is normally very capable for soft matter surfaces. Its probing depth is around 20 nm below the surface with a depth resolution of a few angstroms close to the surface area. NICISS has been employed extensively for determining the elemental concentration depth profiles at soft matter surfaces.[3] This ion spectroscopic technique utilises ionised helium atoms as projectiles and detects backscattered neutral helium atoms.[4] The energy of the backscattered projectiles is determined by their time of flight (TOF). This time of flight is detected by a detector which measured the time of the

projectile when it travels from the target to the detector. The projectiles lose their energy during the backscattering process due to their interaction with the atoms or molecules in the sample, and the energy transfer can be associated with the mass of the target atom due to the inelastic scattering between the helium ion as a projectile and the heavier atom presenting on the sample as a target atom. This first type of energy loss which associated with the target atom mass is used to identify the element from which a projectile is backscattered. Additionally, the projectiles continuously lose energy on their trajectory through the bulk due to small angle scattering from and electronic excitations of the molecules constituting the target. This energy loss, known as stopping power, and is used to determine the depth of the atom from which the projectile is backscattered. By combining these two typical energy losses, we can determine the concentration depth profiles of the elements. A typical NICISS spectrum consists of energy loss spectra for each element constituting the sample. The shape of the spectrum measured of a single element is determined by its concentration depth profile in the sample. The depth resolution of NICIS spectra are mainly influenced by small angle scattering of the projectile. The small angle scattering depends on the trajectory of the projectiles within the sample. The magnitude of the small angle scattering increases with increasing length of the trajectory. Small angle scattering of the projectile is least in the top several Å of the surface, leading to a depth resolution of only a few Å.

The spectra collected from NICISS are also influenced by the distribution of inelastic energy losses during the backscattering process and the straggling of the energy loss caused by low angle scattering and electronic excitations[5]. The inelastic energy loss during the backscattering process can be determined from the NICIS spectra of the respective elements in the gas phase. The energy loss straggling of low energy projectiles has been determined experimentally.[6]

The inelastic energy loss during backscattering and the energy loss straggling of projectiles in the bulk is known experimentally, and thus it is possible to deconvolute the measured profiles to obtain more details of the concentration depth profiles. The deconvolution is performed with a program based on the genetic algorithm [4]. In the genetic algorithm the result of the deconvolution is independent of the starting conditions of the program and that the statistical error of all suitable solution can be used to determine the error bars of the deconvoluted profile. In order to determine the energy of a projectile backscattered from an element in the outermost layer of the sample, NICIS

spectra of the elements in a low density gas jet are employed[4].

5.2.3 Spherical Nature of Titania Particles

The shape of the surface, i.e, the spherical nature of the titania particles needs to be taken into account since the porous titania substrate consists of nano-particles. However, the nano-porous titania surface is not completely flat. This physical condition cannot be neglected because the size or the nano-porous titania is significantly larger than the size of the dye molecule. Due to the curvature of the titania surface, the energy loss struggling of the spectra needs to be taken into account. The brief description of the this evaluation is that the helium ions will travel a longer path length through the dye layer than the actual thickness of this layer when impacting the surface at any point that is not the centre of a particle. Consequently, the spectra will show that bromine seemingly located at a greater depth. It means that the thickness of the dye layer is less than the depth of the atomic target shown by the evaluated spectra which does not make more sense. To address this problem, the more rational way to clarify the concentration depth profile of the dye layer on the top of titania nano-particles can be derived by taking into account the length of the projectile trajectory to the depth in the dye layer as shown in other study.[7]

L0Br dye molecule consists of a bromine atom instead of cyano-acrilic functional group. The presence of bromine in the L0Br as a heavier atom enables NICISS to determine the concentration depth profile of them. In this case, the bromine atom behaves as a spy atom to represent the presence of L0Br molecule near to the TiO_2 surface.[8]

5.3 Result and Discussion

NICIS spectra of the L0Br dye adsorbed on the porous titania is shown in Figure 5-1. Features due to the presence of the main elements constituting the samples such as carbon, oxygen, titanium, and bromine, can be seen in the spectrum. Carbon and oxygen are part of the dye and the substrate, while titanium is presenting as one component of the substrate, and bromine is representing of the dye molecules. Due to the probing depth of NICISS is less than the depth of titania in the substrate, the bromine appears as a single step with only has an onset in the TOF spectrum of the dye on the porous titania substrate as shown in Fig 5-1. This bromine peak has been used to quantify the amount of dye molecules adsorbed on substrates and also it can be used to analyse the thickness and its concentration depth profile of the adsorbed layer. The amount of nitrogen in the sample is too low to appear in the spectrum, in particular, since their signal appears on top of a large

background. The position of nitrogen on the TOF NICISS diagram is at 6,5 microsecons (shown in Figure 5-1). To separate each contributions of component, we can subtract the experimental spectrum by a polynomial function. However, it needs to be beared in mind that the polynomial function should have been fitted to the reference spectrum.[6] In this case it is the prestine titania without the dye molecules on it.
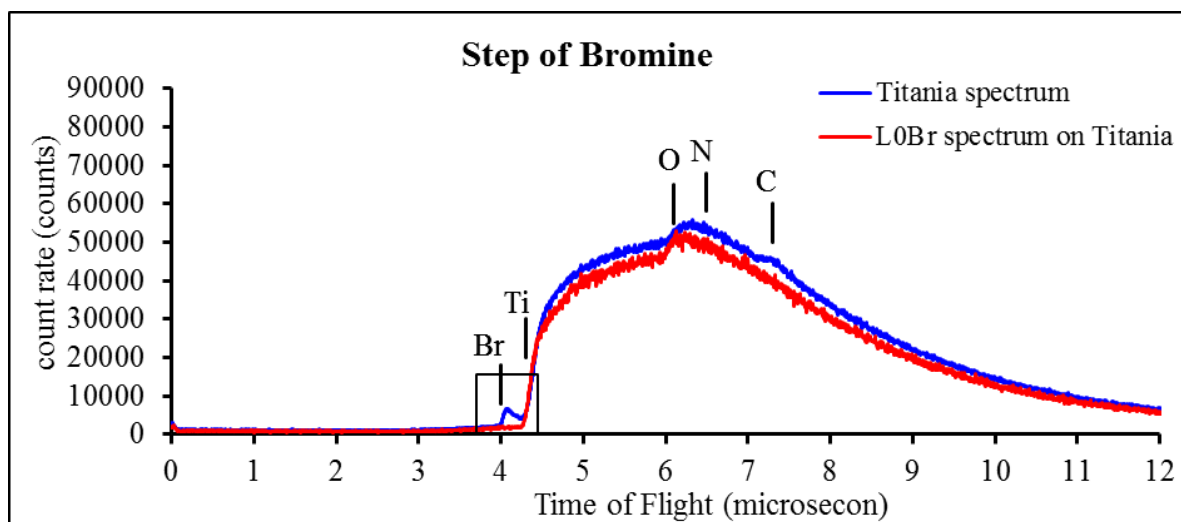
Figure 5-1. NICIS spectrum of plain nanoporous Titania and 0.1 mM L0Br on nanoporous Titania.

In general, from the concentration depth profiles of bromine the morphology of the dye including the coverage of dye molecule on the nano-porous titania, as well as the thickness of the dye and homogeneity of the dye thickness, can be determined. Determining the contribution of helium back scattered from bromine to the overall spectrum is described in the appendix section. The procedure considering the spherical shape of the substrate has been applied as well to the spectra measured here because a porous substrate has been used. The procedure is described in detail in.[7]

The surface coverage of L0Br dye on nanoporus TiO_2 has been determined by integrating the bromine concentration depth profile. The molecular coverage is plotted as a function of L0Br dye concentration is shown in Figure 5-2.
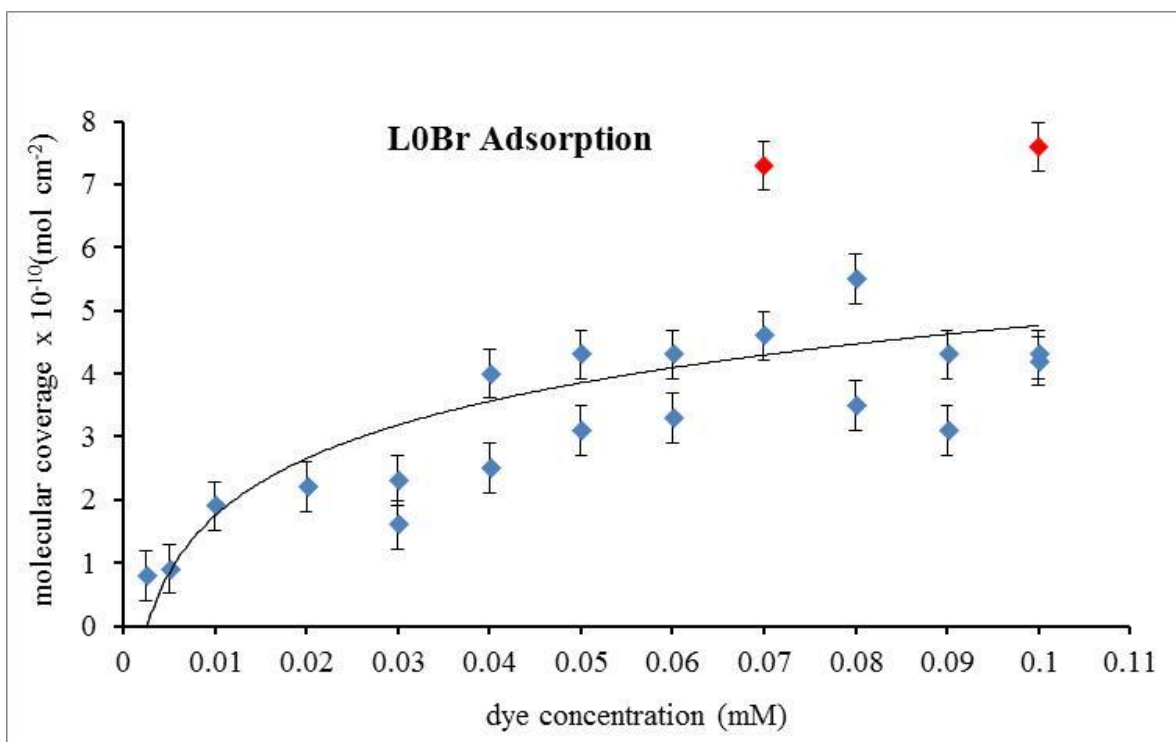
Figure 5-2 Adsorption isotherm of L0Br molecule coverage from 0.01 down to 0.0025 mM on nanoporous titania. The line is only intended to guide the eye.

In general, the plot of dye coverage increases with increasing of dye concentration and it reaches maximum coverage around 4×10^{-10} mol.cm^{-2}, which is in the dye solution concentration range 0.07 to 0.1 mM . At the lowest concentration around 0.0025 mM the coverage is around 1.2×10^{-10} mol.cm^{-2}. The plot of coverage as a linear concentration in Figure 5-2 depicts that there is still a finite coverage at the lowest concentration investigated. In addition, at higher concentration (> 0.07 mM) there are two data points with higher coverage level (red dot point). The concentration depth profiles of these measurements were distinctly different to the other concentration depth profiles showing higher concentrations at a depth > 15 Å. These concentration depth profiles show agglomeration of the dye molecules. None of the preparation conditions could be identified as origin for the agglomeration of the L0Br dye.

The concentration depth profiles determined via NICISS not only are used to determine the amount of dye adsorbed to the titania but also to confirm of the shape of the concentration depth profiles informs whether the dye adsorbs in monolayer or multilayers.[7] It is very crucial to know how the dye molecule attached on the titania rather than only knowing the amount of the dye on the titania as the molecular coverage is representing clearer about the morphology of the dye on the titania.

5.4 Conclusion

Measurement of molecular coverage for L0Br on meso-porous TiO_2 using NICISS has been carried out, and after deconvolution procedure of energy step resolution the concentration depth profile shows that L0Br dye on nano-porous titania forms mostly a monolayer with a small contribution of multilayers. The range coverage is between $1x10^{-10}$ mol·cm^{-2} and $4x10^{-10}$ mol·cm^{-2} or between 1.6 and 0.4 nm^2 per L0Br molecule. In addition, perfect monolayer dye coverage is around 0.5 nm^2 per molecule calculated in theory, which is similar to our measured molecular coverage of sample with around 0.04 mM in concentration. This fact provides the evidence that the L0Br was able to provide quicker electron transfer from dye into titania in DSSC. In term of the used dye concentration, the lowest dye concentration was still able to be detected in NICISS.

References

1. Cao Y, Cai N, Wang Y, Li R, Yuan Y, Wang P. Modulating the assembly of organic dye molecules on titania nanocrystals via alkyl chain elongation for efficient mesoscopic cobalt solar cells. Physical Chemistry Chemical Physics. 2012;14(23):8282-6.

2. Hagberg DP, Jiang X, Gabrielsson E, Linder M, Marinado T, Brinck T, et al. Symmetric and unsymmetric donor functionalization. comparing structural and spectral benefits of chromophores for dye-sensitized solar cells. Journal of Materials Chemistry. 2009;19(39):7232-8.

3. Gabrielsson E, Tian H, Eriksson SK, Gao J, Chen H, Li F, et al. Dipicolinic acid: a strong anchoring group with tunable redox and spectral behavior for stable dye-sensitized solar cells. Chemical Communications. 2015;51(18):3858-61.

4. Andersson G, Morgner H. Impact collision ion scattering spectroscopy (ICISS) and neutral impact collision ion scattering spectroscopy (NICISS) at surfaces of organic liquids. Surface Science. 1998 5/12/;405(1):138-51.

5. Ellis-Gibbings L, Johansson V, Walsh RB, Kloo L, Quinton JS, Andersson GG. Formation of N719 Dye Multilayers on Dye Sensitized Solar Cell Photoelectrode Surfaces Investigated by Direct Determination of Element Concentration Depth Profiles. Langmuir. 2012 2012/06/26;28(25):9431-9.

6. Ishii H, Sugiyama K, Ito E, Seki K. Energy Level Alignment and Interfacial Electronic Structures at Organic/Metal and Organic/Organic Interfaces. Advanced Materials. 1999;11(8):605-25.

7. Osikowicz W, de Jong MP, Salaneck WR. Formation of the Interfacial Dipole at Organic-Organic Interfaces: C60/Polymer Interfaces. Advanced Materials. 2007;19(23):4213-7.

8. Chen C, Yang X, Cheng M, Zhang F, Sun L. Degradation of cyanoacrylic acid-based organic sensitizers in dye-sensitized solar cells. ChemSusChem. 2013 Jul;6(7):1270-5. PubMed PMID: 23775933. Epub 2013/06/19. eng.

9. Heo N, Jun Y, Park JH. Dye molecules in electrolytes: new approach for suppression of dye-desorption in dye-sensitized solar cells. Scientific Reports. 2013 04/24

6 CHAPTER SIX: Photoelectron and Ion Spectroscopy Investigation on PD2 and LEG1 Dye Layer after Applied in Real Cells

Abstract

The aging process and the effects of electrolyte exposure on two different organic dyes, namely PD2 and LEG1 have been carried out. Those two effects aging process and electrolyte exposure were investigated after the working electrode sensitized by two different organic dyes had been applied in real cells. After the application for hours used as the real cells, the change in the molecular level was investigated by electron and ion spectroscopy. XPS, UPS, and MIES are capable to investigate the structure of the PD2 and LEG1 dyes as those spectroscopic techniques have different probing depth. The analysis of UPS, MIES, and XPS reveals information in molecular level corresponds to the sample such as the molecular orientation of some functional groups, the electronic structures, and the material composition of the sample. This study shows that the PD2 and LEG1 have different effect upon either the electrolyte exposure or the aging process after applied for hours in the real cells. The NICISS spectrum did not show the difference between the untreated sample and the treated one due to the absence of the heavier atom on the organic dyes PD2 and LEG1.

6.1 Introduction

The surface analysis of two organic dyes PD2 and LEG1 were necessary to be carried out to investigate what actually occurred on the surface as those two different dyes have been showing an efficient ion transfer on DSSC performance. To do this, NICISS as a surface analysis technique needs to be done upon the surface to provide the concentration depth profile of the surface. Together with the NICISS technique, Photoelectron Spectroscopy e.g. UV Photoelectron Spectroscopy (UPS) and Metastable Induced Electron Spectroscopy (MIES) are also necessary to be done through the samples confirming the structural changes on the surface of the sample after used in the real DSSC.

The NICISS experiment was run first to look at the concentration depth profile of the sample, then photoelectron spectroscopy experiments (e.g. XPS and UPS) and the most

surface sensitive technique MIES were run on ultra-high vacuum (UHV) chamber. The angle resolved XPS (ARXPS) was also run on the sample before UPS and MIES were taken. The UPS and MIES were carried out to semi-quantitatively to confirm the chemical composition and chemical bound changes.

6.2   Material section

Two organic dyes are employed in this study. PD2 dye is one of metal-free dye for DSSCs and it has N-heterocycles including pyridine as the acceptor group. It also a novel ethylene free dye which provides two carboxylic acids as a functional group, which enables a stronger adsorption of the dye to the TiO_2. It has bithiophene linker instead of ethylene to link between the donor and the acceptor unit. While LEG1 is also one of metal-free dye for DSSCs with cyanoacrylic acid as the electron acceptor and anchoring group. Some DSSCs based on a few contemporary cyanoacrylic acid based dyes display promising conversion efficiencies beyond 10%.[1] Both PD2 and LEG1 dyes are organic incorporate the donor unit from the D35 dye, which has been shown to efficiently retard electron recombination.[2] The molecular structure of PD2 and LEG1 dye are shown in Figure 6-1.
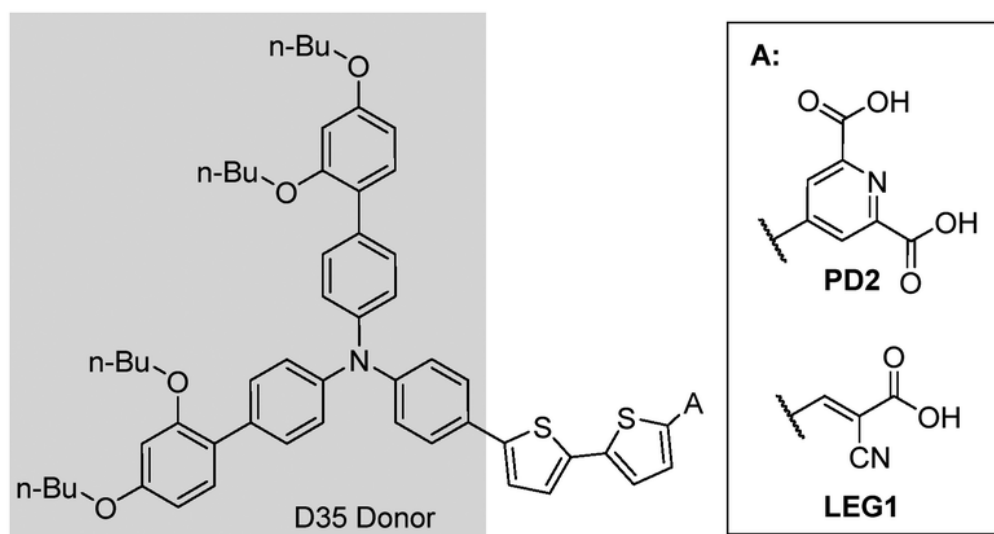
Figure 6-1. LEG1 and PD2 dye molecular structures

Two different electrolytes are used in this study. The first electrolyte is a Co(bpy)₃ based electrolyte without containing *4-tert*-butylpyridine (TBP), and the second electrolyte is containing the TBP. Previous work relates to the presence of TBP in the Co(bpy)₃ based electrolyte was showing that it can cause minor hypsochromic shift (a change of spectral band position in the absorption or emission spectrum of a molecule to a shorter wavelength) in LEG1 but it cause large shift in PD2 dye. It was thought to involve protonation of the pyridine nitrogen in PD2 dye in particular.[3]

6.3 Experimental Section

The detail for the spectroscopy techniques used in this study (e.g. XPS, UPS, MIES and NICISS has already provided in chapter 3. However, the specific configuration called ARXPS was used in this research as an effort to investigate the effect of the titania nano-porous surface. The ARXPS is Angle Resolved XPS which investigate the composition of material by analysing the kinetic energy of the electron emission from different angle thus the trajectory of the electron can are different as a function of the incident angel of the X-ray beam.

6.4 Result and Discussion

There was no significant peak appears on the NICIS spectrum before the bulk titania spectrum contribution as shown in appendix B. It is potentially due to the composition of LEG1 and PD2 dye which just consist of two sulphur atoms as the heavier atoms in bithiophene linker and the rest of the molecule is just light elements (C, H, N and O). The sufficient presence of heavier element on the target sample in NICISS leads to the evidence that the measured spectrum of bare titania and dyed mesoporous titania has no difference.

The Angle Resolved XPS (ARXPS) through PD2 and LEG1 samples in two different X ray incident angle (e.g. 0 and 55 degree) have been carried out as shown in appendix B. However, the variation of the peak intensity which indicates the percentage of each element does not show reasonable correlation of the molecular structure. It might be due to the shape or curvature of the sample surface as the nano-porous titania is not a flat surface obviously.[4] As a result, the intensity variation due to the modified x-ray incident angle is difficult to be associated to the molecular structure of both samples (PD2 and LEG1 dyes) as the curvature shape of the titania surface will affect the trajectory of the incoming projectile as a function of the position of the dye molecule relatively to the centre of titania curvature.

The work function of each sample can be determined from UPS measurement as UPS technique is capable to probe the electrons in the valence level. The value of its work function is associated to the onset of the spectrum. Table 6-1 provides the work functions of each sample.

Table 6-1 Work function of PD2 dye (A series) and LEG1 (B series)

Sample	Work Function (eV)
A2 (fresh)	3.1
3 (electrolyte 1/no TBP)	3.5
A6 (electrolyte 2/with TBP)	3.2
B1 (fresh)	3.2
B3 (electrolyte 1/no TBP)	3.8
B5 (electrolyte 2/with TBP)	3.5
B6 (electrolyte 2/with TBP)	3.4

The work function seems to have slight differences due to the exposure into either the first electrolyte or the second electrolyte. The work functions of both dyes show larger increase due to the first electrolyte immersion rather than the second electrolyte immersion. This evidence can be associated to the dipole layer formation on the dye/titania interface.

6.4.1 PD2 Dye

The fresh and the exposed sample by the second electrolyte showing a similar feature in regard of UPS and MIES spectrum among The PD2 samples. The sample exposed by the first electrolyte (A3) has a different feature, which is showing a shift of whole spectrum. This evident usually indicates the formation of dipole layer [5] between titania as a semiconductor and dye as organic material. titania and the dye interface. Fig 6-4 is showing the UP and MIE Spectra of sample A and the magnitude of 0.3 eV of the shift appears on the A3 sample.
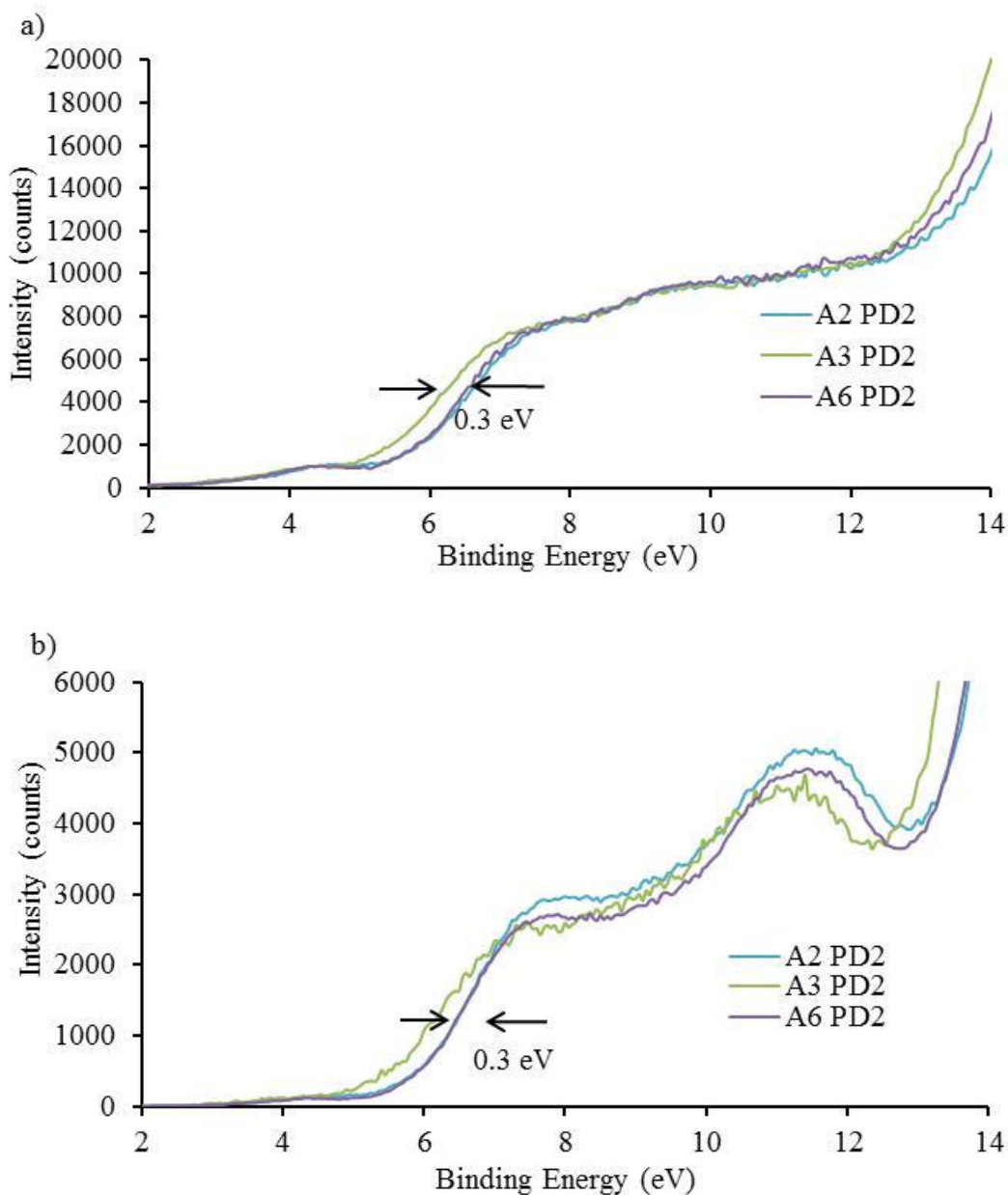
Figure 6-2. The UP Spectrum (a) and MIE Spectrum (b) of A3 sample exposed by the first electrolyte both are showing a shift about 0.3 eV.

Another feature associated with the A3 sample is that the peak contribution around lower binding energy region is decrease. This feature needs to be confirmed more detail by fitting procedure to check which orbital corresponds to this decrease. The confirmation of the fitting peak is shown on the table 6-2 for both PD2 and LEG1 dyes in section 6.4.3. While section 6.4.4 is determining its molecule orbital contribution by finding the matching peak position between theoretical and experimental data and taking into account the variation of peak intensity on MIE spectrum.

6.4.2 LEG1 Dye

LEG1 has two main features on UPS spectrum. They have reasonable peaks in lower binding energy region and more secondary electron intensity for fresh sample. By exposing into the first and second electrolytes, these features are changing by showing a slightly decrease in intensity at higher binding energy regions.

For samples exposed by the 2nd electrolyte (B6), they were forming a dipole layer[6] between the titania and the dye layer, indicated by appearing a shift of whole UPS spectrum (around 0.3 eV). In addition, the MIE spectrum undergoes a shift around 0.6 eV on these samples (the shift can be shown in Fig 6.5); however, the shift did not appear in both samples exposed into the first electrolyte (B4 sample).
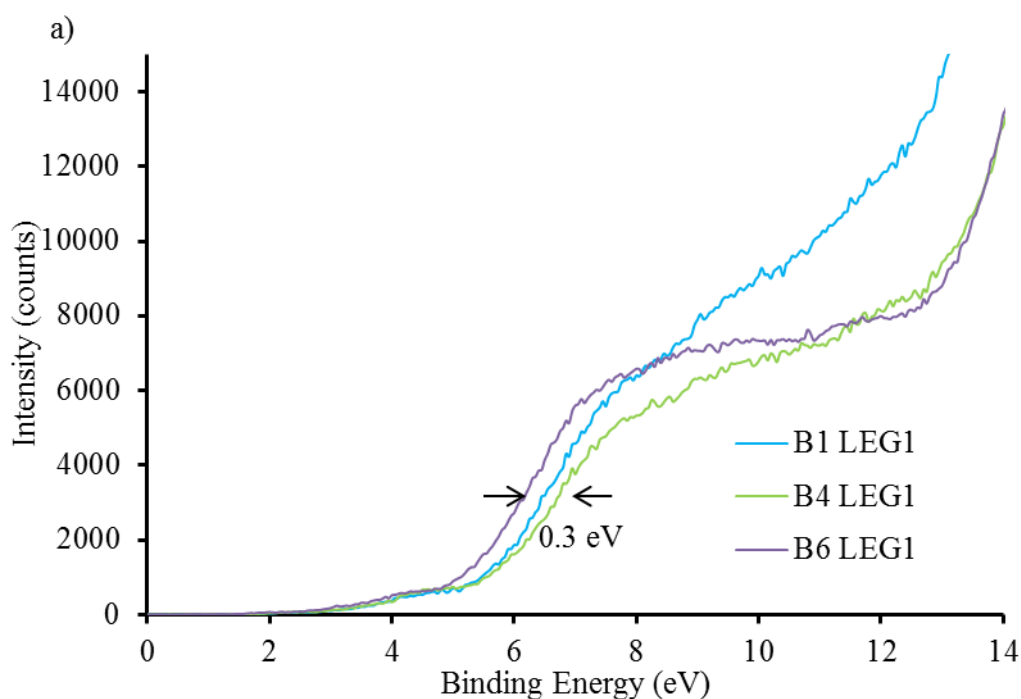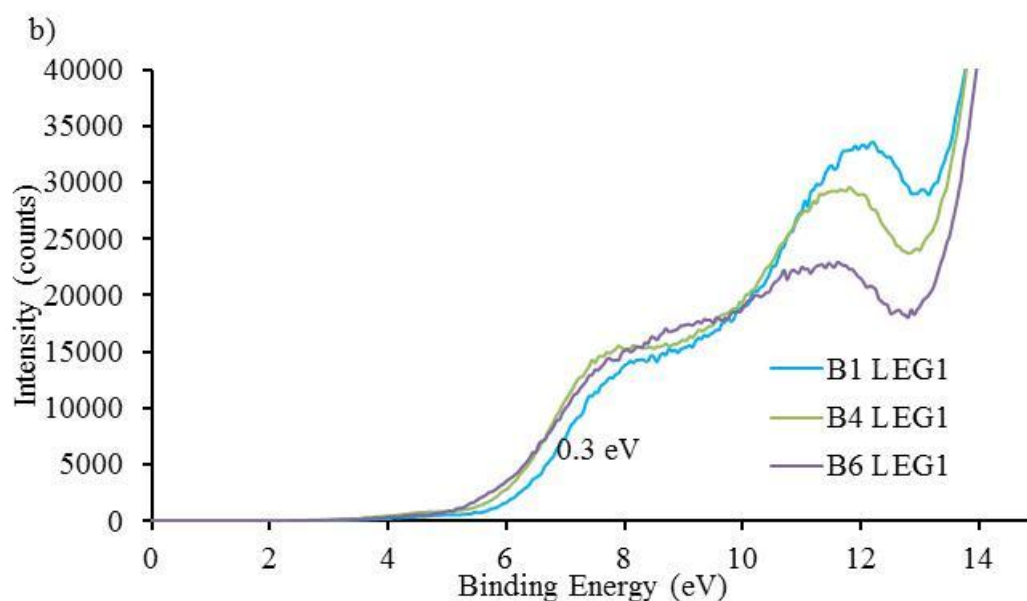
Figure 6-3. The UP Spectrum (a) and MIE Spectrum (b) for B6 samples exposed by the second electrolyte. The UP and MIE Spectra show the shift about 0.3 eV

6.4.3   Fitting Procedure

Fitting procedure enables to resolve each electron orbital contribution in the UP and MIE Spectrum. The reason why both UP and MIE spectrum need to be fitted similarly is that because the UP and MIE spectrum were taken simultaneously on the apparatus. So, the UP and MIE spectra representing the same condition of the sample. The UPS fitting needs to be done to determine the peak positions associated to which functional group while the fitting to the MIES needs to be done to determine the orientation of the represented functional group on the top most layer. On the fitting procedure, each of gaussian curves were developed in a certain position, and its FWHM, position and intensity are set as parameters which will be optimised such that the sum of those gaussian forms a curve which fit to the measured spectrum. Firstly, the spectrum obtained from the fresh dyed nano-porous TiO_2 layer is used as an experimental spectrum. Secondly, the spectrum can be obtained by applying fitting procedure through some parameters (e.g. FWHM, intensity, position, and background). Once the spectrum is well fitted, the next step is using the spectrum as a model to run the fitting procedure for other measured spectra from electrolyte-exposed samples. By comparing between the spectrum from the fresh sample and exposed sample, then it can be seen their changes or how difference they are after the electrolyte immersion.

The intensity, FWHM, and position of each sample are provided in table 6-2.

Table 6-2 Fitting peaks on both UP and MIE spectra of PD2 and LEG1 dyes

PD2 dye					
Intensity	345.61	3867.6	17966.8	2154.87	8570.52
FWHM (eV)	0.83	0.76	1.61	0.58	0.83
Position (eV)	4.52	7.29	9.63	10.92	11.99
LEG1 dye					
Intensity	803.47	841.18	6234.81	14286.8	31115.9
FWHM (eV)	1.21	0.46	0.65	1.01	1.07
Position (eV)	5.57	6.37	7.46	9.2	11.55

6.4.4 Determination of Molecular Orbital Contributions

Comparison between molecular orbital calculation and peak fitting on both UP spectrum and MIE spectrum is necessary to assign the molecular orbital contribution of electrons emitted from the valence level. This matching procedure is carried out only upon the fresh sample on PD2 and LEG1 samples. Figure 6-6 and 6-7 show each contribution attributed to corresponding molecular orbital based on the molecular orbital calculation.
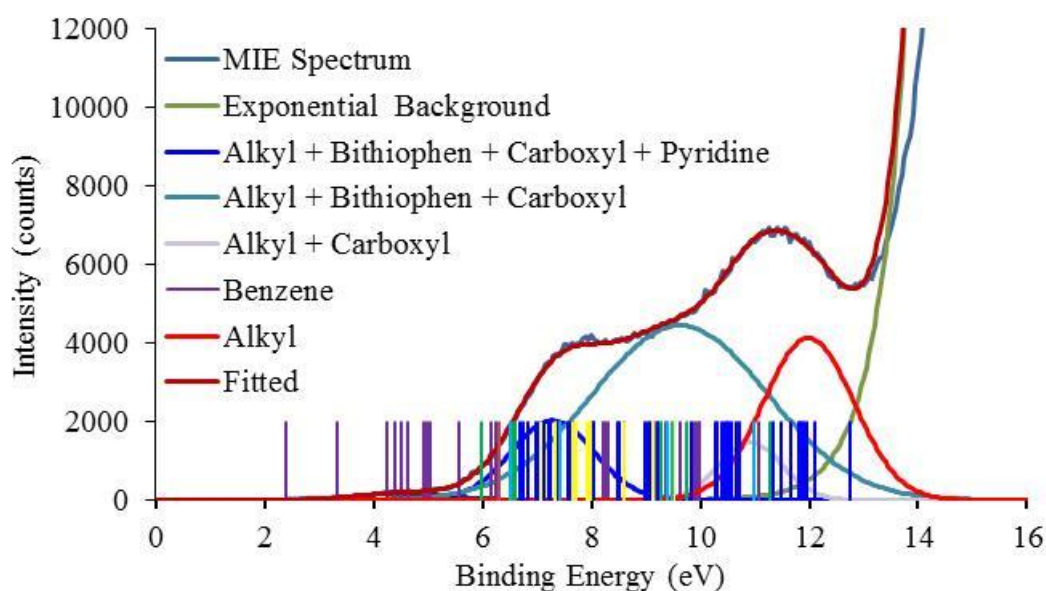
Figure 6-4. Molecular orbital contributions of MIE spectrum of PD2 dye assigned by comparing between the fitted spectrum and computational calculation.
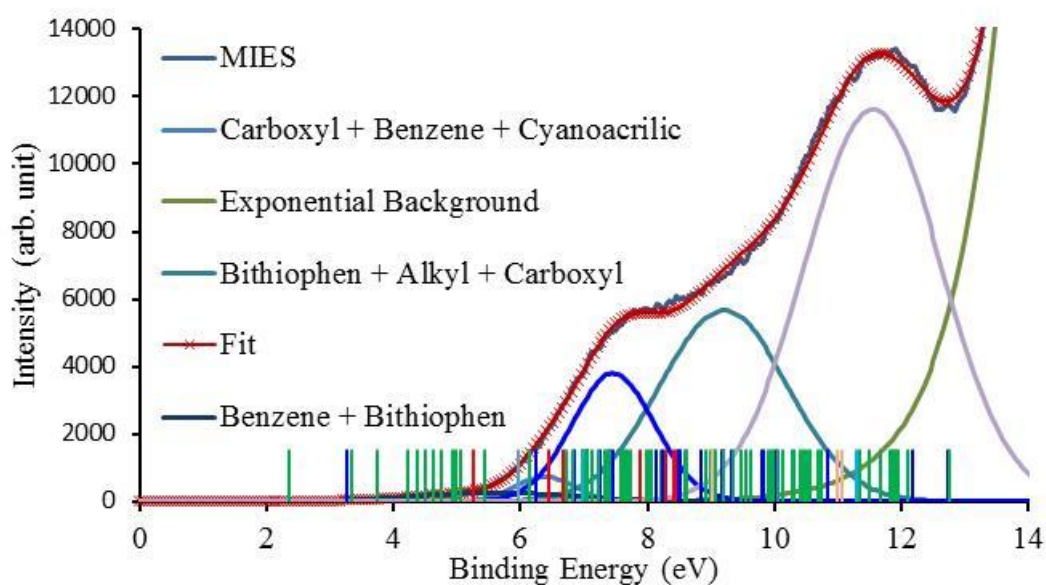
Figure 6-5. Molecular orbital contribution of MIE spectrum of LEG1 dye assigned by comparing between the fitted spectrum and computational calculation.

There are some main features on MIE spectra on PD2 dye samples. From the fitted MIE spectrum of PD2 dye (Figure 6-6), the first molecular orbital contribution in lower binding energy seems to be associated to benzene ring and bithiophene functional group. The second peak contribution can be associated to alkyl, bithiophene, carboxyl, and pyridine. Then the third peak is occupied by alkyl, bithiophene, and carboxyl functional group. Alkyl and carboxyl contribute again on the fourth peak then alkyl also occupied the fifth peak as well besides the bithiophene.

The interpretation of each peak contribution needs to be interpreted more detail as the following. The most dominant contribution of alkyl in PD2 dye molecule was presumed that this functional group equally spreads out around the D35 molecule as a donor unit which is the largest molecule. It can be seen that the intensity variation of PD2 dye due to the immersion into the electrolyte 1 did not show significant changes (Figure 6-8). It is found that the electrolyte 1, which is not containing TBP, does not affect to the PD2 dyed meso-porous titania structure. The stability of peak 1 and 3 relates primarily to the bithiophene ability to maintain a stable dye molecule attachment on the meso-porous titania as the first and the third peaks are occupied by bithiophene functional group. This phenomena could be verified to the previous study that the replacement of the previous linker as ethylene group by the bithiophene as a novel linker enables better dye stability under illumination.[7]

A few changes occur on the second, fourth, and fifth peak contributions due to the immersion into the electrolyte 2. The slightly increased intensity on peak 2 contribution can be associated to the increasing of the pyridine functional group contribution since the alkyl, bithiophene, and carboxyl are not showing significant changes in peak 1 and peak 3. This increase could be accounted that additional pyridine was adsorbed on the surface. Therefore the intensity of the peak 5 which occupied by bithiophene is decreasing because of the presence of pyridine from the electrolyte 2 (Figure 6-8).
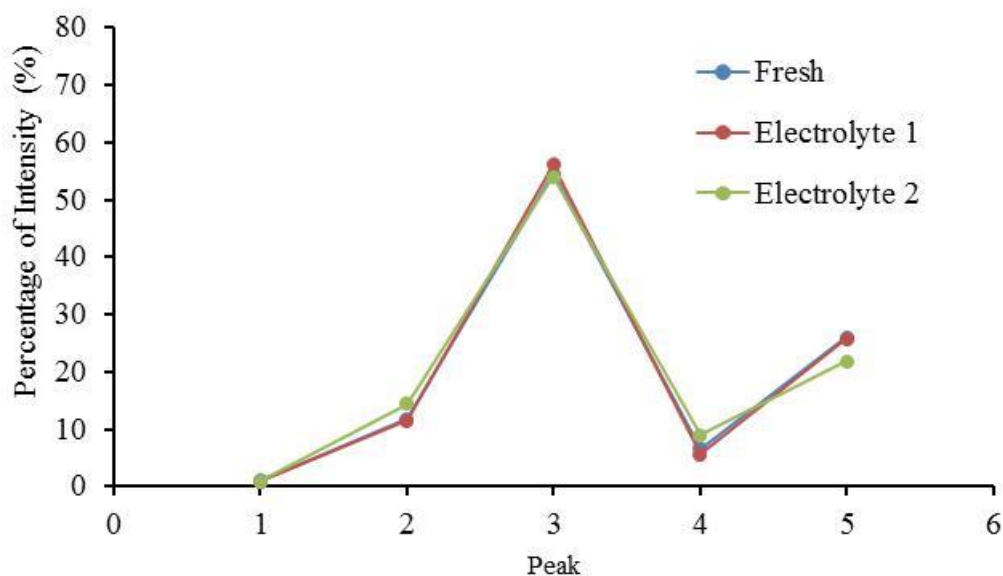
Figure 6-6. Variation of MIES peak Intensity of PD2 dye
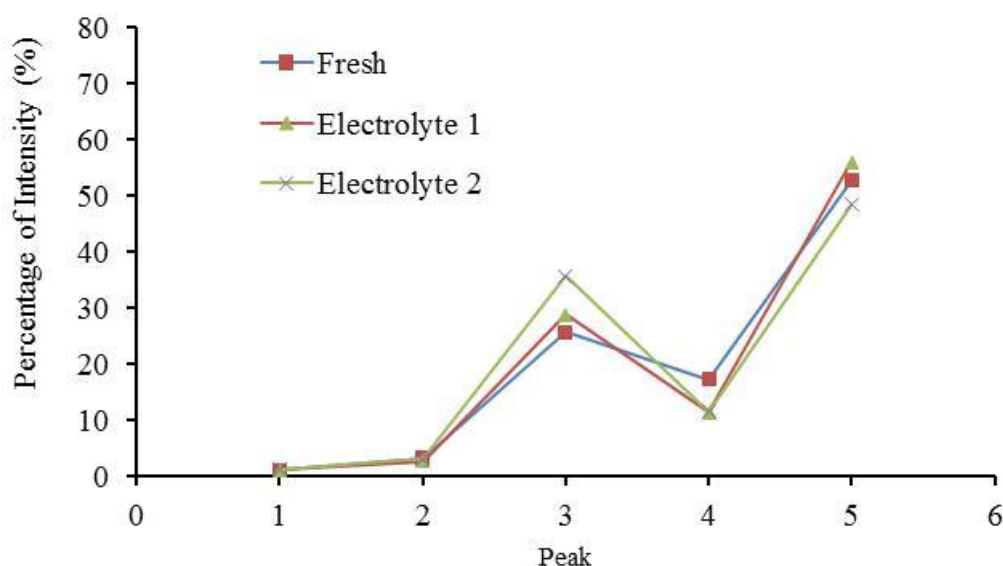
Figure 6-7. Variation of MIES peak intensity of LEG1 dye

The LEG1 main feature is showing some changes of peak contributions. From the fitted MIE spectrum of LEG1 dye (Figure 6-9), the first molecular orbital is occupied by

benzene and bitiophene. The second peak consists of carboxyl, benzene, and cyanoacrylic functional group. The third peak contribution can be associated to benzene, carboxyl, alkyl, and bithiophene. Then the fourth and the fifth peak is occupied by bithiophene, alkyl, and carboxyl functional group.

A significant increase of the peak 3 contribution in LEG1 dye (Fig 6-9) could be estimated as carboxyl contributions, because alkyl is the most dominant ligand, which potentially affects uniformly to all peak contributions. Another reason is due to the carboxyl presence contribution. The carboxyl contribution occupied on three unstable peaks namely peak 3, peak 4, and peak 5. Bithiophene as a linker does not show clear contribution upon peak 4 and 5 as it shows very stable contribution in peak 1. This evidence supports the contribution of carboxyl to the variation of peak 3, 4, and 5.

By immersing into the electrolyte 1, from XPS spectrum it can be seen that the intensity of titania is increasing significantly from 6 to 7.80 which accounted to dye desorption as the sulphur is slightly reduced from 0.48 to 0.32 per cent. In addition, as shown in MIE spectrum, the peak 4 decreases significantly and it can be estimated that the linker (bithiophene functional group) is decreasing because of the dye desorption. It also indicates that the increased contributions of peak 3 and 5 are more likely due to the appearance of donor and acceptor (benzene and carboxyl functional group) where from the XPS the nitrogen as part of the donor (D35) is increasing from 1.53 to 1.74 per cent. This is also can be estimated that the donor and the acceptor are closer to the surface rather than that of the contribution of the linker functional group. It also supports that single carboxylic ligand as the anchoring group in cyanoacrylic acid based dye such as LEG1 dye relates primarily to desorption of the dye, which has been shown to have a large effect on the long-term device performance.[8]

In contrast, by evaluating the XPS it can be seen that after immersing into the electrolyte 2 the percentage of nitrogen increases from 1.53 to 6.57 per cent and the percentage of titanium decreased from 6 to 4.06 percent. This nitrogen is most likely from the pyridine functional group in the electrolyte 2, which contains TBP and it was adsorbed on the surface thus the percentage of titania is decreasing significantly. As a result, the MIE spectra could be interpreted that the increased contribution in peak 3 correspond to the presence of the pyridine on the surface while the decreased peak contributions in peak 4 and 5 correspond to less linker contribution as the percentage of sulphur decreases from 0.48 to 0.35 per cent in XPS. The XPS result is provided in the Appendix B.

6.5 Conclusion

The effect of the electrolyte and aging process to the organic dye also has been investigated using electron spectroscopy (XPS UPS and MIES). As part of XPS technique, the Angle-Resolved XPS (ARXPS) through PD2 and LEG1 samples in two different X-ray incident angle (e.g. 0 and 55 degrees) has been carried out. However, the variation of the peak intensity which indicates the percentage of each element does not show a reasonable correlation of the molecular structure due to the structure of the nano-porous titania as a substrate might not be completely flat. It was shown that the work function of both dyes increased due to the electrolyte exposure. The LEG1 showed a larger change of work function than that of the PD2 dyes. The effect of the second electrolyte exposure, however, formed less dipole layer on both PD2 and LEG1 dyes, than that of the electrolyte with the TBP. As a consequence, the work functions have also changed larger due to the exposure of the second electrolyte than that of the first electrolyte without the TBP. Reorientation of the dye molecules was also occurring for both dyes due to the electrolyte and aging process.

References

1.   Cao, Y., et al., *Modulating the assembly of organic dye molecules on titania nanocrystals via alkyl chain elongation for efficient mesoscopic cobalt solar cells.* Physical Chemistry Chemical Physics, 2012. **14**(23): p. 8282-8286.

2.   Hagberg, D.P., et al., *Symmetric and unsymmetric donor functionalization. comparing structural and spectral benefits of chromophores for dye-sensitized solar cells.* Journal of Materials Chemistry, 2009. **19**(39): p. 7232-7238.

3.   Gabrielsson, E., et al., *Dipicolinic acid: a strong anchoring group with tunable redox and spectral behavior for stable dye-sensitized solar cells.* Chemical Communications, 2015. **51**(18): p. 3858-3861.

4.   Ellis-Gibbings, L., et al., *Formation of N719 Dye Multilayers on Dye Sensitized Solar Cell Photoelectrode Surfaces Investigated by Direct Determination of Element Concentration Depth Profiles.* Langmuir, 2012. **28**(25): p. 9431-9439.

5.   Ishii, H., et al., *Energy Level Alignment and Interfacial Electronic Structures at Organic/Metal and Organic/Organic Interfaces.* Advanced Materials, 1999. **11**(8): p. 605-625.

6.   Osikowicz, W., M.P. de Jong, and W.R. Salaneck, *Formation of the Interfacial Dipole at Organic-Organic Interfaces: C60/Polymer Interfaces.* Advanced Materials, 2007. **19**(23): p. 4213-4217.

7.   Chen, C., et al., *Degradation of cyanoacrylic acid-based organic sensitizers in dye-sensitized solar cells.* ChemSusChem, 2013. **6**(7): p. 1270-5.

8.   Heo, N., Y. Jun, and J.H. Park, *Dye molecules in electrolytes: new approach for suppression of dye-desorption in dye-sensitized solar cells.* Scientific Reports, 2013. **3**: p. 1712.

7 CHAPTER 7: Cooperative Adsorption of the Dye N719 and Chenodeoxycholic Acid on Titania

Abstract

The effects of the co-adsorbent Chenodeoxycholic Acid (CDCA) up to a concentration of 20 mM on the adsorption of the dye N719 have been investigated using Neutral Impact Collision Ion Scattering Spectroscopy (NICISS). It is shown that the co-adsorption of CDCA changes the adsorption mode of N719 from multilayer toward monolayer. FTIR absorption spectroscopy shows that the adsorption of CDCA increases with increasing CDCA concentration. In contrast, the amount of N719 adsorbed onto titania shows a minimum at 10 mM CDCA and the relationship between the amount of CDCA and of N719 adsorbed onto titania depends non-monotonically on the CDCA concentration. The co-adsorption of CDCA and N719 can be described as cooperative. The effect is observed for both low and high N719 concentrations.

7.1 Introduction.

The most attractive properties of dye sensitized solar cells (DSSCs) in relation to other types of solar cells are their potential low-cost and simple manufacturing processes together with numerous advantageous attributes like lightweight, environmentally benign materials, and excellent performance also in diffuse light conditions[1]. DSSCs are based on sensitizing dyes for converting solar energy into electrical energy. Photons absorbed by the dye molecules promote electrons from the occupied to the unoccupied electron energy levels which are then transferred to the titania together forming the photoanode of the DSSCs. The oxidised dye is then regenerated from the cathode via the electrolyte solution. Optimising dye adsorption onto the titania is therefore of paramount importance. Both dye load and dye organization on the titania support surface will affect the amount and efficiency by which photoexcited electrons will contribute to the photocurrent.

Adding co-adsorbents like chenodeoxycholic acid (CDCA) and phosphonic acid is known to improve the efficiency of DSSCs[2]. It is assumed that the reason for the increase in

efficiency is the change in conformation, in terms of a reduced tendency to aggregation, of the dye layer due to the presence of the co-adsorbent[3].

A crucial structural aspect of the dye layer is whether or not the dye molecules form monolayers or multilayers on the titania electrode surface. While it is unclear how the formation of dye monolayers or multilayers on titania can be influenced, it is also discussed [4] whether or not the dye molecules actually form monolayers or multilayers. In recent studies we have applied the depth profiling method Neutral Impact Collision Ion Scattering Spectroscopy (NICISS) with results showing that the Ru based dye molecules N719 and Z907 form multilayer islands while the organic dye L0Br rather is adsorbed in monolayers.[4, 5]

One of the compounds frequently used as co-adsorbent in DSSCs is CDCA, which is a saturated polycyclic molecule with a sterol group separated from the carboxylic acid (anchoring) group by a 4-carbon chain[6] as shown in Figure 7-1(b). CDCA is expected to bind to TiO_2 via the carboxylic acid group.[7] It is assumed that CDCA is promoting the formation of dye monolayers rather than multilayers by reducing dye aggregation. However the influence of CDCA on the formation of the Ru based dye layers on titania has not been studied and the role of CDCA in DSSCs is still under discussion. Other suggested roles of CDCA in DSSCs include shifting the TiO_2 conduction band edge and shielding the TiO_2 surface retarding electron recombination loss reactions with the oxidized species in redox electrolyte[8]. Interesting studies employing N719 and CDCA as co-adsorbent has been carried out by Cisneros[9] and Salvatory.[7] However they only analysed the change of the total light absorption of the photosensitized electrode in the presence of CDCA. Cisneros found a decrease in total light absorption and conversion of the dye giving evidence for a competition between CDCA and dye for adsorption onto the substrate surface. This observation was associated with the crucial factor of the cell performance improvement, such as the photocurrent conversion efficiency (PCE) and retardation of the recombination rate between photo-injected electrons and the oxidized mediator (shield effect). From FT-IR analyses they found that the CDCA could also possibly be creating a bulky insulating network, such as a strong shield effect, on the TiO_2 surface.[7, 9] It was shown that the CDCA had a stronger effect than bis(4-methoxyphenyl) phosphinic acid (BMPP) on reducing the interaction between two neighbouring sensitizer (dye) molecules attached to the surface of titania (an anti-π-stacking effect).[9] The authors

also made computational modeling of CDCA on titania and found that the agglomeration of dye molecules on the titania is energetically favourable.

Co-adsorption as such is also of more general interest because in complex systems close to reality co-adsorption onto surfaces and interfaces never involve adsorption of a single substance. Such systems are normally confined to model systems for systematic laboratory studies. In this sense, DSSCs can be considered as a system closer to real systems in terms of adsorption complexity.

Domain formation is typically observed at liquid surfaces of binary surfactant systems forming islands when differences in surface energy are large. It has been found that 1-palmitoyl-2-oleoyl-sn-glycero-3-phosphocholine (POPC) and cholesterol mutually influence the adsorption of each other at surfaces of polar liquids.[10] Levy et al. have found that cholesterol and phospholipids form domains in biological membranes, and it is assumed that the weak interaction with the substrate plays a role in the domain formation.[11] Miao et al. have shown that in the adsorption of self-assembled monolayers onto solid substrates both molecule–substrate interaction and solvent effects play a role in the formation of bi-molecular layers.[12] Woodruff came to a similar conclusion in his review covering, amongst other themes, co-adsorption onto surfaces published in 2002.[13] Ootani et al. investigated co-adsorption in DSSCs and concluded that the energy levels and the molecular orbital distribution did not change upon co-adsorption of components forming the sensitizing layer in DSSCs.

The aim of the present work is to investigate how the presence of CDCA as co-adsorbent in the dye solution for photoelectrode adsorption influences the formation of the Ru-based N719 dye layer adsorbed onto titania. In particular, the study is aimed to investigate how the presence of CDCA influences the amount of N719 adsorbed onto the titania and whether or not the adsorption of the CDCA influences the formation of multilayer N719 islands. NICISS has been applied to determine the amount of dye adsorbed in multilayers. It will be shown that in the co-adsorption process of CDCA and N719 both substances strongly influence the mutual adsorption on the titania surface. The co-adsorption process can be characterised as being cooperative. Such cooperative co-adsorption is of general interest and will have impact on the understanding of co-adsorption processes in general.

7.2 Experimental Section

7.2.1 Material
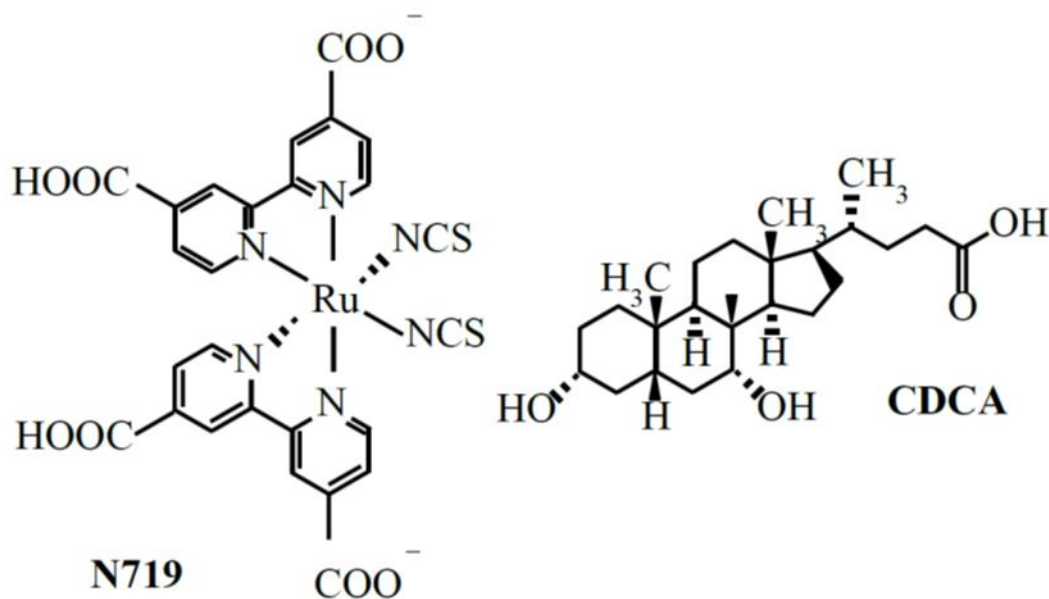
Figure 7-1. (left) N719 and (right) chenodeoxycholic acid (CDCA) molecular structures.

The CDCA was purchased from Sigma Aldrich and was used without further purification. Titania DSL18NR-T paste was purchased from Dyesol (Australia). Also the N719 dye powder was purchased from Dyesol, Australia. The molecular structures of N719 and CDCA are shown in **Error! Reference source not found.**.

7.2.2 Sample Preparation and NICISS measurement

The titania DSL18NR-T paste contains 19.4% TiO_2 with an average particle size of 20 nm. Nanoporous titania films were made by a standard doctor blade and sintering procedure[4, 14]. The TiO_2 films were sintered at 450 ^{o}C for 30 minutes to burn the organic filler. Indium doped tin oxide (ITO) coated glass slides were used as the substrate, obtained from Kintec (China) with 1.1 mm in thickness and sheet resistivity of 15 ohm/sq.

The nanoporous titania films were immersed into N719/CDCA ethanol solutions. N719 solutions used were of two different concentrations (0.1 mM and 0.005 mM). The two dye concentrations were chosen such that one (0.1 mM) is close to the concentration used as a standard in the fabrication of DSSCs, and the other concentration (0.005 mM) is low as compared to standard dye concentrations. Freshly made solutions were consistently used. The CDCA in 1:1 volume ratio concentration was of 0 mM to 20 mM in steps of 5 mM.

Firstly, two solutions of N719 and CDCA with the same volume were prepared. Subsequently, both solutions were mixed and thus the volume of the solution doubled. The concentration of the initial solutions was chosen such that the above listed concentration of the final solutions were achieved. Then, the titania films were immersed into the dye solutions for 24 hours with or without the CDCA present. Finally, the dye-coated sample was rinsed with ethanol to remove excess dye weakly bound to the surface. Subsequent to fabrication, samples were investigated with NICISS. A plain titania sample was used as reference sample for the NICISS measurements.

7.2.3 NICISS

NICISS usually uses He ions (He^+) as a projectile and is described in detail in[15] and will be described here briefly. In the present work He^+ with a primary energy of 3 keV have been used to bombard the sample. The time of flight of backscattered projectiles is measured to determine their energy. During the backscattering process, the projectiles undergoes energy loss processes and the energy transfer from the ion to the target depends on the mass of the target atom. This first type of energy loss is used to identify the element from which a projectile is backscattered. Projectiles backscattered from deeper layers also experience a continuous energy loss when they pass through the bulk because of small angle scattering and electronic excitations when passing by of the atoms forming the target. This second type of energy loss is called stopping power and is used to determine the depth of the atom from which the projectile is backscattered. Combining both types of energy loss, the concentration depth profile of the elements in the sample can be determined. NICISS has also been used before to investigate liquid samples[16], polymer surfaces and thin organic layers. Generally, a NICISS spectrum consists of energy loss spectra for each element in the sample. The shape of the spectrum of each element is determined by its concentration depth profile in the sample. The depth resolution of NICISS spectra is mainly influenced by small angle scattering of the projectile while on its trajectory through the bulk, which increases with trajectory length. Therefore, in the top several Å of the surface this effect is minimal, leading to a depth resolution of only a few Å. The spectra are also influenced by the distribution of inelastic energy losses during the backscattering process and the straggling of the energy loss caused by low angle scattering and electronic excitations[15] related to charge exchange mechanisms leading to the neutralization of the projectile, such as the auger neutralization and de-excitation

processes and more likely excitations to bound states with subsequent radiative decay are possible.

For a NICISS measurement, the dyed titania sample is placed on a rotating sample holder in the NICISS apparatus to prevent the surface damaging due to the helium on bombardment. The dose for the measurements was kept below a dose of 5×10^{13} ions/cm^2. The TOF spectrum for each sample is measured. The contribution of each element to the spectra are isolated from the spectra and converted into concentration depth profiles as described in detail in.[4, 17]

7.3   Result and Discussion

7.3.1   Results

Figure 7-2 shows the concentration depth profiles of samples prepared from exposure to solutions with 0.005 and 0.1 mM N719 and with CDCA concentrations from 0 to 20 mM. In Figure 7-2, the Ru NICIS spectra are shown as energy loss spectra and not as concentration depth profiles. The reason is that the changes of the spectra with the change of the CDCA concentration can be demonstrated more directly using energy loss spectra rather than the concentration depth profiles, because the former is more related to the path length of the projectile. The titania surface onto which the N719 molecules have been deposited is not flat. Therefore, determining the correct concentration depth profiles requires a deconvolution procedure as demonstrated in reference.[18]

Figure 7-2 also shows that an energy loss of 0 eV corresponding to the surface of the dye layer, which has been established in previous publications.[18] Increasing energy loss means increasing depth. The energy loss spectra in Figure 7-2 show that the region between 10 and 30 Å decrease in intensity indicating that the amount of dye molecule is lower upon CDCA application.
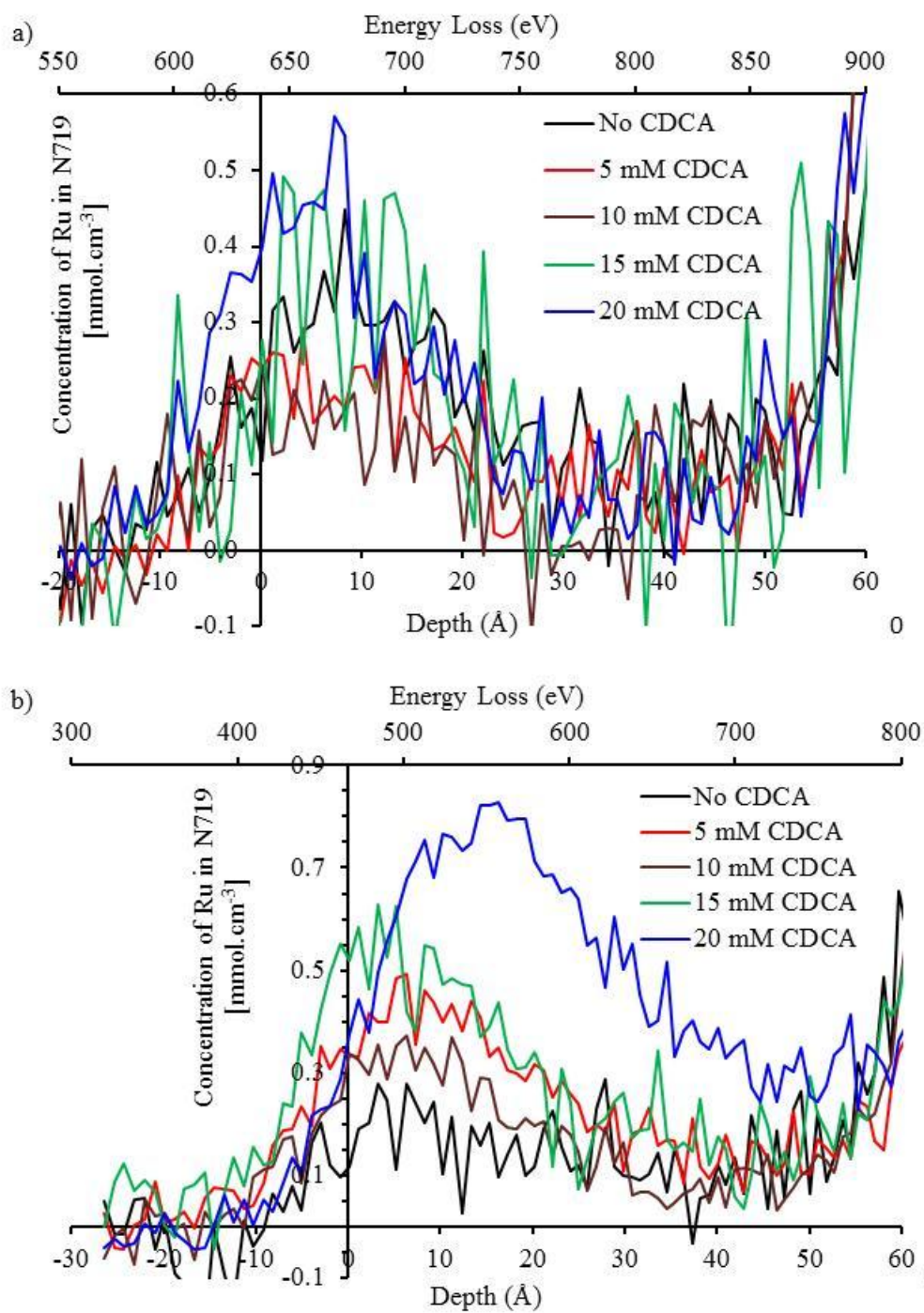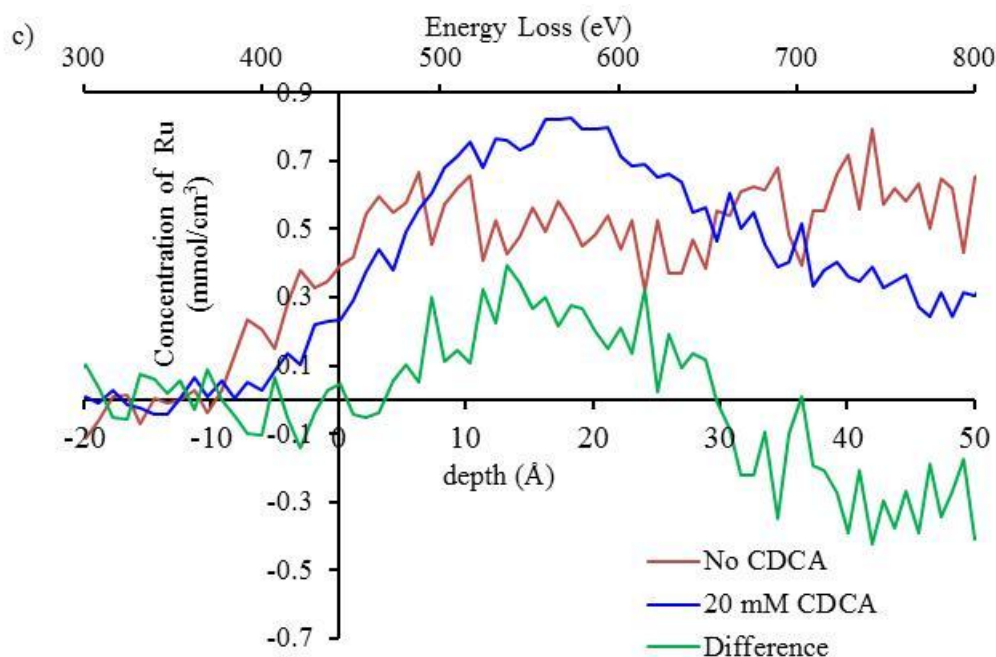
Figure 7-2: Path lengths of the projectiles as a function of energy loss for low dye solution concentration (a) and high dye solution concentration (b). Significant decrease of multilayer formation after exposure to 20 mM CDCA (c). The depth scale is shown as well to give an indication of the approximate depth.

In Figure 7-2c Ru NICIS spectra of surfaces exposed to 0.1 mM N719 with 0 mM and 20 mM CDCA are shown, as well as the difference between the spectra. The difference shows that in the spectrum from a pure N719 solution, the ruthenium is found at larger depths as compared with the spectrum from a surface exposed to the solution also containing 20 mM CDCA. This observation means that N719 multilayers are formed to a lesser degree when CDCA is added to the solution. This is also demonstrated by the difference in the spectra, shown as green line. The difference is positive between 0 and 170 eV loss energy (approximately 0 and 20Å in depth) upon addition of the co-adsorbent, while the difference is negative in the region larger than 30 Å (270 eV energy losses). This difference in the energy loss profiles and concentration depth profiles, respectively, highlights a decrease in the formation of multilayers upon addition of CDCA. Overall, the amount of dye adsorbed to the titania is unchanged.
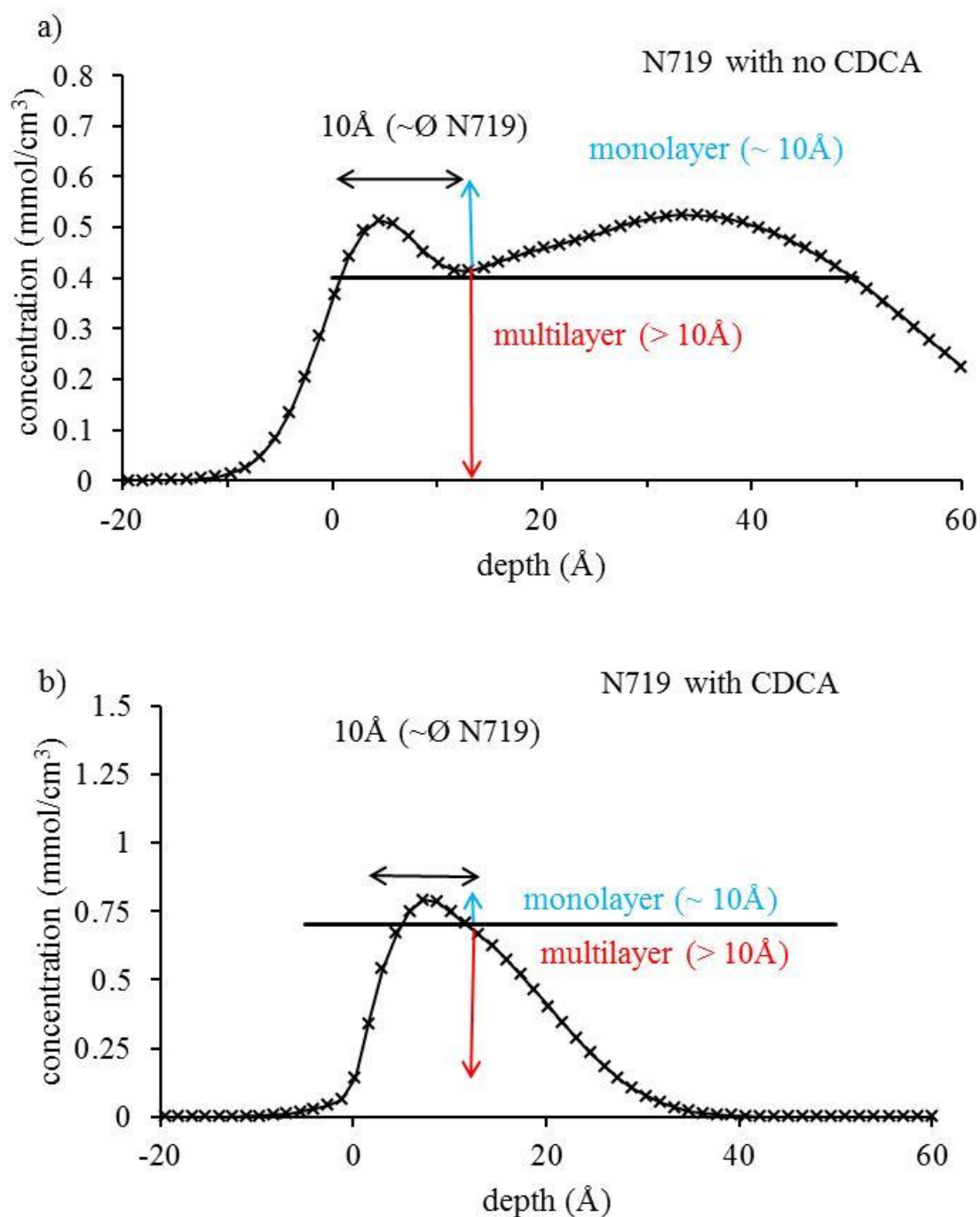
Figure 7-3: Concentration depth profile of N719 after correcting for the spherical shape of the titania particles forming the substrate and deconvolution of the concentration depth profiles. In a) the concentration depth profiles of Ru for surfaces exposed to solutions containing 0 mM CDCA is shown, and in b) the Ru concentration depth profile when exposed to a solution containing 20 mM CDCA.

The profiles shown on Figure 7-3 are the concentration depth profile of the dye after taking into account the spherical shape of the titania particles forming the substrate and also after deconvolution for the energy resolution.

Figure 7-3 also clearly shows how the presence of CDCA in the dye bath affects the morphology of dye layer formed on the titania. The vertical line at 10 Å is a guideline, approximately corresponding to the molecular size of N719, suggesting that at this thickness the dye is adsorbed preferably as monolayers. As we can note, the concentration depth profile decreases significantly in the region >30 Å for the surfaces exposed to a dye bath containing 20 mM CDCA.

If we compare this result with the previous work by Ellis-Gibbings et al[4], the concentration depth profile of dye layer formed from a solution of N719 with no CDCA added in this study, there are some differences. There is a larger contribution of dye multilayers in this study as compared to our previous work. The measurements in this work were reproducible, as well as the measurements in our previous work. Thus, it is not clear which parameter is causing the difference in concentration depth profiles of the dye. However, the main results from the present and past work are not affected by this difference. The main finding is that the thickness of the multilayer decreases upon addition of CDCA in the dye solution used. It should also be noted that the dye multilayer region of the surface exposed to a solution containing 20 mM CDCA is smaller in thickness than in our previous work.[4]

a)

b)
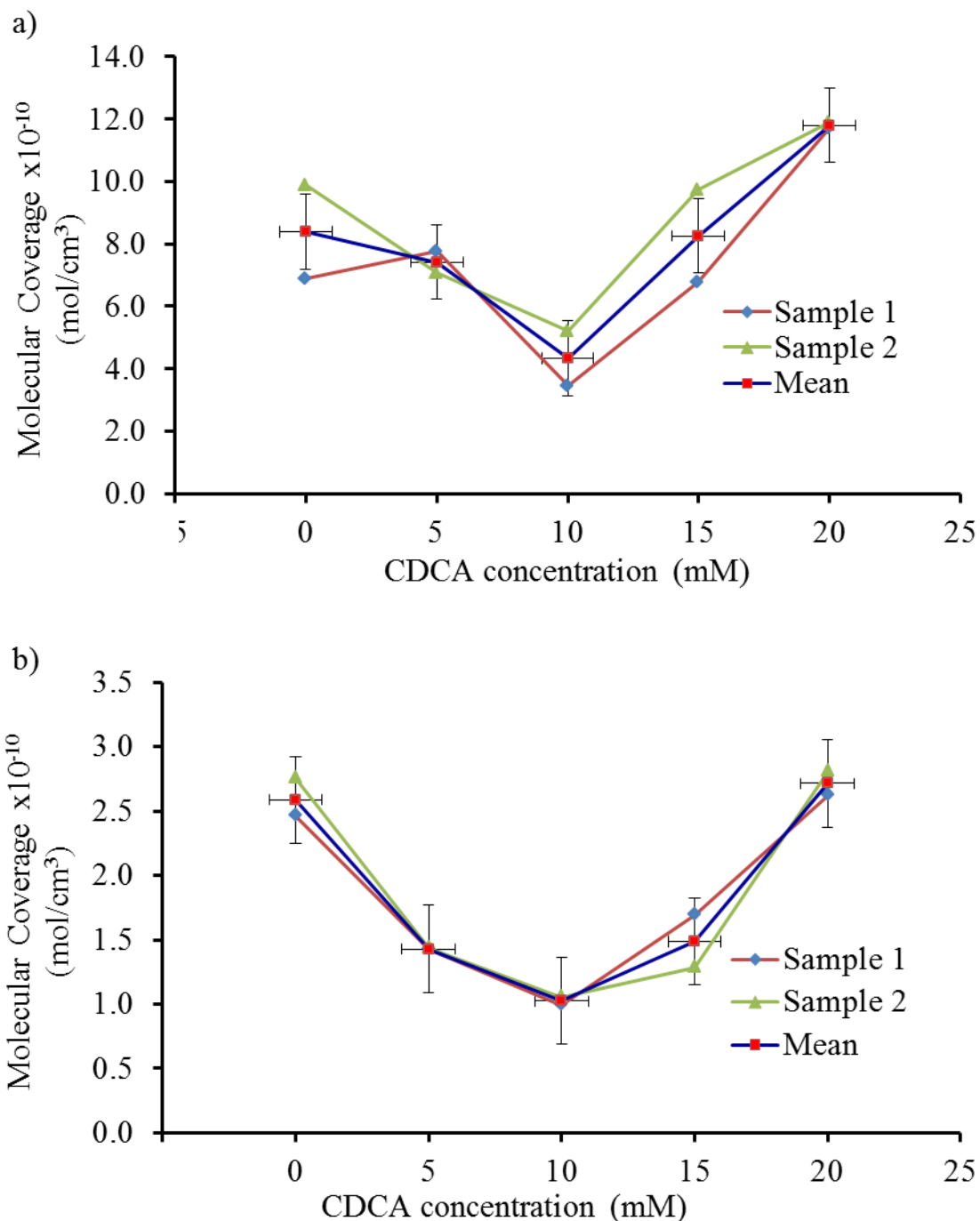
Figure 7-4. Molecular coverage of N719 as a function of CDCA concentration in the dye solution for low (a) and high (b) dye solution concentrations.

Concentration depth profiles of ruthenium as constituent of the N719 layer on titania have been determined with NICISS. In total, 10 combinations of N719 and CDCA concentrations were investigated. Data from each combination were recorded twice. Tables 7-1 and 7-2 show the N719 coverage of titania for the samples with low (0.005 mM) and high (0.1 mM) dye concentration, respectively. As there are two samples for

each CDCA concentration, we also provide the mean coverage and its uncertainty in the last column in the tables. The dye coverage is defined as the amount of dye molecules on the titania surface per square centimetre, while the dye load is a quantity to measure the amount of dye molecule on the titania per unit volume.

Table 7-1. Molecular coverage resulting from the 0.005 mM N719 solution on the nanoporous titania with CDCA

No	CDCA concentration (mM)	Sample 1 Molecular coverage $\times 10^{-10}$ (mol.cm^{-2})	Sample 2 Molecular coverage $\times 10^{-10}$ (mol.cm^{-2})	Mean Molecular coverage $\times 10^{-10}$ (mol.cm^{-2})
1	Without CDCA	0.69	0.99	(0.84 ± 0.2)
2	5 mM CDCA	0.78	0.71	(0.74 ± 0.05)
3	10 mM CDCA	0.35	0.52	(0.4 ± 0.12)
4	15 mM CDCA	0.68	1	(0.83 ± 0.21)
5	20 mM CDCA	1.2	1.2	(1.18 ± 0.01)

Table 7-2. Molecular coverage resulting from the 0.1 mM N719 solution on the nanoporous titania with CDCA

No	CDCA concentration (mM)	Sample 1 Molecular coverage $\times 10^{-10}$ (mol.cm^{-2})	Sample 2 Molecular coverage $\times 10^{-10}$ (mol.cm^{-2})	Mean Molecular coverage $\times 10^{-10}$ (mol.cm^{-2})
1	Without CDCA	2.5	2.8	(2.6 ± 0.2)
2	5 mM CDCA	1.4	1.3	(1.4 ± 0.1)
3	10 mM CDCA	1	1.1	(1.0 ± 0.1)
4	15 mM CDCA	1.7	1.4	(1.5 ± 0.3)
5	20 mM CDCA	2.6	2.8	(2.7 ± 0.1)

By integrating the concentration depth profiles, the total amount of ruthenium on the surface can be determined. **Error! Reference source not found.** depicts the molecular coverage of N719 on the titania as a function of CDCA in the dye solution. It can be seen that the coverage of titania with N719 decreases with increasing CDCA concentration from 0 to 10 mM and then increases when increasing the CDCA concentration from 10 to 20 mM. A minimum coverage of N719 is found when using dye solutions of 10 mM CDCA. This phenomenon is found for both high and low N719 dye solution concentration.

NICISS is not suitable for determining the CDCA coverage of the titania surface. The reason is that NICISS is sensitive to the weight of the elements and not primarily to their chemical nature. CDCA consists only of the light elements O, C and H, and the O-to-C ratio is similar to the one in N719. Thus NICISS cannot be used to uniquely identify the amount of CDCA on the titania surface. In order to determine the amount of adsorbed CDCA, FT-IR measurements on the exposed photoelectrode surfaces were applied instead. The FT-IR spectra in **Error! Reference source not found.**(a) change with changes in the CDCA dye bath concentration. The FT-IR absorbance spectra show three main peaks at 2876, 2924, and 2961 cm^{-1}.

The peak around 2876 cm^{-1} has also been found in other studies using CDCA and has been attributed to the –CH stretch vibrational modes.[19] The absorption in N719 around 2876 cm^{-1} is at a minimum in the spectrum of an electrode exposed to a pure N719 solution, and it is stronger in the spectrum of an electrode exposed to a pure CDCA solution (blue dashed line, Figure 7-5a. This observation shows that the intensity of the peak around 2876 cm^{-1} is expected to increase with increasing CDCA concentration in a dye solution. The change in absorption in this wavenumber region can therefore be used to determine the amount of CDCA adsorbed onto the titania surface in the presence of N719.

In order to determine the CDCA and N719 concentration, a baseline is drawn between 2823 cm^{-1} and 3028 cm^{-1} (purple line, Figure 7-5b). The relative height of absorption intensities h_1 and h_2 at 2876 cm^{-1} (red line) and 2924 cm^{-1} (green line) were determined, as illustrated in **Error! Reference source not found.**b, and the ratio was calculated. The ratio is used as a relative measure for the amount of CDCA adsorbed onto titania in the presence of N719 in the dye solutions.
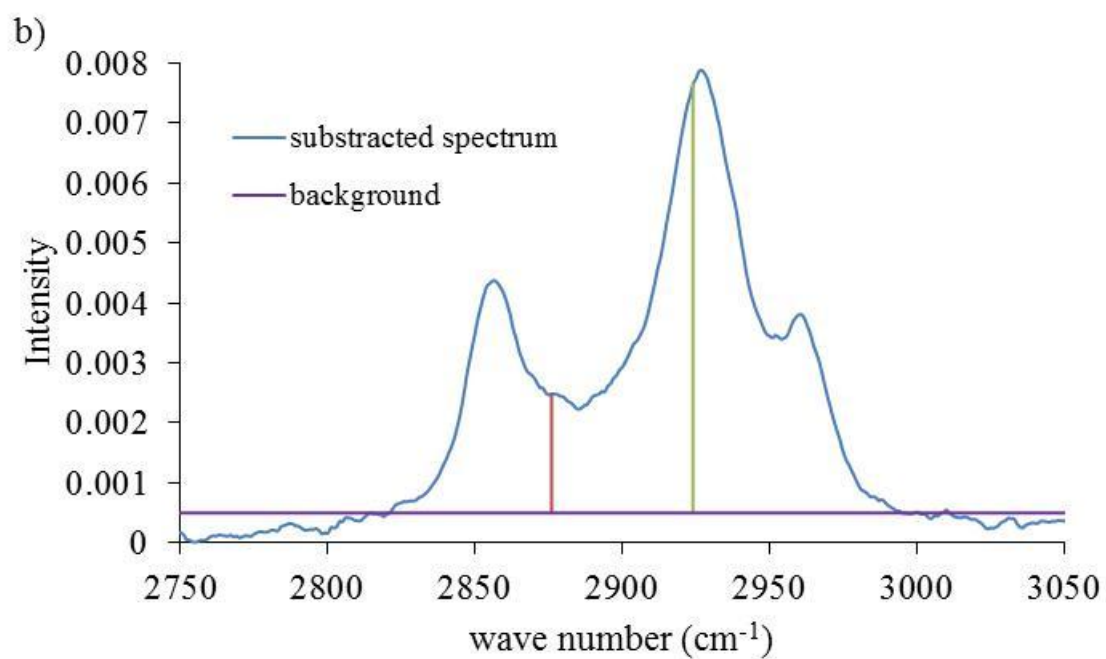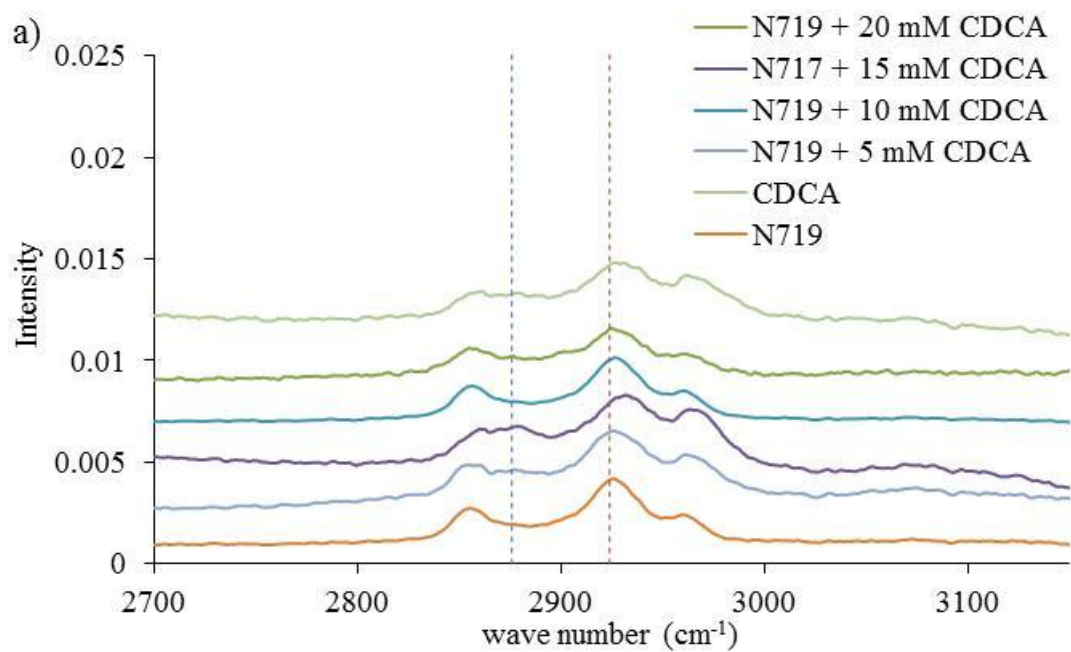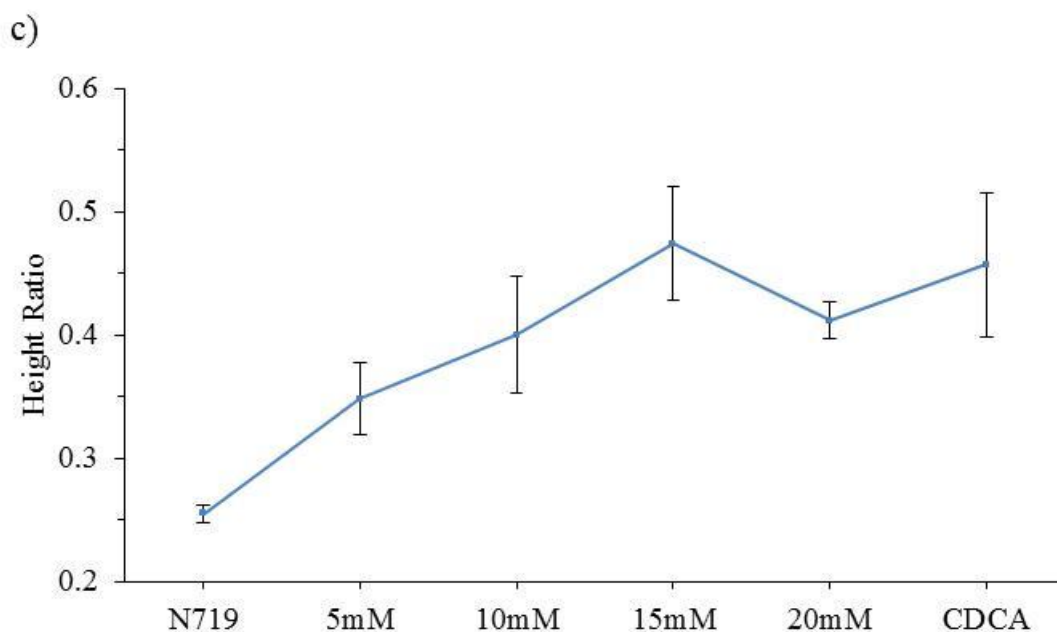
Figure 7-5. (a) FT-IR spectra of photoelectrodes exposed to 0.1 mM N719 and the CDCA with varying concentration. (b) The ratio h_1 and h_2 show a change of CDCA and N719 contribution (c) The ratio of peak contributions between 2876 cm^{-1} and 2924 cm^{-1} on FT-IR spectra (h_1 and h_2) is used as a relative measure for the amount of CDCA adsorbed onto the titania.

Regarding FT-IR analysis depicted on Figure 7-5(c) it seems that the increase of CDCA on titania surface after the strong minimum at 10 mM dye solution are not parallel with the fact shown on the ion spectroscopy where the amount of N719 decreases. Due to this result the FT-IR cannot investigate the presence of the CDCA quantitatively in this study, however NICISS is capable to measure it. However, it is impossible to plot the amount of CDCA in absolute intensity rather than a ratio intensity because the intensity for sample without the CDCA is not zero which means that some functional group on the N719 also seems behaves similarly as CDCA on the FT-IR measurement.

The ratio in absorbance intensity is given in **Error! Reference source not found.** (b) and shows that the ratio between CDCA and N719 increases monotonously with increasing amount of CDCA in the dye solution. It is important to notice that the FT-IR analysis is not a fully quantitative analysis because the absorption intensities at 2876 cm^{-1} and 2924 cm^{-1} cannot be associated to either pure N719 nor pure CDCA. Thus, the analysis of the FT-IR data represents a semi-quantitative measure of the amount of CDCA in the adsorbed layer.

7.3.2 Discussion

The two main results in this study are that *i)* the total coverage of titania with N719 depends on the concentration of CDCA in the dye solution and has a minimum at a concentration of 10 mM CDCA, and *ii)* that the fraction of the titania surface covered by a dye monolayer rather than a dye multilayer depends on the CDCA concentration in the dye solution used. These observations are similar to those found in a previous study, which reported that an addition of CDCA to the solution of organic dyes (e.g. D29 and D35) reduces the dye load on titania surfaces and increases the Incidence Photon to Current Efficiency (IPCE).[20]

The coverage of titania with N719 is the same for the concentration of 0 and 20 mM CDCA but goes through a minimum at 10 mM CDCA. Increasing the CDCA concentration also leads to a decrease in the thickness of the N719 layer, i.e. the degree of formation of multilayers decreases with increasing CDCA concentration. At 0 mM CDCA in the dye solution used a strong contribution of multilayers can be found, while at 20 mM CDCA the formation of a N719 monolayer is dominant. It is plausible to assume that both phenomena have the same origin. A possible explanation for both phenomena is that the CDCA molecules reduce the inter-dye molecular interaction[21] and as a consequence strengthens the molecular interaction between the adsorbents (N719 and CDCA) and titania substrate. The observation that the amount of N719 dye adsorbed onto the titania substrates goes through a local minimum as function of the CDCA concentration shows that a minimum amount of CDCA molecules have to adsorb onto the titania surface to generate this effect. However, it is still unclear why reducing the interaction between the N719 molecules leads to an increase of the amount of dye molecules on the titania surface. A possible explanation could be that the orientation of the N719 molecules also changes when the interaction between N719 and titania becomes more dominant, and as a result a larger number of N719 molecules adsorb on the surface. It must be noted that the experiments in this study do not give results that allow us to draw conclusions about the orientation of the adsorbed N719 molecules, and thus no evidence for the above hypothesis can be given. Irrespective of the reason for the increase in N719 coverage at CDCA concentrations of 10 mM and higher, it can be noted that N719 and CDCA cooperatively adsorbed onto titania. Supporting the formation of dye monolayers rather than dye multilayers is expected to support the electron injection from the dye to the metal oxide electrode because the transfer of the electrons from the excited dye molecule to the

electrode becomes more directly. As a consequence the efficiency of the DSSC is expected to increase.[22]

7.4 Conclusion

The investigation of dye-titania interface using NICISS technique has been performed to study the effect of the application of CDCA as co-adsorbent in a dye layer formation. Monolayer formation of the dye improves the injection of electrons into the titania. It had been known that CDCA improves the function of DSSCs but it was the reason why the CDCA is able to do this was not known yet. In this study, we have now revealed at least one of the reasons that the CDCA reduces the formation of multilayer dye and increases the monolayer dye. The key phenomena to reveal the changes is due the inter-dye molecule interaction. The CDCA strengthens the molecular interaction between the adsorbents and titania substrate and a possible explanation could be that the orientation of the N719 molecules also changes and as a result a larger number of N719 molecules adsorbed on the surface.

References

1. Grätzel, M., *The advent of mesoscopic injection solar cells.* Progress in Photovoltaics: Research and Applications, 2006. **14**(5): p. 429-442.

2. Li, J., et al., *Effect of chenodeoxycholic acid (CDCA) additive on phenothiazine dyes sensitized photovoltaic performance.* Science China Chemistry, 2011. **54**(4): p. 699.

3. Allegrucci, A., et al., *Improved performance of porphyrin-based dye sensitised solar cells by phosphinic acid surface treatment.* Energy & Environmental Science, 2009. **2**(10): p. 1069-1073.

4. Ellis-Gibbings, L., et al., *Formation of N719 Dye Multilayers on Dye Sensitized Solar Cell Photoelectrode Surfaces Investigated by Direct Determination of Element Concentration Depth Profiles.* Langmuir, 2012. **28**(25): p. 9431-9439.

5. Liu, P., et al., *EXAFS, ab Initio Molecular Dynamics, and NICIS Spectroscopy Studies on an Organic Dye Model at the Dye-Sensitized Solar Cell Photoelectrode Interface.* ACS Applied Materials & Interfaces, 2017. **9**(23): p. 19773-19779.

6. Grätzel, M., *Conversion of sunlight to electric power by nanocrystalline dye-sensitized solar cells.* Journal of Photochemistry and Photobiology A: Chemistry, 2004. **164**(1–3): p. 3-14.

7. Salvatori, P., et al., *Supramolecular Interactions of Chenodeoxycholic Acid Increase the Efficiency of Dye-Sensitized Solar Cells Based on a Cobalt Electrolyte.* The Journal of Physical Chemistry C, 2013. **117**(8): p. 3874-3887.

8.   Neale, N.R., et al., *Effect of a Coadsorbent on the Performance of Dye-Sensitized TiO2 Solar Cells: Shielding versus Band-Edge Movement.* The Journal of Physical Chemistry B, 2005. **109**(49): p. 23183-23189.

9.   Cisneros, R., M. Beley, and F. Lapicque, *A study of the impact of co-adsorbents on DSSC electron transfer processes: anti-π-stacking vs. shield effect.* Phys. Chem. Chem. Phys., 2016. **18**(14): p. 9645-9651.

10. Andersson, G. and H. Morgner, *Thermodynamics and structure of liquid surfaces investigated directly with surface analytical tools**.* Annalen der Physik, 2017. **529**(6): p. 1600230-n/a.

11. Levy, D. and K.A. Briggman, *Cholesterol/Phospholipid Interactions in Hybrid Bilayer Membranes.* Langmuir, 2007. **23**(13): p. 7155-7161.

12. Miao, K., et al., *Hydroxyl versus Carboxyl Substituent: Effects of Competitive and Cooperative Multiple Hydrogen Bonds on Concentration-Controlled Self-Assembly.* The Journal of Physical Chemistry C, 2016. **120**(26): p. 14187-14197.

13. Woodruff, D.P., *Solved and unsolved problems in surface structure determination.* Surface Science, 2002. **500**(1): p. 147-171.

14. Johansson, V., et al., *On the correlation between dye coverage and photoelectrochemical performance in dye-sensitized solar cells.* Physical Chemistry Chemical Physics, 2014. **16**(2): p. 711-718.

15. Andersson, G. and H. Morgner, *Impact collision ion scattering spectroscopy (ICISS) and neutral impact collision ion scattering spectroscopy (NICISS) at surfaces of organic liquids.* Surface Science, 1998. **405**(1): p. 138-151.

16. Ridings, C., G.G. Warr, and G.G. Andersson, *Composition of the outermost layer and concentration depth profiles of ammonium nitrate ionic liquid surfaces.* Physical Chemistry Chemical Physics, 2012. **14**(46): p. 16088-16095.

17. Andersson, G., T. Krebs, and H. Morgner, *Activity of surface active substances determined from their surface excess.* Phys Chem Chem Phys, 2005. **7**(1): p. 136-42.

18. Andersson, G. and H. Morgner, *Determining the stopping power of low energy helium in alkanethiolates with Neutral Impact Collision Ion Scattering Spectroscopy (NICISS).* Nuclear Instruments and Methods in Physics Research Section B: Beam Interactions with Materials and Atoms, 1999. **155**(4): p. 357-368.

19. Yang, L., et al., *FT-IR spectroscopic study on the variations of molecular structures of some carboxyl acids induced by free electron laser.* Spectrochimica Acta Part A: Molecular and Biomolecular Spectroscopy, 2005. **62**(4–5): p. 1209-1215.

20. Jiang, X., et al., *Structural Modification of Organic Dyes for Efficient Coadsorbent-Free Dye-Sensitized Solar Cells.* The Journal of Physical Chemistry C, 2010. **114**(6): p. 2799-2805.

21.   Hara, K., et al., *Effect of Additives on the Photovoltaic Performance of Coumarin-Dye-Sensitized Nanocrystalline TiO2 Solar Cells.* Langmuir, 2004. **20**(10): p. 4205-4210.

22.   Hagfeldt, A. and M. Graetzel, *Light-Induced Redox Reactions in Nanocrystalline Systems.* Chemical Reviews, 1995. **95**(1): p. 49-68.

8 CHAPTER 8: Conclusions and Summary

The work described in this thesis has focused on the formation of dye on the titania layer in the DSSCs from the perspective of monolayer /multilayer dye formation and the effect of the electrolyte exposure, aging process, and the application of the co-adsorbent. The dye structure changes were found to be dependent on the chemical boundaries of the interface between the dye and the substrate. Those processes are very important in the operation of DSSCs as an effort to suppress the recombination reaction that could be the unwanted process in the cell which could potentially hinder the electron flows in right effective path way, thus it will be improving their performance.

While the techniques used in this research are used to probe the depth of the surface based on their probing depth, XPS is the less surface sensitive than that of UPS and MIES but its probing depth is able to investigate the chemical composition of the material. MIES is the most surface sensitive and UPS is in between of XPS and UPS. When the spectrum contribution appeared on the UPS and it did not on the MIES, it indicates that the component is sitting underneath of the surface. In addition, NICISS as one of ion spectroscopy technique is able to probe until 30 nm in depth. Thus we can classify in which depth the components are sitting on the sample.

In the study of the investigation of iodine as one component of the electrolyte, it is focusing on how the iodine interacts with the sensitized-dye molecules on the mesoporous titania. After the iodine exposure, the interaction between the iodine and the dye molecule could occur at the dye/titania interface or shallower. The investigation is possible to be carried out as the thickness of the dye layer is in the range of the probing depth of the photoelectron spectroscopy technique used in this study (XPS, UPS, and MIES). The results have been able to determine the change of the dye formation due to the presence of the iodine after the exposure to the electrolyte solution. Interestingly, the N719 dye does not show a significant shift of the secondary electron cut-off in the UP spectra in comparison with the Z907 dye. This evidence indicates that the N719 has fewer changes of the work function where the iodide as the chemical boundary.

In term of the restructuring of the outermost molecules, the N719 dyes underwent reorientation of the dye and iodide adsorption after iodine exposure. However, we conclude that the iodide adsorption is more likely, which was shown by the additional

peak around low binding energy in the MIE spectra. The Z907 dye, however, did not show additional peaks after iodine exposure. The Z907 more likely formed stronger dipole layers across the dye/titania interface rather than the N719 dye.

The more iodine presenting on the Z907 dye layer, the stronger dipole layer will occur across the dye/titania interface. For the N719 dye, on the other hand, the more iodine on the surface, the more dye molecule reorientation occurred. However, it does not significantly affect the change of its work function. The finding of where the iodide adsorbs to the dye layer on this study has implications for charge transfer from dye to titania. However, for understanding the influence on the operation DSSCs would have to be built.

The application of some organic dyes like L0Br has also been investigated. The aim of the research using the L0Br is to determine the formation of the dye layer in the titania. Using an ion spectroscopy technique (NICISS), which employs the presence of a heavier element to scatter back the helium atom, is a favourable technique as a direct measurement to investigate the concentration depth profile of the sample. As part of the L0Br molecule, bromine could scatter back the helium atom, therefore the measurement of its concentration depth profile of the L0Br on the titania, is possible to be carried out. It was also acknowledged that by using NICISS, the concentration depth profile of the L0Br dye on nano-porous titania showed that the L0Br formed mostly a monolayer dye with a small contribution of multilayers after the deconvolution of the NICISS spectrum.

By calculating the molecular coverage of each sample, the plot of the adsorption isotherm can be determined. The range coverage is between $1\text{x}10^{-10}$ mol·cm^{-2} and $4\text{x}10^{-10}$ mol·cm^{-2} or between 1.6 and 0.4 nm^2 per L0Br molecule. In addition, perfect monolayer dye coverage is around 0.5 nm^2 per molecule calculated in theory, which is similar to our measured molecular coverage of sample with around 0.04 mM in concentration. The result also provides the evidence that the L0Br dye was forming more monolayer rather than building some islands before forming a multilayer. This evidence is expected to provide more efficient charge transfer to titania.

The effect of the electrolyte and aging process to the organic dye also has been investigated using electron spectroscopy (XPS UPS and MIES). The investigation was focusing on the effect of the electrolyte exposure and aging process of the PD2 and LEG 1 dyes. Two different electrolytes were used to look at how they influence the dye layer. The

first electrolyte is Co(bpy)$_3$ based electrolyte which is the electrolyte without contained *4-tert*-butylpyridine (TBP), and the second electrolyte contained the TBP.

The Angle-Resolved XPS (ARXPS) through PD2 and LEG1 samples in two different X-ray incident angle (e.g. 0 and 55 degrees) has been carried out. However, the variation of the peak intensity which indicates the percentage of each element does not show a reasonable correlation of the molecular structure. It might be due to the shape or curvature of the sample surface as the nanoporous titania may not be completely flat.

It was shown that the work function of both dyes increased due to the electrolyte exposure. The LEG1 showed a larger change of work function than that of the PD2 dyes. The effect of the second electrolyte exposure, however, formed less dipole layer on both PD2 and LEG1 dyes, than the electrolyte with the TBP. As a consequence, the work functions have also changed larger due to the second electrolyte than that of the first electrolyte without the TBP. Reorientation of the dye molecules was also occurring for both dyes due to the electrolyte and aging process.

The application of the adsorbent on the DSSC is also promising and in this study, the effect of CDCA as a co-adsorbent on the N719 dye was revealed. The formation of the N719 dye on the titania was found to be dependent on the presence of the CDCA. This investigation has been carried out using ion NICISS technique. It has been shown that at least one of the reasons that the CDCA reduces the formation of multilayer dye and increases the monolayer dye is because of the titania surface passivation, or suppressing the intramolecular dye interaction, which led to the dye aggregation, even though the reason why the CDCA is able to improve the function of DSSCs was not known yet.

The effect of the co-adsorbent on the N719 dye was found to be dependent on the concentration of both the dye and the adsorbent. The higher concentration of the N719, mostly experienced multilayer formation without the application of CDCA.,This phenomenon was proposed to explain the change of the concentration depth profile of the N719 dye on the titania by comparing with the one which was containing the CDCA.

It was shown that there was a minimum molecular coverage of the N719 as a variation of the CDCA concentration. When the concentration of the CDCA application increased from 0 to 20 mM, the molecular coverage of the N719 on the titania was decreasing initially then increasing after reaching minimum coverage. The minimum coverage can be attributed to the region where the dye more likely formed less multilayer and increased

more monolayer. Based on this evidence, it was found that the CDCA work cooperatively with the N719 dye to reduce the aggregation of the dye and also to passivate the titania. Therefore the application of the CDCA as a co-adsorbent with fully organic composition material would be potentially improving the cell performance in the future application due to the low-cost production in making the DSSCs with the abandoned material.

While this Ph.D. work was focussed on studying the interfacial properties of the electrolyte/dye/titania interface on the DSSCs, the fundamental understanding of the factors influencing the formation of the dye on the substrate corresponding to other materials are relevant to a wide range of applications.

As the studies of the work-function, restructuring of some outermost atom on the surfaces, and the concentration depth profiles, in this research highlighted the importance of actual properties of the surface, it can potentially have critical implications on the interfacial energetic in many applications. Thus, the results of this study are not only important for the surface science community where electron and ion spectroscopy can be used as a method of choice for measuring molecular properties of the interface, but these findings could potentially be useful in better understanding of the film devices.

The future work that can be carried out related to this Ph.D. research can be associated with several aspects. One of the potential issues could be related to the electrolyte exposure upon different dyes. Redox couples in the electrolyte are interacting in a different way to corresponding dye, some combination of the dye-electrolyte pair will expand the knowledge how to get the best material matching to improve the cell performance. Another potential work could also be related to the use of different co-adsorbent, where another type of the co-adsorbent also could be possibly investigated together with different dyes either based on metal complexes or fully organic dyes in correlation with the different dye treatment that is normally used in the effort to improve the cell performance. Another co-adsorbent based on phosphonic acid such as DPA (decylphosphonic acid) is the second champion co-adsorbent material in DSSCs application. Thus it would be a potential research area in which relevant to a wide range of material studies. The more complex of electron and ion spectroscopy techniques such as more powerful ARXPS, UPS-MIES, IPES, and NICISS would be very interesting to be carried out to reveal more complex information in the molecular energetic level for dye/titania interface analysis.

Appendix A

Considering the shape/curvature of nanoporous titania

Figure A.1 shows the concentration depth profiles of four samples, namely 0.0025 mM (the lowest concenteration), 0.03 mM, 0.08 mM, and 0.1 (the highest concentration). Purple and red lines are the deconvoluted spectra after applying deconvolution procedure to resolve the energy step of bromine and taking the shape of titania into account respectively.
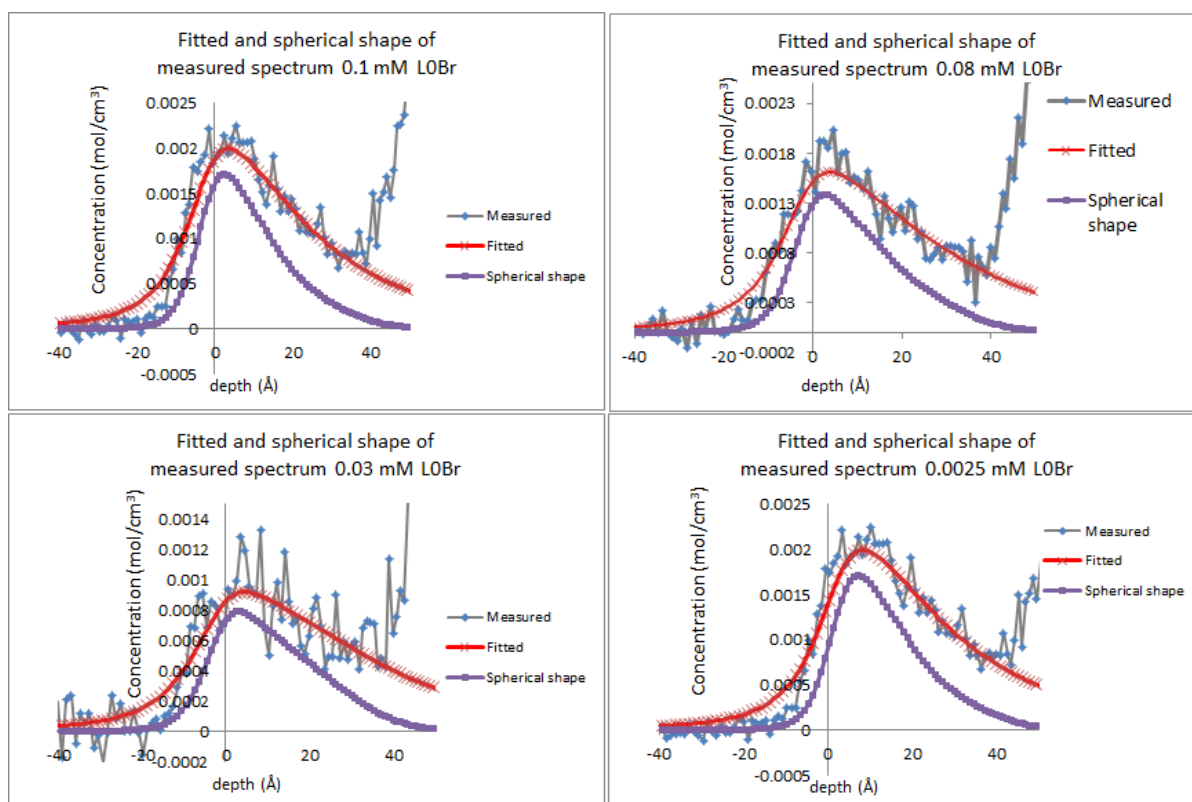

Figure A.1 Corrected spherical shape of measured L0Br 0.1 mM, 0.08 mM, 0.03 mM and 0.0025 mM

Figure A.1 depicts the L0Br spectrum of measured spectra after taken the shape of titania into account. Among the distinct bromine peak on the deconvoluted spectrum, it seems that all of the deconvoluted L0Br dye coverages on the mesoporus titania have distinct sharp and narrow peaks with a width of ~5 angstroms indicating that the L0Br dye layer forms mostly a monolayer with a small fraction of the surface covered with a multilayer.(Figure A.2) This evidence shows that the proportion of multilayer dye island is much smaller than what has been found in previous works for N719[1] and Z907[2].
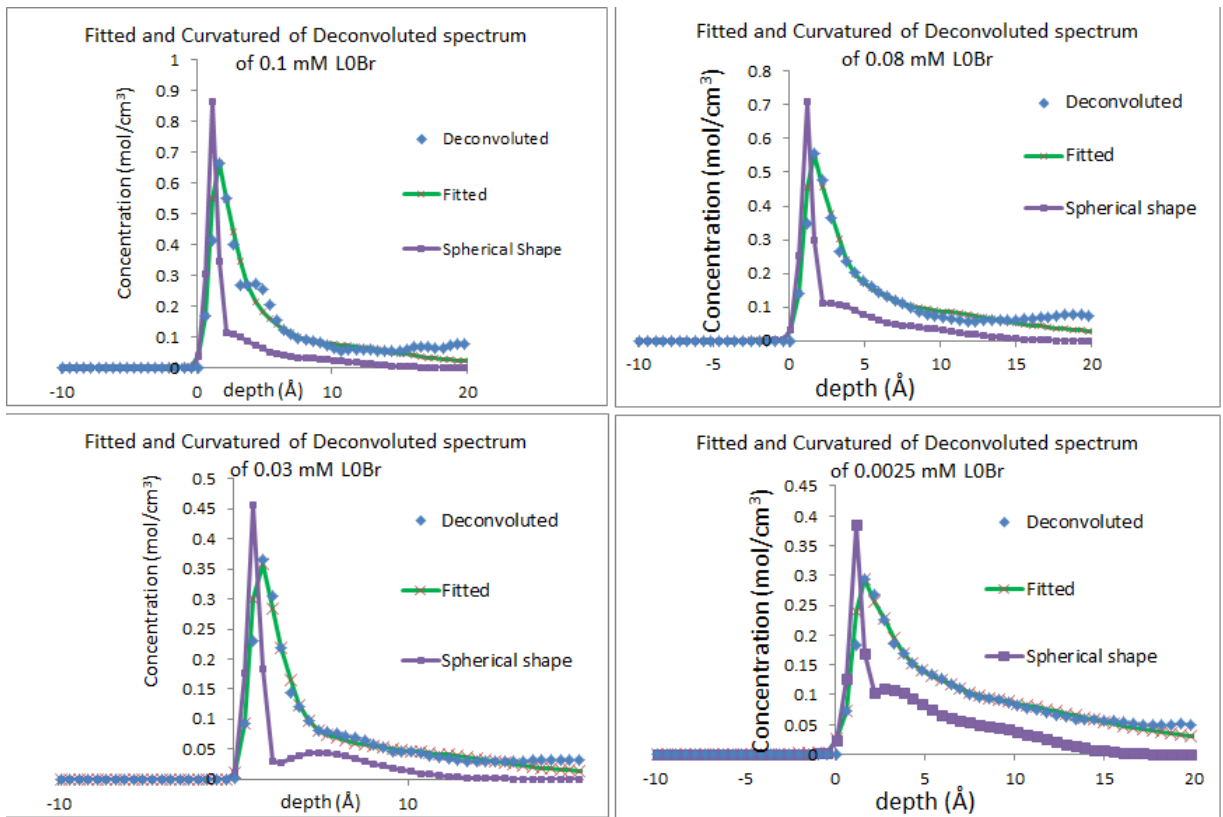
Figure A.2 Corrected spherical shape of deconvoluted L0Br 0.1 mM, 0.08 mM, 0.03 mM and 0.0025 mM

High dose ion bombardment

In high dose of helium ion bombardment, the indium leads to appears between -15 to 5 in depth scale as an additional contribution (Figure A.3) more likely due to the pinhole on the titania layer indicating that this contribution leads to unclear data evaluation of the exact molecular coverage of L0Br. This measurement needs to be taken to show the presence of pinhole on the titania surface affects to the bromine peak because indium is sitting close by to bromine on TOF spectrum in NICISS. However, the presence of pinholes only covers a small fraction of the surface.
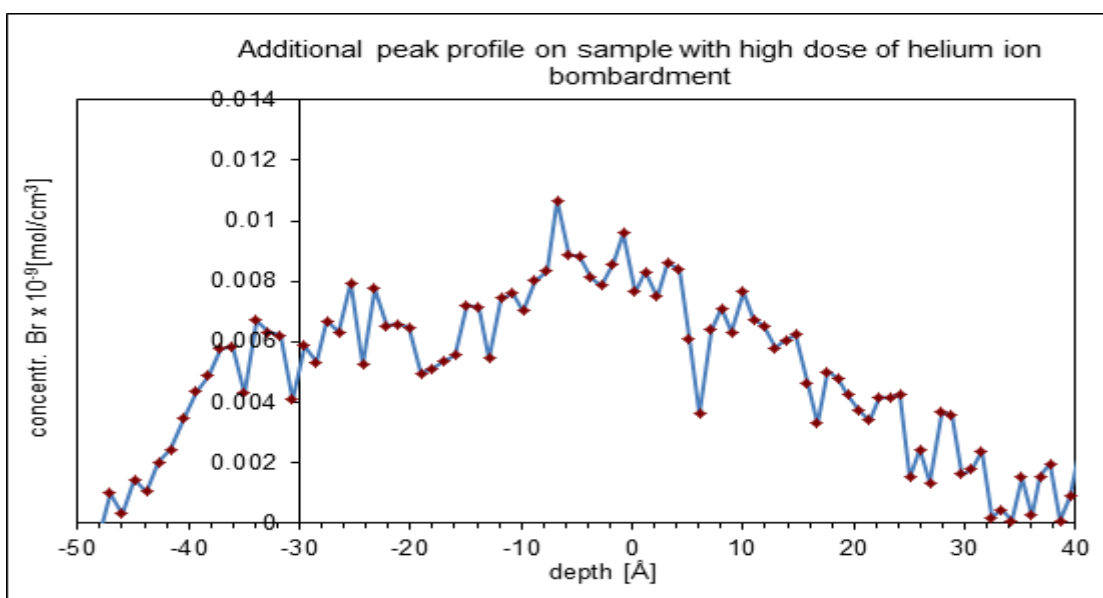

Additional peak profile on sample with high dose of helium ion bombardment

Figure A.3 Profile of indium peak on high dose helium ion bombardment

XPS (X-ray Photoelectron Spectroscopy)

XPS measurement on the 0.09 mM sample with high ion dose of bombardment has been carried out, and table A1 indicates the presence of indium spectrum around 444 eV in binding energy on the L0Br dye sample surface. Table A.1 also depicts the percentage of each element on the dyed sample surface was measured from XPS. The percentage of indium is around 0.05 per cent. It is larger than the percentage of bromine which is only 0.01 per cent. The indium (444 eV) is associated as a single indium atom rather than indium hydroxide as the binding energy position of $In(OH)_3$ is 445.2 eV. The possibility that the indium appears as additional contribution could be assumed in various ways. One of the factor might be the migration of indium through the mesoporus titania due to the sintering process. The other factors why indium contributes to the bromine peak could be assumed that either the sample surface has some pinholes due to the improper coverage of

ITO glass substrate by the mesoporus TiO_2 using doctor blade method or the damaging of the surface due to the high dose exposure of helium ions as showed in Figure A.3.

Table A.1 Chemical composition one of dyed sample surface from XPS measurement

Element	Calibration	% int
O 1s peak 1	530	23.27
O 1s peak 2	532	14.60
C 1s peak 3	288	2.89
C 1s peak 2	286	21.57
C 1s peak 1	285	27.88
Ti 2p3/2	458.9	6.87
Br 3d5/2	70.3	0.02
In 3d5/2	444	0.05

Reference

1. Ellis-Gibbings, L., et al., Formation of N719 Dye Multilayers on Dye Sensitized Solar Cell Photoelectrode Surfaces Investigated by Direct Determination of Element Concentration Depth Profiles. Langmuir, 2012. **28**(25): p. 9431-9439.

2. Johansson, V., et al., On the correlation between dye coverage and photo-electrochemical performance in dye-sensitized solar cells. Physical Chemistry Chemical Physics, 2014. **16**(2): p. 711-718.

Appendix B

NICISS spectrum of PD2 and LEG1 dye

The NICISS spectra measurement for both PD2 and LEG1 can be seen on the Figure B.1 below. The sulphur is estimated appears on the early onset of the bulk Titania as the position of sulphur is very close in comparison with titania on NICISS.
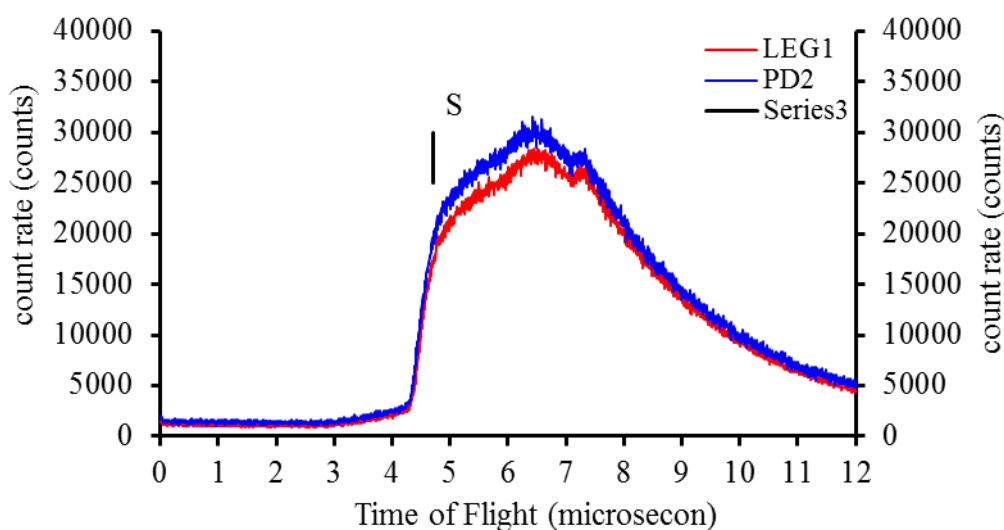

Figure B.1 The absence peak in front of the onset of the titania shows that the sulphur contribution on the both dyes (PD2 and LEG1) is not sufficient as a target in NICISS investigation.

Orbital Contribution on MIE Spectra

Regarding to the main component of PD2 dye which is one of promising organic sensitising dye, there are three main part components including donor, linker and acceptor. Donor, linker, and acceptor in PD2 and LEG1 dyes associate to several chemical groups such as alkyl and benzene, bithiophene, carboxyl and pyridine (PD2) or cyanoacrylic (LEG1) respectively.

PD2 dye Orbital Contribution

Number of molecular orbital on PD2 dye peak contribution assignment for peak 3, 4 and 5 is shown in the table B.1 below.

Table B.1. Molecular orbital assignment of PD2 dye for peak 3, 4 and 5 MIE spectra

Number of molecular orbital	Peak	Associated Functional Group
33	Donor in peak 3 and 4	Alkyl
11	Donor in peak 5	Alkyl
6	Acceptor in peak 3 and 4	Carboxyl
0	Acceptor in peak 5	-
10	Linker in peak 3 and 4	Bithiophene
2	Linker in peak 5	Bithiophene

LEG1 dye Orbital Contribution

Number of molecular orbital on LEG1 dye peak contribution assignment for peak 3, 4 and 5 is shown in the table B.2 below.

Table B.2 Molecular orbital assignment of LEG1 dye for peak 3, 4 and 5 MIE spectra

Number of molecular orbital	Peak	Associated Functional Group
21	donor peak 3	Benzene, Alkyl
21	donor peak 4	Alkyl
21	donor peak 5	Alkyl
4	acceptor peak 3	Carboxyl
4	acceptor peak 4	Carboxyl
4	acceptor peak 5	Carboxyl
4	linker peak 3	Bithiophene
9	linker peak 4	Bithiophene
3	linker peak 5	Bithiophene

XPS Result

The XPS measurement has been done for both PD2 and LEG1 with Angle Resolved XPS (ARXPS). Angle represents the position of normal sample surface relatively to the impinging X-ray. While the number is representing the percentage composition of each components on the sample (Nitrogen, Oxygen,Titanium, and Sulphur). As a variation of the incident angle, the change of intensity or percentage intensity could represent different depth if the surface could be assumed as a flat surface.

Table XPS of PD2 dye

PD2 sample A2

Angle	N peak 1	O peak 1	O peak 2	O peak 3	O peak 4	C peak 1	C peak 2	C peak 3	C peak 4	Ti peak 1	S peak 1
0 deg	1.54	17.51	3.97	3.22	6.99	32.66	18.09	9.26	1.19	4.97	0.61
55deg	1.39	17.21	3.96	3.42	6.67	24.70	20.11	11.46	5.23	5.13	0.71

PD2 sample A3

Angle	N peak 1	O peak 1	O peak 2	O peak 3	O peak 4	C peak 1	C peak 2	C peak 3	C peak 4	Ti peak 1	S peak 1
0 deg	1.54	17.51	3.97	3.22	6.99	32.66	18.09	9.26	1.19	4.97	0.61
55deg	1.39	17.21	3.96	3.42	6.67	24.70	20.11	11.46	5.23	5.13	0.71

PD2 sample A6

Angle	N peak 1	O peak 1	O peak 2	O peak 3	O peak 4	C peak 1	C peak 2	C peak 3	C peak 4	Ti peak 1	S peak 1
0 deg	1.54	17.51	3.97	3.22	6.99	32.66	18.09	9.26	1.19	4.97	0.61
55deg	1.39	17.21	3.96	3.42	6.67	24.70	20.11	11.46	5.23	5.13	0.71

Table XPS of LEG 1 dye

LEG1 sample B1

Angle	N peak 1	O peak 1	O peak 2	O peak 3	O peak 4	C peak 1	C peak 2	C peak 3	C peak 4	Ti peak 1	S peak 1
0 deg	1.54	17.51	3.97	3.22	6.99	32.66	18.09	9.26	1.19	4.97	0.61
55deg	1.39	17.21	3.96	3.42	6.67	24.70	20.11	11.46	5.23	5.13	0.71

LEG1 sample B3

Angle	N peak 1	O peak 1	O peak 2	O peak 3	O peak 4	C peak 1	C peak 2	C peak 3	C peak 4	Ti peak 1	S peak 1
0 deg	1.54	17.51	3.97	3.22	6.99	32.66	18.09	9.26	1.19	4.97	0.61
55deg	1.39	17.21	3.96	3.42	6.67	24.70	20.11	11.46	5.23	5.13	0.71

LEG1 sample B4

Angle	N	O	O	O	O	C	C	C	C	Ti	S

	peak 1	peak 1	peak 2	peak 3	peak 4	peak 1	peak 2	peak 3	peak 4	peak 1	peak 1
0 deg	1.54	24.20	3.70	3.29	5.79	29.24	16.02	7.57	0.99	7.17	0.47
55deg	1.83	24.85	3.66	3.53	5.54	27.23	17.10	7.72	0.78	7.25	0.51

LEG1 sample B5

Angle	N peak 1	O peak 1	O peak 2	O peak 3	O peak 4	C peak 1	C peak 2	C peak 3	C peak 4	Ti peak 1	S peak 1
0 deg	6.57	13.73	6.27	4.21	4.74	38.90	17.87	2.68	0.64	4.06	0.35
55deg	6.33	13.46	6.25	4.48	3.82	39.88	18.35	2.73	0.57	3.79	0.34

LEG1 sample B6

Angle	N peak 1	O peak 1	O peak 2	O peak 3	O peak 4	C peak 1	C peak 2	C peak 3	C peak 4	Ti peak 1	S peak 1
0 deg	9.77	12.04	6.23	3.54	2.90	23.09	21.40	16.78	0.72	3.24	0.30
55deg	10.93	11.85	5.62	3.51	1.79	23.78	21.99	16.34	0.75	3.13	0.31

Appendix C

Measured NICISS Spectra

Figure. C.1 to Figure. C.8 are showing the concentration depth profile between N719 dye after CDCA application and the pristine N719 with various concentration of coadsorbent. Figure. C.1 to B.4 and Figure C.5 to B.8 are representing low dye loading with 0.005 mM and high dye loading with 0.1 mm of N719 respectively. Figure C.8b is showing two different regions of the depth. The region less than 10 Å is representing the monolayer region while the region more than 10 Å is associated with the depth for multilayer. The purple dashed line shown in the figure helps as a mark to differentiate between the monolayer and multilayer regions. Plots of the differences between the N719 with CDCA and without CDCA also help us to look at how the changes among the samples.
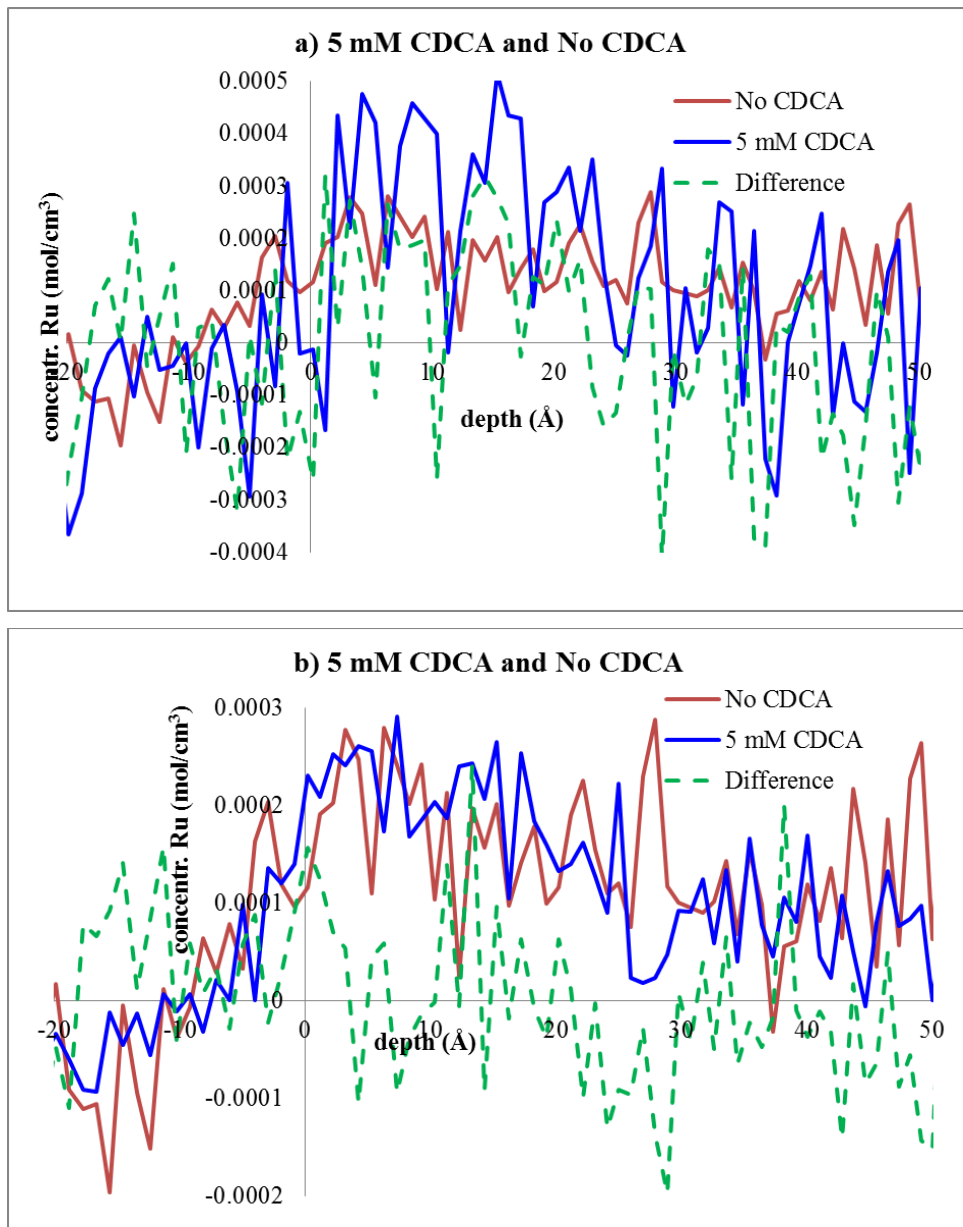
Figure C.1. The difference between 5 mM of 0.005 mM N719 CDCA and the pristine one
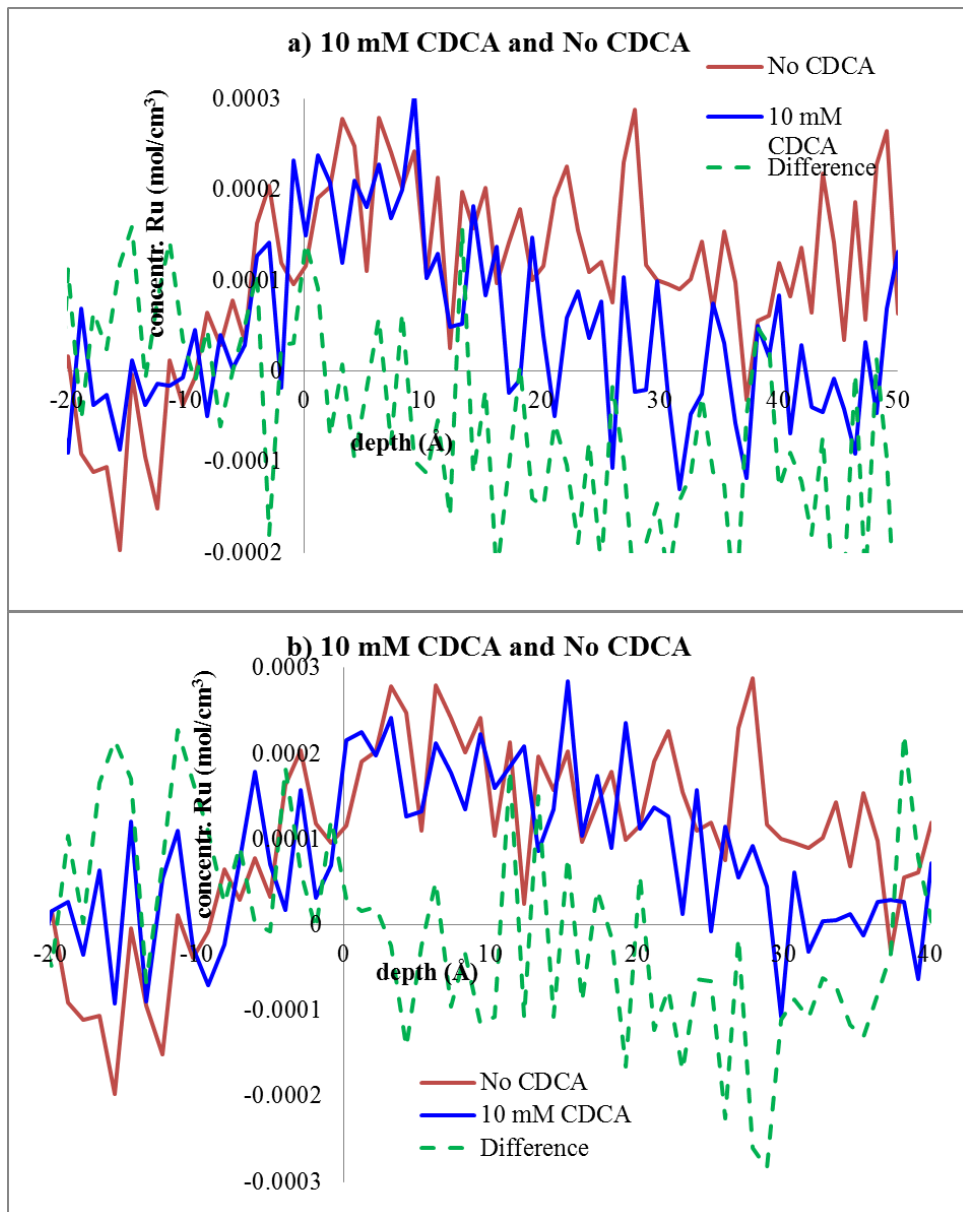
Figure C.2. The difference between 10 mM of 0.005 mM N719 CDCA and the pristine one.
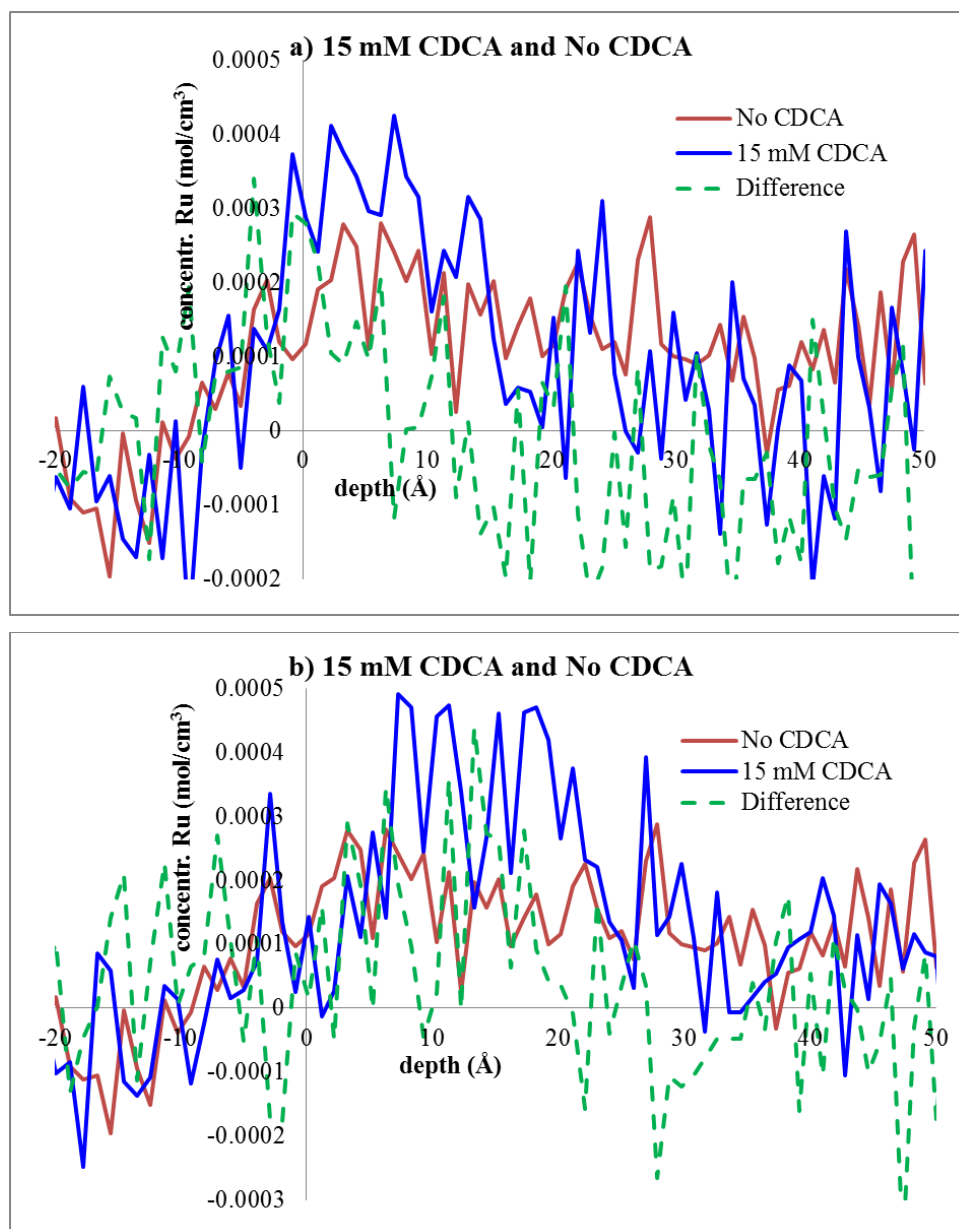
Figure C.3. The difference between 15 mM of 0.005 mM N719 CDCA and the pristine one.
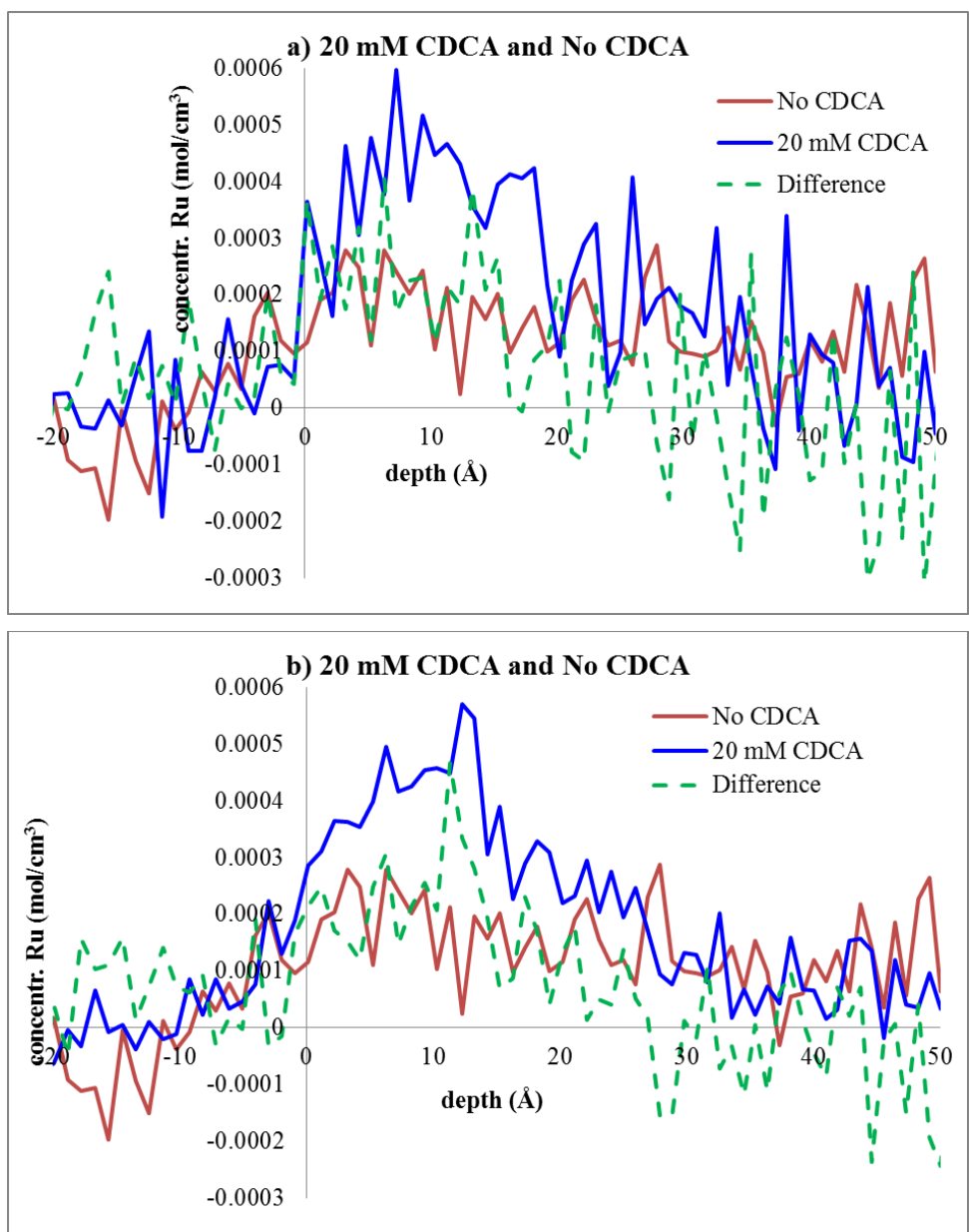
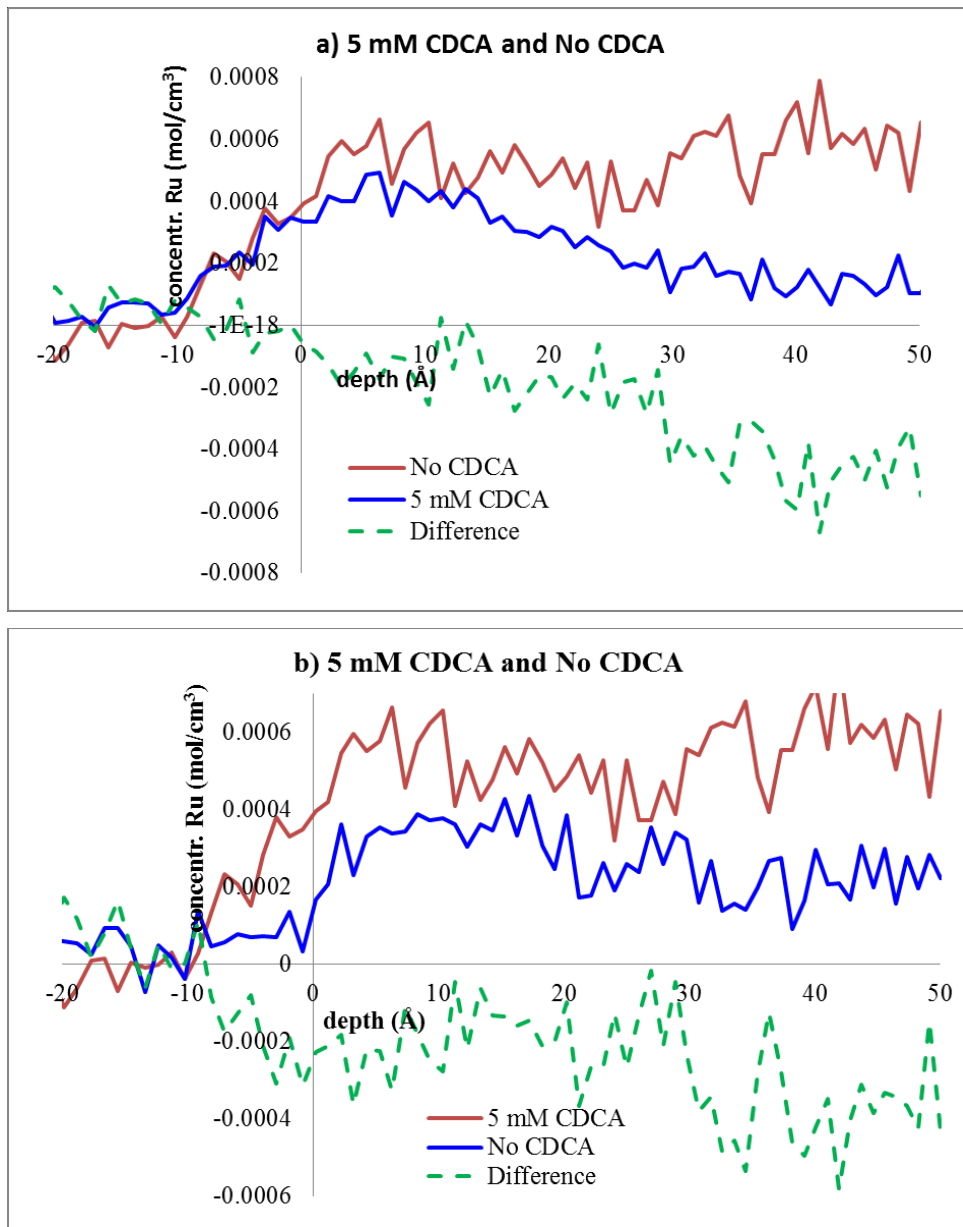*Figure C.4. The difference between 20 mM of 0.005 mM N719 CDCA and the pristine one.*

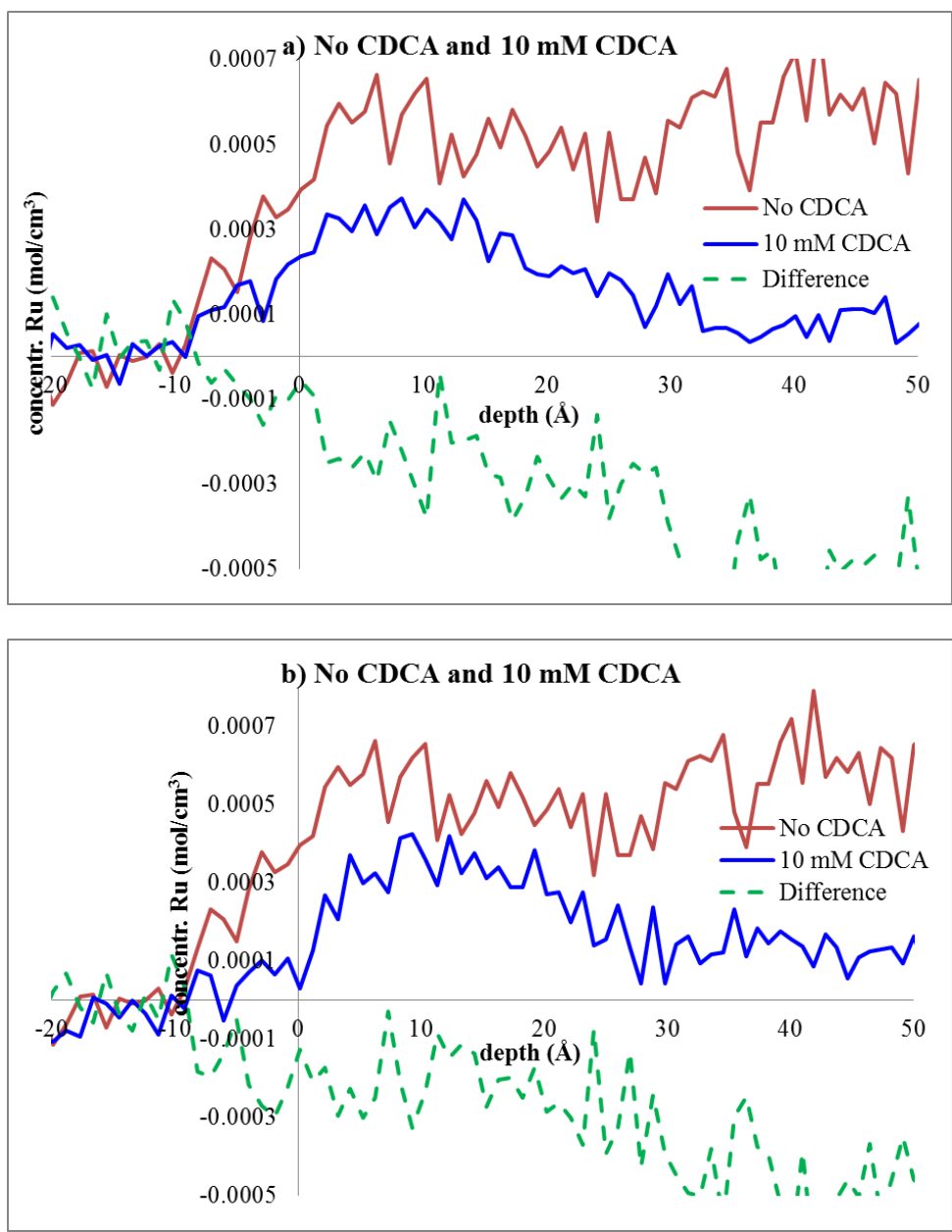*Figure C.5. The difference between 5 mM of 0.1 mM N719 CDCA and the pristine one*

a) No CDCA and 10 mM CDCA

b) No CDCA and 10 mM CDCA

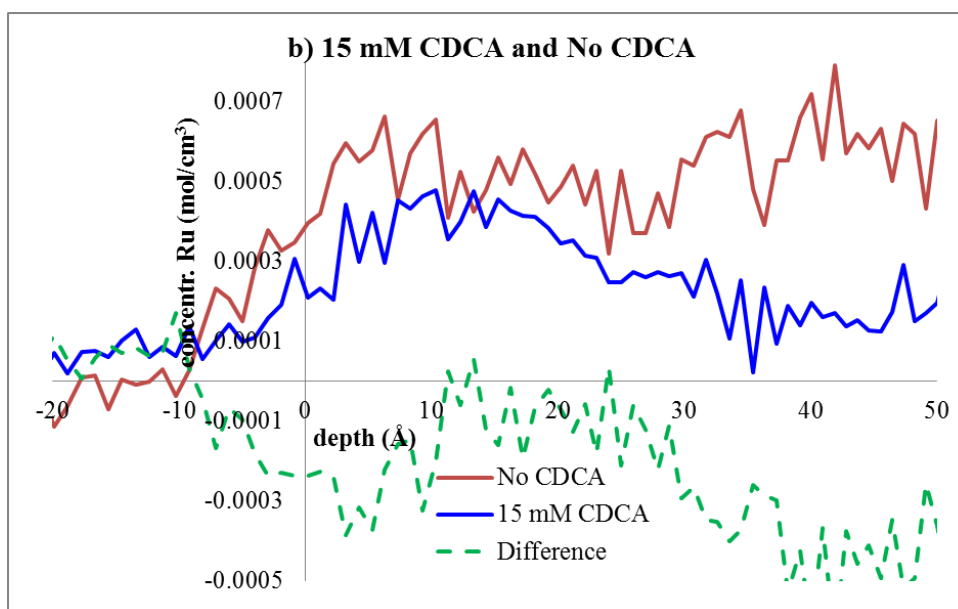*Figure C.6 The difference between 10 mM of 0.1 mM N719 CDCA and the pristine one.*
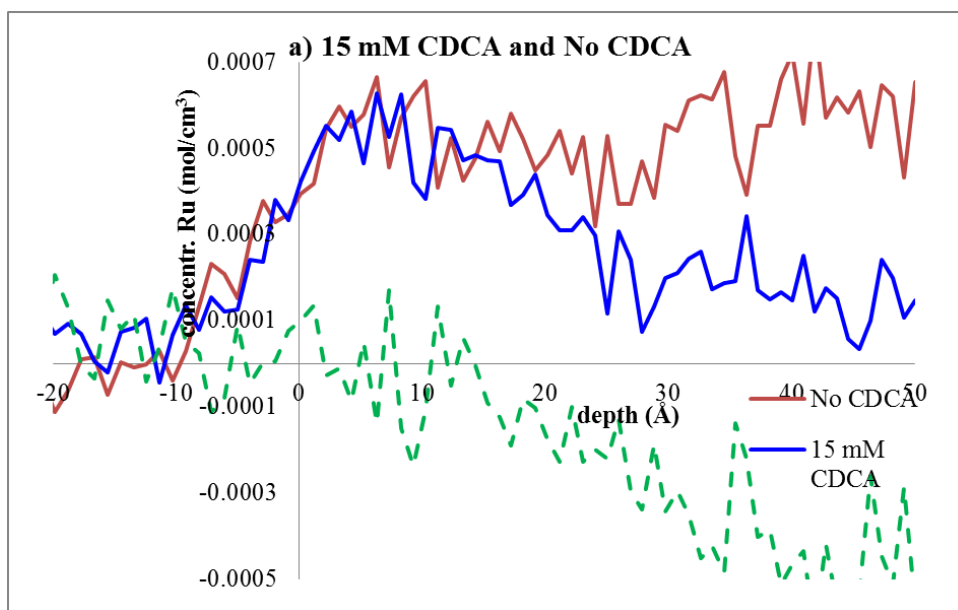
Figure C.7. The difference between 15 mM of 0.1 mM N719 CDCA and the pristine one.
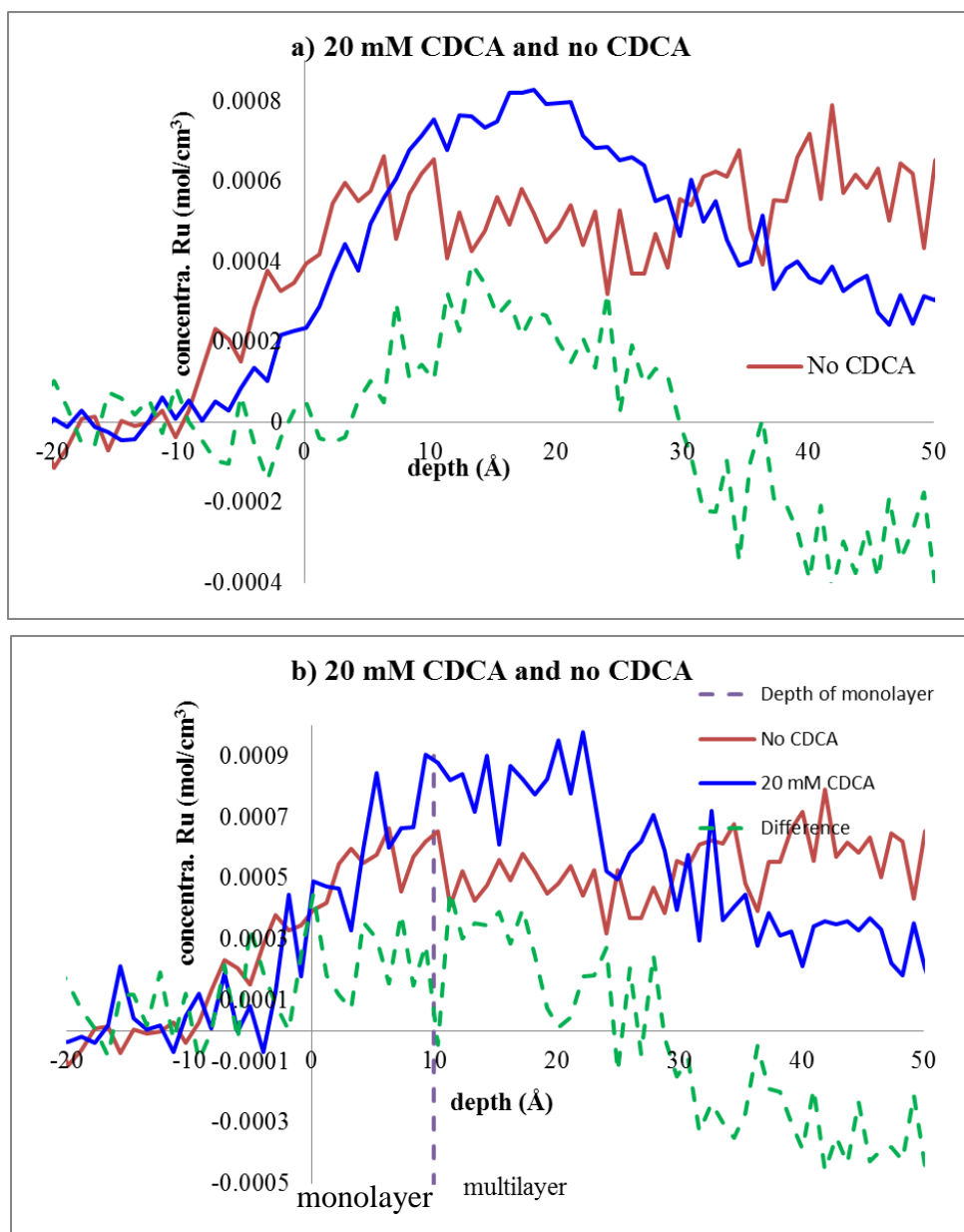
Figure C.8. The difference between 20 mM of 0.1 mM N719 CDCA and the pristine one.

The differences of NICISS spectrum between sample with CDCA and without the CDCA (pristine) are shown in Fig B.1 to Fig B.8. In general, it can be seen that the concentration at deeper layer has decreased or at least retained at a constant number after adding the CDCA as a coadsorbent as shown in both sample group. However, the concentration depth profile of the outermost layer less than 20Å showed some variation.

In terms of monolayer dye formation, seven samples showed increases of monolayer formation which associated in Fig B1a, B.3a, B.3b, B.4a, B.4b, B.8a and B.8b. Four samples correspond to Fig B.1b, B.2a, B 2b, and B 7a showed constant number of monolayer, and five samples showed decreases of monolayer (e.g Fig B.5a, B.5b, B.6a,B. 6b, and 7b). In deeper region which is more than 20Å, there were six samples showing a

constant number of concentration depth profile namely Fig B.1a, B.1b, B.3a, B.3b, B.4a, and B.4b. The most interesting finding was that in this particular region, ten samples which are shown in Fig B.2a, B.2b, B.5a, B.5b, B.6a, B.6b, B.7a, B.7b, B.8a, and B.8b showed decreases of number of ruthenium. It is very crucial aspect in dye sensitised solar cell that the less multilayer formation on the substrate is more promising to enable more efficient electron transfer from the excited dye into the semiconductor.

The difference shown in the green dashed line has been taken by subtracting between the sample feature with the CDCA application and the sample without the CDCA application to see how the CDCA changes and how deep the ruthenium can go below the surface. When the difference was going positive (upward) it indicates that the number of ruthenium is increasing. While it going negative on the other hand, it is indicating that the number of ruthenium is lower in that depth relatively to the sample without CDCA. It can be interpreted that the presence of the CDCA suppressed the multilayer and led to the monolayer dye formation.